UNIVERSITY OF OKLAHOMA

GRADUATE COLLEGE

GEOCHEMICAL CHARACTERIZATION OF THE UPPER MISSISSIPPIAN GODDARD FORMATION, SPRINGER GROUP, IN THE ANADARKO BASIN OF OKLAHOMA

A THESIS

SUBMITTED TO THE GRADUATE FACULTY

in partial fulfillment of the requirements for the

Degree of

MASTER OF SCIENCE

By

CATHERINE AGNES PEARSON
Norman, Oklahoma
2016

GEOCHEMICAL CHARACTERIZATION OF THE
UPPER MISSISSIPPIAN GODDARD FORMATION, SPRINGER GROUP, IN THE
ANADARKO BASIN OF OKLAHOMA

A THESIS APPROVED FOR THE
CONOCOPHILLIPS SCHOOL OF GEOLOGY AND GEOPHYSICS

BY

_____

Dr. R. Paul Philp, Chair

_____

Dr. Michael Engel

_____

Dr. R. Douglas Elmore

Acknowledgments

As meaningful accomplishments are rarely achieved without the help of others, I'd like to thank all those who supported and guided me over the past two years.

In particular, I'd like to recognize my adviser, Dr. Paul Philp. I'm grateful for both your guidance and patience these past two years. Thank you for supporting this project from its infancy to its fruition.

I would also like to thank my committee members, Dr. Mike Engel and Dr. Doug Elmore for their instruction, feedback, and time. I'd also like to thank Dr. Roger Slatt for his input and assistance in acquiring samples for this project.

Many thanks are owed to those who gave me the skills and knowledge to fully realize this project. I am indebted to Dr. Thanh Nguyen for his instruction, patience, and time in the lab. My thanks also go to Dr. Lara Heister for sharing her experience and insights into the field of geochemistry.

I'd like to express my gratitude to all the individuals in the Organic Geochemistry Group. Thank you for the thoughtful conversations, laughs, and companionship during long hours in the lab.

I'd also like to extend my appreciation to the faculty and staff of the ConocoPhillips School of Geology and Geophysics. Thank you for your support, instruction, and timely deadline reminders.

My thanks also go to the Oklahoma Geological Survey, with particular thanks to Dr. Brian Cardott for assisting with sample analysis.

This project would not have been possible without the generous donations of sam-

ples and data from the following companies: ConocoPhillips, Echo Energy, Newfield Exploration Company, and Vitruvian Exploration II. I would also like to thank GeoMark Petroleum Services Ltd. and IFP Energies nouvelles for donating their services and and ZetaWare Inc. for donating the use of their software.

Finally, I'd like to thank my parents and family, my first and foremost advisers, for their unwavering support.

Table of Contents

List of Tables

List of Figures

Abstract

The Goddard Formation is the basal unit of the Late Mississippian-Early Pennsylvanian Springer Group of Oklahoma. This Formation is part of a stacked oil and condensate play in the South Central Oklahoma Oil Province (SCOOP). Unconventional production of the Goddard has been ongoing since 2012. However, published geochemical interpretations for this formation are still few. This study characterized regional trends in the organic geochemistry of the Goddard Formation within the Anadarko Basin. Bulk geochemical and biomarker analyses were used to develop an organofacies model for the Goddard. Bulk geochemical and biomarker data were also used to conduct source rocks and oil correlations. Explanations for an unusual abundance of tricyclic terpanes in this Formation were also evaluated.

This study evaluated 15 source rocks and 11 oils from the Goddard in the Anadarko Basin. An outcrop sample and oil seep from the neighboring Ardmore Basin were also included in the sample set. Analyses were conducted using Rock-Eval pyrolysis, whole oil-gas chromatography, gas chromatography (GC), gas chromatography-mass spectrometry (GCMS), and gas chromatography-mass spectrometry-mass spectrometry (GCMSMS) methods.

Geochemical data collected in this study classified the Goddard Formation as a Type B organofacies. This organofacies type reflects a marine depositional environment dominated by siliciclastic sedimentation. Biomarker analyses indicated that the depositional environment for the Goddard was suboxic with normal to slightly elevated salinity and a non-stratified water column. The presence of fusinite and benzo(e)pyrene supported

a periodic but minor contribution of oxidized terrestrial plant matter following wildfire events. Comparison of the biomarker signature for both the source rock and oils revealed a striking similarity. The most useful biomarker family for correlation of Goddard source rocks and oils was the tricyclic terpanes.

Tricyclic terpanes dominated the *m/z* 191 chromatogram for both Goddard oils and extracts. Neither thermal stress nor biodegradation were able to account for the abundance of tricyclic terpanes. Fractionation mechanisms were also inconsistent with the geochemical similarity between the oils and extracts. Finally, the abundance of algae-like *Tasmanite* fossils, a proposed precursor for tricyclic terpanes, was low in the Goddard. Interpretations in this study support a non-*Tasmanite* precursor for the tricyclic terpanes. A non-*Tasmanite* precursor may still have been a marine algae similar to *Tasmanite*. Glacial production of iron-rich loess and a major mass extinction during the Late Mississippian would have been conducive to blooms of low-diversity algal communities in setting such as the Anadarko Basin.

Future work in the Goddard could include studies of stable carbon isotopes to look for indicators of algal blooms and explore correlation with total organic carbon. Additional biomarker studies could focus on outcrops in the nearby Ardmore Basin to assess whether abundant tricyclic terpanes are only found in the Goddard Formation within the Anadarko Basin.

1. Introduction

1.1. The Goddard Formation

The Goddard Formation is a Chesterian mudstone found in both the Ardmore and Anadarko Basins of Oklahoma (Figure 1). This formation defines the base of the Mississippian-Pennsylvanian Springer Group (Figure 2). The first unconventional production from the Goddard began in 2012 in the South Central Oklahoma Oil Province (SCOOP) of the Anadarko Basin. Both oil and condensate are currently produced from the Goddard. Total organic carbon (TOC) in the Goddard is typically three to four percent and formation thickness varies from 60-120 feet (Eagle Rock Energy Partners, 2015). The Goddard Formation joins a long list of unconventional reservoirs in both Oklahoma and the United States as a whole (U.S. EIA, 2011; Jacobs et al., 2014).

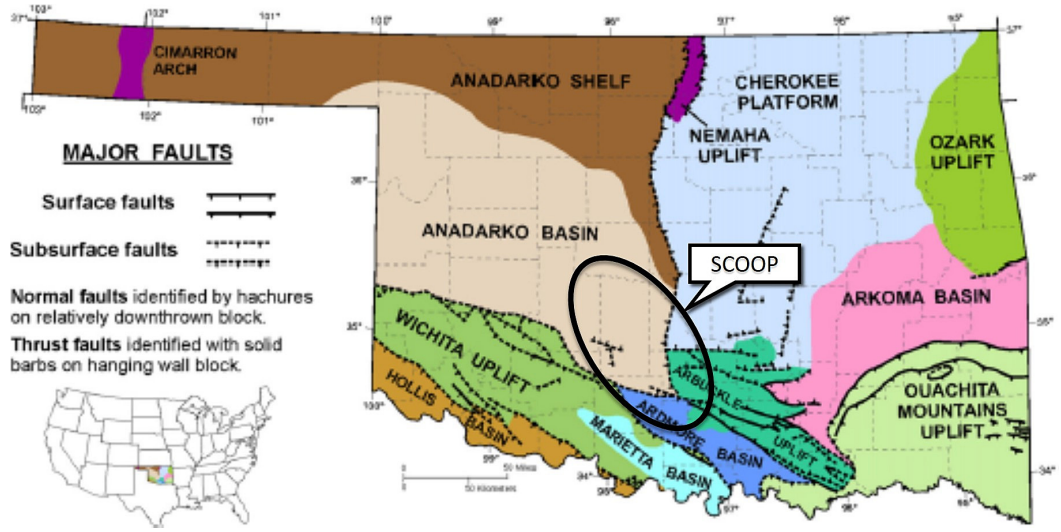

Figure 1: Present day geologic provinces of Oklahoma and South Central of Oklahoma Oil Province (SCOOP) (modified from Cardott, 2012b)

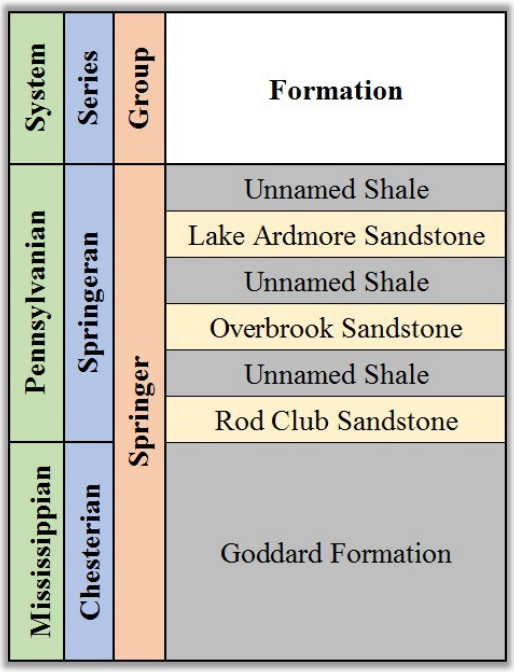

Figure 2: Simplified stratigraphic column for the Springer Group (after Cardott, 2012b; after Eagle Rock Energy Partners, 2015)

Prior to 2012, descriptions of the Goddard Formation in publicly available literature were cursory and typically overshadowed by the overlying sands in the Springer Group. This paucity of literature was due not only to historic naming discrepancies discussed in the following chapter, but also to the historic economic importance of the Springer Sands in Oklahoma. Before 2012, the Goddard Formation was only recognized as a potential source rock for the gas produced from Springer Group Sands. Even now that the Goddard Formation has been recognized as an unconventional resource in its own right, the Goddard is still often referred to as the Springer Shale (Nash, 2014; Bates, 2015).

The Springer Group's reputation as a conventional reservoir in Oklahoma was established in the mid 1900s (Reedy and Sykes, 1959; Peace, 1965). Gas production from Springer reservoirs began as early as 1925 in areas such as the Carter-Knox and Sho-

Vel-Tum fields (Reedy and Sykes, 1959; Peace, 1965; Andrews, 2008). Gas production was greatest during the 1960s until the mid-1980s when rates peaked (Andrews, 2008). Since 1992, gas production from Springer Sands has held steady around 200 billion cubic feet (Bcf) per year (Andrews, 2008). In 2005, the Oklahoma Geological Survey (OGS) reported that Springer reservoirs, combined with the Morrow, accounted for 28 percent of gas production for Oklahoma (Boyd, 2008). In comparison, oil production from Springer sand reservoirs has been in a steady decline. As of 2004, oil production from Springer sands had fallen below five million barrels a year (Andrews, 2008).

At present, the economic importance of the Goddard relative to the Springer Sands is more balanced. Production data for horizontal, hydraulically-fractured Goddard wells indicates several favorable characteristics: slow decline from initial production; a high siliciclastic content that promotes formation brittleness; and minimal produced water (Stratas Advisors, 2014; Davis et al., 2015). These characteristics contribute to a lower cost for unconventional production relative to similar domestic plays (Stratas Advisors, 2014; Bates, 2015). Well tests performed in 2014 estimated that the expected ultimate recovery for a 4,500 ft. horizontal well in the Springer would average 940 thousand barrels of oil equivalent (Mboe) (Nash, 2014; Oil and Gas Investor This Week, 2015a). A single Goddard well completed in 2015 reported a daily production of over 1300 barrels (bbl) oil and 456 million cubic feet (Mcf) gas (Oil and Gas Investor This Week, 2015b). In 2014, the breakeven estimate for unconventional production in the Goddard Formation was approximately 43 USD (Bates, 2015; Stratas Advisors, 2015). These characteristics may allow the Goddard Formation to remain economically resilient during the current bear market for the oil and gas industry (Bates, 2015; Oil and Gas Investor This Week,

2015a; Oil and Gas Investor This Week, 2015b; Stratas Advisors, 2015).

1.2. Purpose and Objectives

While the amount of production data for the Goddard are increasing, geochemical interpretations for this formation are still sparse in publicly available literature (Jones and Philp, 1990; Kim and Philp, 2001; Wang and Philp, 2001; Continental Resources, 2014). This scarcity is unfortunate, because geochemical data can add tremendous value to production and exploration strategy for new petroleum systems (Magoon and Dow, 1994; Moldowan et al., 1985; Peters and Cassa, 1994). Additionally, geochemical analysis of the Goddard would improve understanding of paleo -depositional, -climatic, and -biologic conditions for the Anadarko Basin during the Late Mississippian-Early Pennsylvanian transition. This boundary marks a critical period that is underrepresented in the geologic record of Oklahoma. Unconventional resources in general are also still a recent type of play; a thorough geochemical evaluation of all such plays should be done whenever feasible.

The objective of this study is to characterize regional trends in the organic geochemistry of the Goddard Formation within the Anadarko Basin of Oklahoma. Interpretations are based on biomarkers and select bulk geochemical data from both source-rocks and oils. From these interpretations, a preliminary organofacies model is developed. This organofacies model can be used to guide future exploration, production, and development in the Goddard play. An additional objective of this study focuses on a specific family of biomarkers: the tricyclic terpanes. These biomarkers are present in unusually high abun-

dances in the Goddard Formation. Possible mechanisms for enrichment will be evaluated using additional biomarkers and the organofacies model developed for the Goddard.

1.3. Organofacies

The approach taken to characterize source rocks in this study is primarily based on the organofacies model developed by Pepper and Corvi (1995). Pepper and Corvi (1995) defined an organofacies as "a collection of kerogens derived from common organic precursors, deposited under similar environmental conditions, and exposed to similar early diagenetic histories" (Figure 3). Organofacies interpretations are also compared to kerogen types defined by the more commonly used Pseudo-van Krevelen (PVK) model. The PVK model is often used to screen source rocks because of the simple dataset needed for classification; more extensive interpretation using the PVK model is limited for the same reason. Justifications for using organofacies as the primary method of source rock characterization are discussed in the following sections.

1.3.1. Thermal Stress

Characterization methods such as the PVK diagram define source rock kerogen using parameters that are sensitive to thermal stress (Peters and Cassa, 1994; Dembicki, 2009). With increasing thermal maturity, kerogen generates hydrocarbons and becomes depleted in both hydrogen and carbon (Peters and Cassa, 1994). This depletion can cause different kerogen types to converge on the diagram (Figure 4a). Mixing of kerogen types can cause shifting into inaccurate zones on the PVK diagram (Figure 4b). When these

Organofacies	Description	Principal Biomass	Environmental Association	Age Association	Kerogen Type Equivalent
A	Aquatic, marine, siliceous or carbonate/evaporite	Marine algae, bacteria	Marine, upwelling zones, clastic-starved basins	Any Age	Type IIS
B	Aquatic, marine, siliciclastic	Marine algae, bacteria	Marine, clastic basins	Any Age	Type II
C	Aquatic, non-marine, lacustrine	Freshwater algae, bacteria	"Tectonic" non-marine basins, minor on coastal plains	Phanerozoic	Type I
D	Terrigenous, non-marine, waxy	Higher plant cuticle, resin, lignin, bacteria	Ever-wet coastal plains	Mesozoic and younger	Type III
E		Higher plant cuticle, lignin, bacteria			
F	Terrigenous, non-marine, wax-poor	Lignin	Coastal plains	Late Paleozoic and younger	Type III/IV

Figure 3: Characteristics of organofacies (after Pepper and Corvi, 1995)

limitations are either avoided or minimized, methods like the PVK diagram may be useful for screening. However, at high thermal maturities these pitfalls are unavoidable and the PVK model cannot be used to meaningfully interpret depositional conditions and kerogen types (Pepper and Corvi, 1995). Organofacies models require more information to create but provide more meaningful and comprehensive interpretations regardless of subsequent thermal alteration.

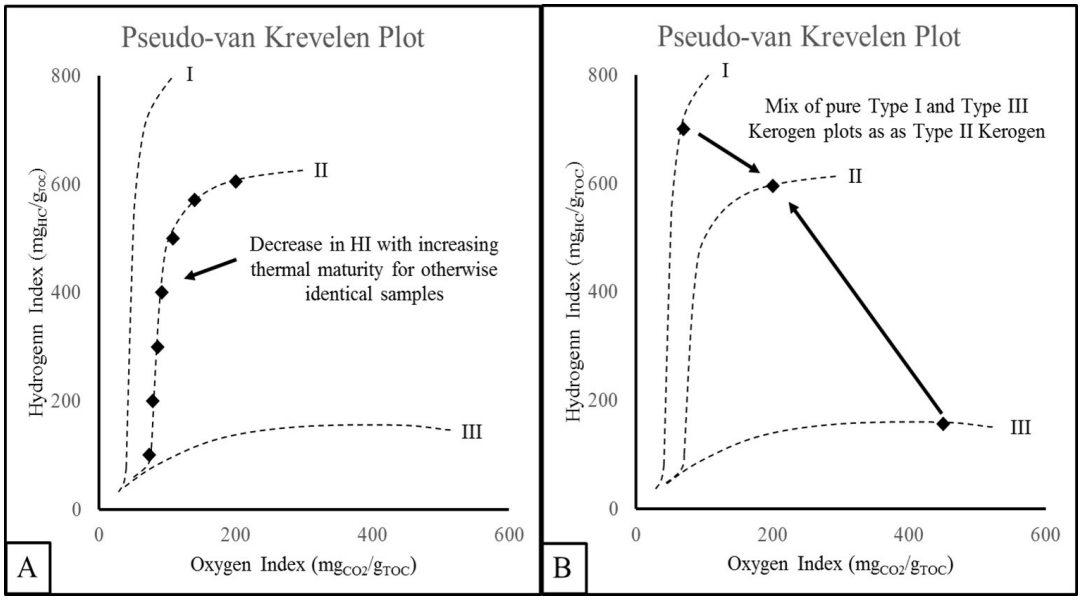

Figure 4: Pitfalls of the Pseudo-van Krevelen diagram for characterizing kerogen type at (a) high thermal maturities and in (b) cases of kerogen mixing (after Dembicki, 2009)

1.3.2. Biomarker Integration

The comprehensive nature of organofacies was also considered compatible with the biomarker-focused approach taken in this study. Biomarkers are molecular fossils that can be associated with precursor compounds from once-living organisms (Treibs, 1936; Tissot and Welte, 1984). The origins and applications of biomarkers are diverse, but

altogether, these chemical fossils can be used to infer the age, thermal history, extent of alteration, and depositional conditions for source rocks and their expelled hydrocarbons (Shanmugam, 1985; Aquino Neto, 1986; McCaffrey et al., 1996; Farrimond, 1999). Organofacies, by definition, integrate all four of these components (Pepper and Corvi, 1995). Biomarkers are also inherently linked to biology. Organofacies are well suited to integrating variables that influence life, such as climate, into a meaningful source rock characterization. By comparison, models such as the PVK Diagram are limited to characterizing kerogen types and this strategy can often be lead to simplistic interpretations of source rocks (Dembicki, 2009).

1.3.3. Exploration and Production Strategy

Organofacies directly apply to exploration and production strategy. Whereas the definition of organofacies has expanded, the original relationship between organofacies and petroleum generation profiles is still applicable (Pepper and Corvi, 1995; di Primio and Horsfield, 2006). For example, Type A or B organofacies would begin generating oil at 95-105°C whereas a Type D or E organofacies would only begin generating oil around 120°C or higher (Pepper and Corvi, 1995; Figure 5). Organofacies also correlate to the type and volume of hydrocarbons generated by a source rock (di Primio and Horsfield, 2006). A Type C organofacies would be more prone to generating oil whereas a Type D organofacies would have a higher gas to oil ratio from the onset of hydrocarbon generation (Pepper and Corvi, 1995).

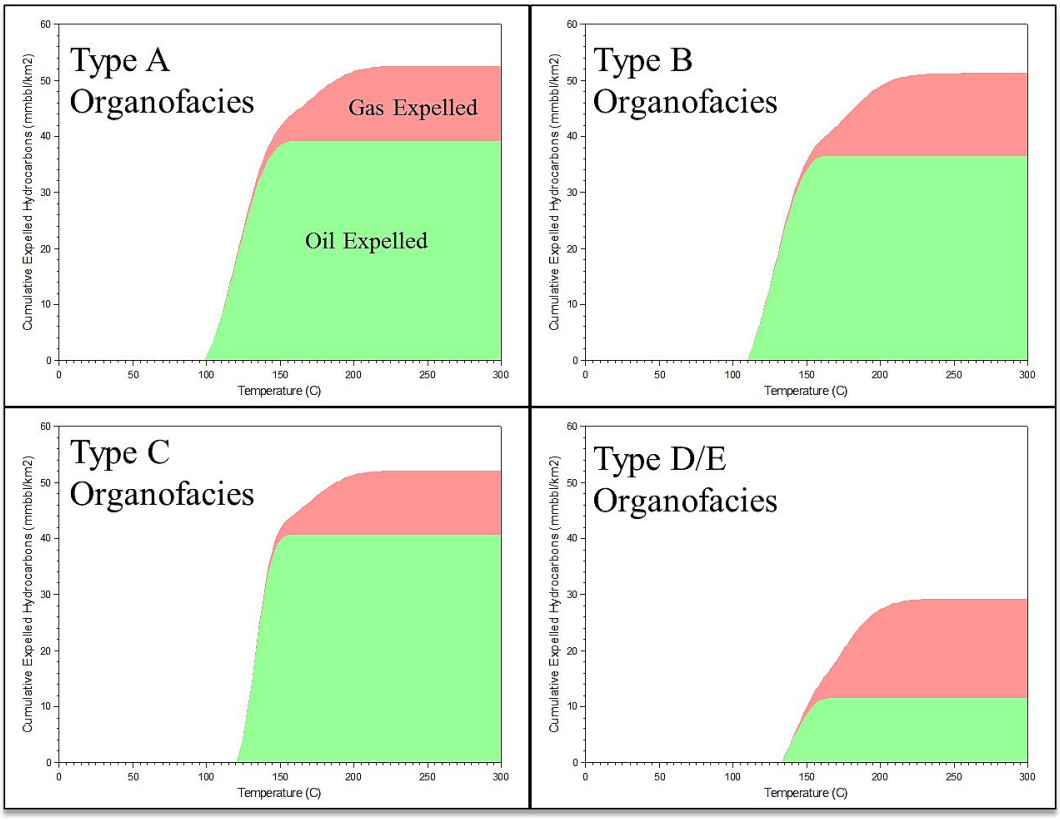

Figure 5: Organofacies generation profiles in MMbbl per square kilometer of source rock (from ZetaWare Inc., 2015)

1.4. Tricyclic Terpanes in the Goddard

The Goddard has a geochemical fingerprint distinct from all other source rocks in the Anadarko Basin. The most diagnostic biomarkers of Goddard-sourced hydrocarbons are the tricyclic terpanes. Tricyclic terpanes are ubiquitous at low levels in almost all oils and source rocks (Chicarelli et al., 1988; Philp et al., 1989; Azevedo et al., 1992; de Grande et al., 1993; Tao et al., 2015). In the Goddard, however, these compounds are present at concentrations so high they obscure the hopanes on the *m/z* 191 chromatogram. Globally, such an abundance of tricyclic relative to pentacyclic terpanes is only seen in a handful of oil families and source rocks (Aquino Neto et al., 1986; Figure 6).

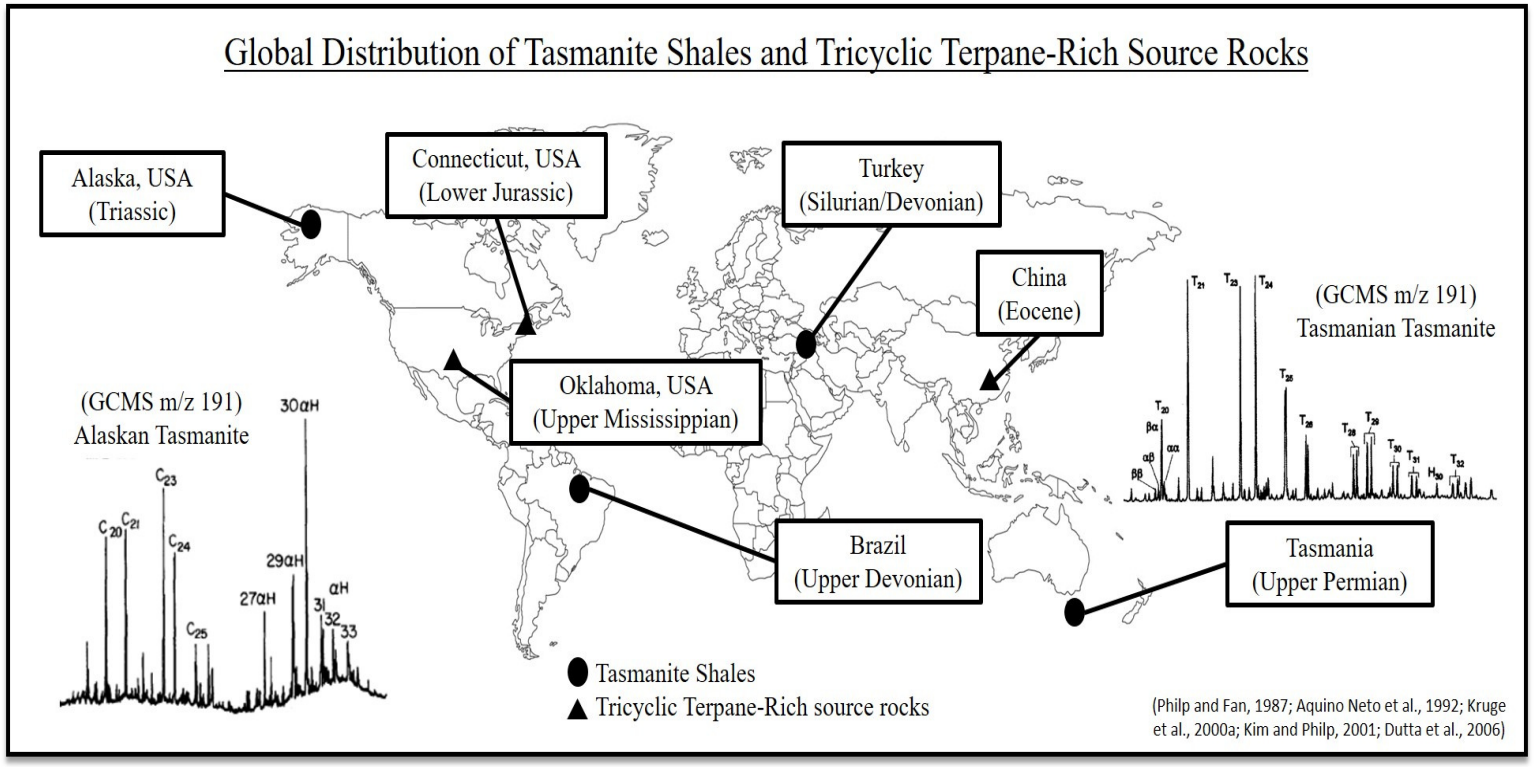

Figure 6: Global distribution of *Tasmanite* shales and tricyclic terpane-rich source rocks

1.4.1. Debated Origins

Tricyclic terpanes, also known as cheilanthanes, are present in almost all known source rocks and oils (Chicarelli et al., 1988; Philp et al., 1989; Azevedo et al., 1992; de Grande et al., 1993; Tao et al., 2015). The lower homolog tricyclic terpanes were first recognized in 1971 in the bitumen and oils of the Green River Shale (Anders and Robinson, 1971; Gallegos, 1971). By definition, lower homolog tricyclic terpanes extend from C_{19}-C_{24} (Aquino Neto et al., 1982). Extended tricyclic terpanes are defined as those C_{25} and greater (Peters, 2000). de Grande et al. (1993) identified tricyclic terpanes extending out to C_{54} and it's likely the series extends even further.

There is still uncertainty regarding precursors for both the lower and extended tricyclic terpanes. Identification of a specific precursor would add greater understanding to organofacies interpretations based on the tricyclic terpanes. Some early work suggested that tricyclic terpanes were derivatives or degradation products of other biomarkers. One hypothesis proposed that lower tricyclic terpanes were derived from the degradation of pentacyclic terpanes (Anders and Robinson, 1971). Subsequent analyses of natural and synthesized tricyclic terpanes were unable to show a direct relationship between pentacyclic terpanes and the lower tricyclic terpanes (Aquino Neto et al., 1982). Other structural differences between the tricyclic and pentacyclic terpanes, such as side chain attachment points, support that tricyclic terpanes are not derived from the hopanes (Philp et al., 1992). Additional research has explored biomarker precursors such as ketones and alkanes but with little success (Azevedo et al., 2001). Some studies have focused specifically on the extended tricyclics and have suggested that these extended compounds

are also produced through degradation of existing biomarkers. (Moldowan et al., 1983). Observations of both *in-situ* and synthesized extended tricyclic terpanes also suggest that extended tricyclic terpanes have different origins than the lower tricyclic terpane homologs (Moldowan et al., 1983). For example, proposed precursors for the extended tricyclic terpanes included the polyprenols (Heissler et al., 1984). Degradation pathways are still uncertain, but the overall importance of biomarker degradation as a source of tricyclic terpanes is probably minimal.

The search for a direct biologic precursor has met with mixed success. Various studies have demonstrated that land plants (Simoneit et al., 1993) and bacteria (Aquino Neto et al., 1982) are unlikely precursors. There is strong support, however, for at least one algae-like organism as a direct precursor for tricyclic terpanes (Simoneit et al., 1990; Guy-Ohlson and Boalch, 1992). This organism, the now-extinct *Tasmanites*, is thought to have been similar to a modern, marine unicellular green algae of the genus Pachysphaera (Simoneit et al., 1990; Boalch and Guy-Ohlson, 1992; Guy-Ohlson and Boalch, 1992).

Product-precursor studies have focused on source-rocks where *Tasmanite* fossils make up the majority of the organic matter (Figure 7). One of the most well-known of these so-called *Tasmanite* shales is a Permian age source rock in Tasmania (Simoneit et al., 1990; Aquino Neto et al., 1992; Azevedo et al., 1992). Simoneit et al. (1990) described a Tasmanian *Tasmanite* sample with 29 percent total organic carbon that was dominated by the *Tasmanite* fossil. Another study by Azevedo et al. (1992) looked at a similar Tasmanian sample where the *Tasmanite* fossil contributed 80 percent of the total organic carbon. Both of these groups extracted the *Tasmanite* rocks and recorded “major amounts” (Simoneit et al., 1990) of tricyclic terpane compounds (Simoneit et al., 1990;

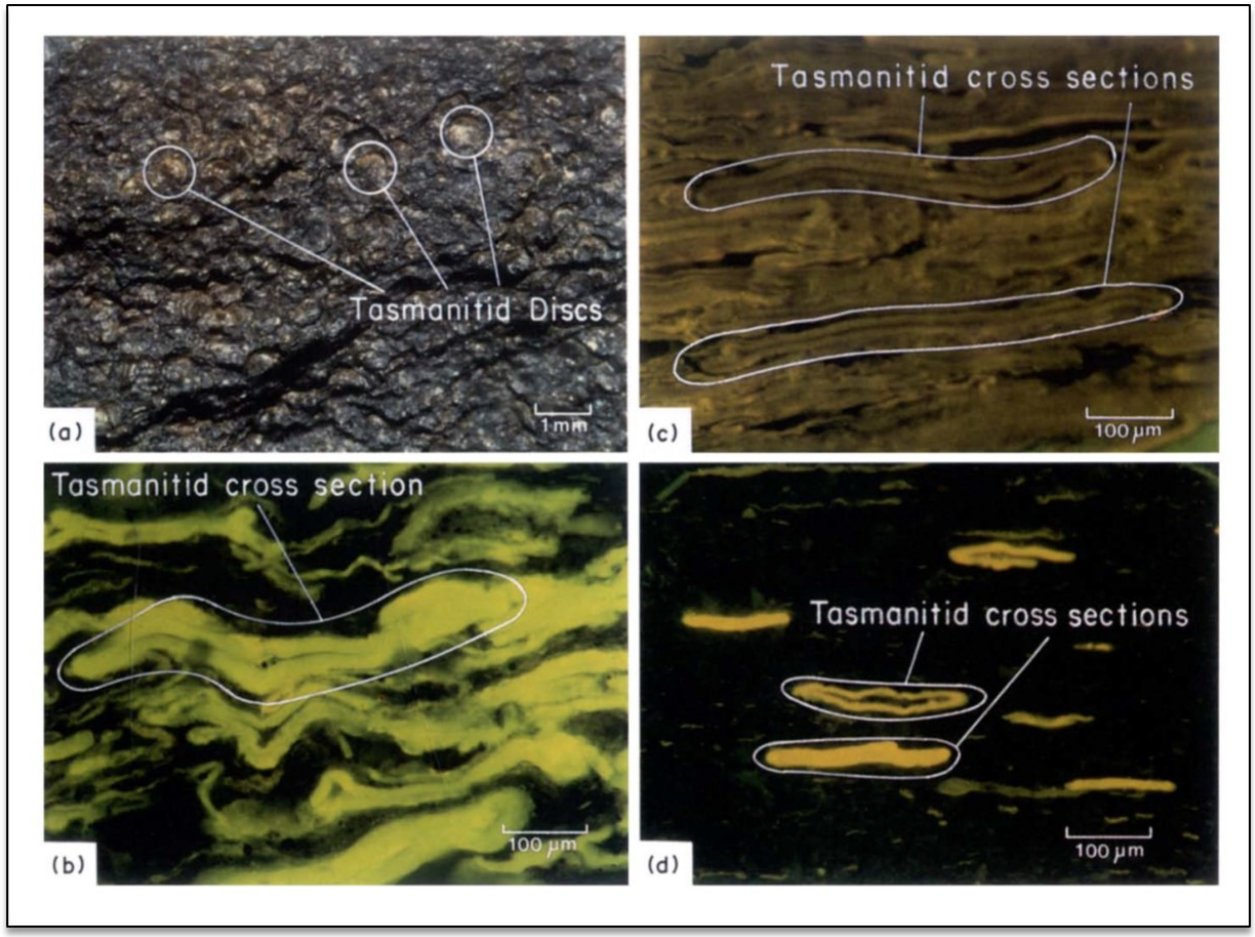

Figure 7: *Tasmanite* fossils in various *Tasmanite* shales: (a) Tasmanian *Tasmanite*; (b) Tasmanian *Tasmanite*; (c) Alaskan *Tasmanite*; (d) Brazilian *Tasmanite* (from Aquino Neto et al., 1992)

Azevedo et al., 1992). The *Tasmanites* studied by Azevedo et al. (1992) were thermally immature (Vitrinite reflectance, or %Ro, of 0.3-0.4) which supports that hypothesis that tricyclic terpanes are derived from *in-situ* biologic precursors and not thermally degraded biomarker precursors.

Other *Tasmanite* shales have been extracted and analyzed with similar results. Work done by Aquino Neto et al. (1992) used Devonian *Tasmanites* from Brazil, Triassic *Tasmanites* from Alaska, and the classic Permian *Tasmanite* from Tasmania. All three samples were either immature or in the early oil window (Aquino Neto et al., 1992). In each of the extracts, tricyclic terpanes were detected in equal or greater abundance relative to the hopanes (Aquino Neto et al., 1992). More recent work has used laser micropyrolysis gas-chromatography mass-spectrometry to analyze individual *Tasmanites* fossils rather than bulk rock extracts (Greenwood et al., 2000). The pyrolysates from these studies contained high abundances of tricyclic terpanes and no bacterial hopane compounds (Greenwood et al., 2000). The only *Tasmanite* shale that has not demonstrated a product-precursor link between the *Tasmanites* fossil and abundant tricyclic terpanes is a Silurian-Devonian *Tasmanite* from Turkey (Dutta et al., 2006). Dutta et al. (2006) analyzed fossils of *Tasmanites* as well as a closely-related algae genus in this sample using Curie point pyrolysis-gas chromatography-mass spectrometry; tricyclic terpanes were not found in the pyrolysates from the *Tasmanite* fossils but were present in pyrolysates for other, closely-related algae genera (Dutta et al., 2006). This work demonstrates that the relationship between *Tasmanites* and tricyclic terpanes is not absolute and supports the existence of other, albeit less common, precursors (Dutta et al., 2006).

Stable isotope analyses also support the product-precursor link between *Tasmanites*

and tricyclic terpanes. For example, a study by Simoneit et al. (1993) looked at extracts from Tasmanian *Tasmanites*. Simoneit observed that the δ^{13}C of the bulk kerogen was enriched (-16.6‰) compared to other Permian marine organic matter (δ^{13}C = -25‰ to -30‰) (Simoneit et al., 1993). Compound-specific isotope analysis showed that tricyclic compounds were further enriched by approximately 10‰ when compared to the normal alkanes and isoprenoids in the extract (Simoneit et al., 1993). The δ^{13}C values for the alkanes and isoprenoids were -18‰ to -24‰ (Simoneit et al., 1993). Simoneit et al. (1993) proposed that this unique enrichment was the result of either unusual environmental conditions related the *Tasmanite*-rich source rocks or unusual biologic fractionation specific to the *Tasmanite* algae. The same enrichment of δ^{13}C values in tricyclic terpanes from Tasmanian *Tasmanite* has been observed in other *Tasmanite* shales (Simoneit et al., 2005).

Uncertainty regarding precursors for the tricyclic terpanes has not diminished their utility as biomarkers. Instead, the applications for the tricyclic terpanes are based on empirical observations.

1.4.2. Response to Alteration

Tricyclic terpanes have several applications as thermal maturity indictors for source rocks and oils. One maturity parameter is based on the isomerization of tricyclic terpanes. Beginning at C_{20}, the primary stereoisomer of the tricyclic terpanes has a 13β(H), 14α(H) configuration (Aquino Neto et al., 1986; Farrimond et al., 1999); in immature sediments, a 13α(H), 14α(H) isomer is also present (Aquino Neto et al., 1986). Other isomers,

including the 13β(H), 14β(H) and 13α(H), 14β(H) have been identified in low maturity sediments (Chicarelli et al., 1988). However, these latter isomers are thermally labile and begin to isomerize during the earliest stages of diagenesis (Chicarelli et al., 1988). Studies of immature sediments in the Espirito Santo Basin of Brazil showed that the 13α(H), 14α(H) isomer decreases with respect to the 13β(H), 14α(H) with depth in the sediment column (Aquino Neto et al., 1986). Aquino Neto et al. (1986) identified an equilibrium ratio of 0.9 which is reached around %Ro 0.5-0.6. By the late oil window, this equilibrium ratio for tricyclic terpanes C_{25}-C_{29} may achieve parity (Farrimond et al., 1999; Peters, 2000). Different organic matter input does not appear to influence isomerization rates, so this maturity parameter is applicable irrespective of kerogen type (Aquino Neto et al., 1986).

Tricyclic terpanes also have a greater resilience to thermal stress than do the hopanes (Zhusheng et al., 1988; Farrimond et al., 1999; Wenger et al., 2002). As an oil or source rock enters the late oil window, hopanes are degraded more quickly than the tricyclic terpanes (Farrimond et al., 1999). By the end of the late oil window, thermal stress only appears capable of bringing the hopane to tricyclic terpane ratio to parity (Zhusheng et al., 1988; Philp et al., 1992; Peters, 2000). Thermal stress sufficient to further degrade the hopanes relative to the tricyclic terpanes would also cause a noticeable alteration to the tricyclic terpanes, steranes, and normal alkanes (Zhusheng et al., 1988; Philp et al., 1992; Peters, 2000).

Ratios and absolute abundances of the lower tricyclic terpanes can also be used as thermal maturity proxies (Zhusheng et al., 1988; Tao et al., 2015). In immature samples, the absolute abundance of the C_{23} tricyclic terpane is greater than C_{21} and C_{20} homologs

(Zhusheng et al., 1988). This ratio often reverses by the late oil window (Zhusheng et al., 1988; Huang et al., 2015; Tao et al., 2015). Tricyclic terpanes from C_{23} to C_{26} are also influenced by depositional conditions (Zumberge et al., 2000), so they are best used as maturity parameters for samples with similar organofacies.

Because of their isoprenoid side chain, tricyclic terpanes are also more resistant to biodegradation than both the hopanes and steranes (Azevedo et al., 1992). During microbial degradation, steranes are destroyed at the same time that hopane and tricyclic terpanes compounds begin to experience demethylation (Alberdi et al., 2001; Wenger et al., 2002). The demethylation occurs at C_{10} for both families and produces 17-nor-tricyclic terpanes and 25-norhopanes (Alberdi et al., 2001). Demethylation of the hopanes begins before demethylation of the tricyclic terpanes (Alberdi et al., 2001). As such, the relative extent of demethylation for the tricyclic and pentacyclic terpanes can be used to compare the extent of biodegradation in different samples.

1.4.3. Organofacies and Exploration Applications

Another application of the tricyclic terpanes, particularly for this study, is organofacies interpretation. Most tricyclic terpane parameters used for inferring depositional conditions are based on the lower homologs. For example, the absence of tricyclic terpanes above C_{20} is well correlated with Type D and E terrigenous organofacies (Alberdi et al., 2001). Lower tricyclic terpane homologs are also less abundant in source rocks and fluids associated with freshwater or hypersaline depositional conditions. Tricyclic terpanes are more abundant in source rocks and oils associated with marine carbonate or saline lacus-

trine conditions (de Grande et al., 1993). As suggested by Mello (1988), this variation in abundance may be due to salinity levels; precursors for the tricyclic terpanes appear to favor conditions of normal to elevated salinity rather than hypersaline or freshwater conditions (de Grande et al., 1993). Indeed, Philp et al. (1989) observed tricyclic terpanes in equal abundance to hopanes in oils from a brackish depositional environment with salinity levels similar to typical marine environments. In the same study, oils generated from source-rocks deposited under inferred hypersaline conditions had much lower abundances of tricyclic terpanes (Philp et al., 1989).

Ratios of lower tricyclic terpane homologs can also be used to distinguish carbonate, lacustrine and marine organofacies. The C_{19} and C_{20} tricyclic terpanes are often abundant in oils associated with terrestrial or freshwater lacustrine depositional environments (Tao et al., 2015). The C_{21}, C_{22}, C_{23}, and C_{24} homologs are primarily used to differentiate source rocks and oils associated with marine carbonate and lacustrine organofacies (Zumberge et al., 2000). Source rocks deposited in saline, lacustrine environments often have C_{23} as the dominant tricyclic terpane homolog (Zumberge et al., 2000; Tao et al., 2015). The C_{25} and C_{26} homologs are useful for differentiating oils associated with lacustrine and marine organofacies (Zumberge et al., 2000). As mentioned above, thermal stress alters the relative abundance of the lower homologs, so lower tricyclic terpane parameters should only be compared among samples of similar thermal maturities (Farrimond et al., 1999).

1.4.4. Mechanisms for Enrichment

While almost ubiquitous in oils and source rocks, tricyclic terpanes are usually less abundant than the hopanes. There are only a handful of source rocks in which the tricyclic terpanes are present in equal or greater abundance than the hopanes; most of these source rocks are the so-called *Tasmanites* (Aquino Neto et al., 1992).

One proposed mechanism for tricyclic terpane enrichment assumes that the *Tasmanite* algae is the precursor for the tricyclic terpanes and that these algae experienced periodic blooms (Guy-Ohlson and Boalch, 1992; Kim and Philp, 2001). Such blooms would not only increase the amount of organic matter being deposited but would also ensure a homogeneous organic matter source. This mechanism was mentioned in several Tasmanian *Tasmanites* studies (Simoneit et al., 1993; Revill et al., 1994).

Kim and Philp (2001) invoked the algal bloom mechanism in a survey study of Mississippian source rocks from the Anadarko Basin. The survey study included several samples that were time-equivalent to the Goddard and displayed a similar abundant tricyclic terpane signal (Kim and Philp, 2001). The Mississippian sample in the study was listed and identified as Chester in age but could likely have been from a stratigraphic interval that today is considered part of the Goddard (Kim and Philp, 2001). This regional study is the only previous instance of a high-tricyclic terpane signal being observed in Oklahoma (Kim and Philp, 2001). Another study of tricyclic terpane-rich source rocks in the Hartford Basin of Connecticut mentions the algal bloom mechanism as well (Kruge et al., 1990b). In the East Berlin Formation of the Hartford Basin, an increase in tricyclic terpanes coincides with indicators of increased precipitation. Increased runoff may have

delivered additional nutrients and triggered blooms (Kruge et al., 1990b).

There are, however, some issues with the *Tasmanite* algae bloom model. Tricyclic terpane enrichment in *Tasmanite* fossil-poor formations has been seen in rock extracts from China as well intervals in the Hartford Basin mentioned above (Philp and Zhao-An, 1987; Kruge et al., 1990a; Kruge et al., 1990b). Conversely, formations within the Anadarko Basin such as the Woodford Shale are known to be rich in *Tasmanite* fossils yet they do not have an abundant tricyclic terpane signal (B. Cardott, Oklahoma Geological Survey, Personal Communication, March 16th, 2016).

One explanation for an apparent lack of precursor fossils could be an incomplete understanding of the *Tasmanite* fossil. If *Tasmanites* are indeed similar to the modern green-algae Pachysphaera, then they may have had a two-phase life cycle (Guy-Ohlson and Boalch, 1992). The commonly recognized morphology of the *Tasmanite* corresponds to the non-motile, spherical of the Pachysphaera (Guy-Ohlson and Boalch, 1992). If the *Tasmanite* has an additional motile-phase similar to the Pachysphaera algae, this phase may be going unrecognized in tricyclic terpane-rich rocks.

There are also discrepancies in δ^{13}C isotope values expected of an algal bloom model (Aquino Neto et al., 1992; Simoneit et al., 1993). Under bloom conditions, rapidly growing algae can cause a local drawdown of CO_2 (Coale et al., 1996). While photosynthesis kinetically favors ^{12}C bearing CO_2, an overall reduction in CO_2 would cause algae to discriminate less against ^{13}C bearing CO_2 (Simoneit et al, 1993). As a result, the δ^{13}C for organic matter would be enriched (Simoneit et al., 1993). However, some *Tasmanite* extracts from Brazil and Alaska are no more enriched in ^{13}C than contemporary *Tasmanite*-poor source rocks (Aquino Neto et al., 1992; Simoneit et al.,

1993). While there is strong evidence that the *Tasmanite* fossil is a precursor for the tricyclic terpanes, there is even more compelling evidence to suggest that there are additional, unknown precursors.

Abiotic mechanisms may also play a role in the enrichment of tricyclic terpanes. A straightforward mechanism for tricyclic terpane enrichment is thermal stress. As previously discussed, tricyclic terpanes are more resistant to thermal stress than the hopanes and steranes. Enrichment of tricyclic terpanes is partially attributed to thermal stress in oil and source rock studies of the Anadarko (Philp et al., 1992), Sichuan (Zhusheng et al., 1988), and Hartford Basins (Kruge et al., 1990a; Kruge et al., 1990b). However, additional biomarker parameters in those studies do not support severe thermal alteration (Zhusheng et al., 1988; Kruge et al., 1990a; Kruge et al., 1990b; Philp et al., 1992). In the Hartford Basin, source rocks dominated alternately by tricyclic and pentacyclic terpanes were observed within the same formation in strata of equal thermal maturity (Kruge et al., 1990a). Therefore, thermal stress may not even play a role in the enrichment of tricyclic terpanes in some cases.

Migration fractionation is another proposed mechanism for tricyclic terpane enrichment. Laboratory studies simulating hydrocarbon expulsion indicate that certain biomarkers elute and migrate at faster rates (Zhao-An and Philp, 1987). In column chromatography simulations, tricyclic terpanes eluted before the hopanes (Zhao-An and Philp, 1987; Zhusheng et al., 1988). Early, immature expulsions of oil could plausibly be enriched in tricyclic terpanes while later charges could have more typical distributions of hopanes and tricyclic terpanes. Migration could further enhance the abundance of tricyclic terpanes relative to hopanes (Zhao-An and Philp, 1987; Zhusheng et al., 1988; Kruge et al.,

1990a).

Unsurprisingly, *in-situ* observations of bitumen and oils indicates that migration fractionation mechanisms are more complex than simulations. Kruge et al. (1990b) observed that mature bitumen in the Hartford Basin were actually enriched in tricyclic terpanes compared to related oils and overlying, less mature source rocks (Kruge et al., 1990b). To explain this apparent contradiction, Kruge et al. (1990b) suggested that asphaltenes in bitumen could be retaining tricyclic terpanes and other maltene compounds. The occlusion (Ekweozor, 1984) of tricyclic terpanes within the matrix of resin and asphaltene fractions has been observed in several other simulations (Ekweozor, 1984; Jones et al., 1987; Zhao-An and Philp, 1987). Polar fractions may act as natural molecular sieves; rather than being expelled, early maltene fractions are trapped and protected in polar fractions (Kruge et al., 1990b). Ekweozor (1984) observed that chemically degraded asphaltenes from two different tar sands generated maltenes dominated by tricyclic terpanes rather than hopanes. A subtler enrichment of tricyclic terpanes was observed by Jones et al. (1987) after pyrolyzing a bitumen from Switzerland. While poorly understood, both fractionation and asphaltene occlusion appear to play a role in enriching the abundance of tricyclic terpanes in oils and source rocks.

2. Geologic Setting

The following chapter reviews the tectonic and paleoclimate conditions controlling the deposition of the Goddard Formation. The problematic history of Upper Mississippian stratigraphy in the Anadarko Basin is also discussed.

2.1. Tectonics of the Late Mississippian

Johnson et al. (1989) divided the Phanerozoic history of North America into three phases. The first phase spanned the Cambrian to the end of the Mississippian and was a time of quiescent deposition within the expansive Oklahoma Basin (Figure 8). The Oklahoma Basin was a broad, shallow marine embayment and was characterized primarily by carbonate deposition (Visher, 1989). The depocenter of the Oklahoma Basin was the Southern Oklahoma Aulocogen, a remnant from the rifting of Laurentia during the late Precambrian and early Cambrian (Hemish and Andrews, 2001). There were numerous proto-basins in addition to the Southern Oklahoma Aulocogen in the Oklahoma Basin (Johnson et al., 1989; Visher, 1989).

As the onset of the Ouachita Orogeny neared in the Late Mississippian, deposition of siliciclastic sediments in the form of mudstones and sandstones increased slowly into the Oklahoma Basin (Johnson et al., 1989). A major deposition of mudstone and sandstones occurred during the Chesterian series of the Late Mississippian and heralded the early stages of tectonic collision between Laurussia and Gondwana (Johnson et al., 1989). It was at this time that the siliciclastic sediments of the Goddard were deposited. Later units in the overlying Springer Group are even richer in coarse-grained siliciclastic sediments

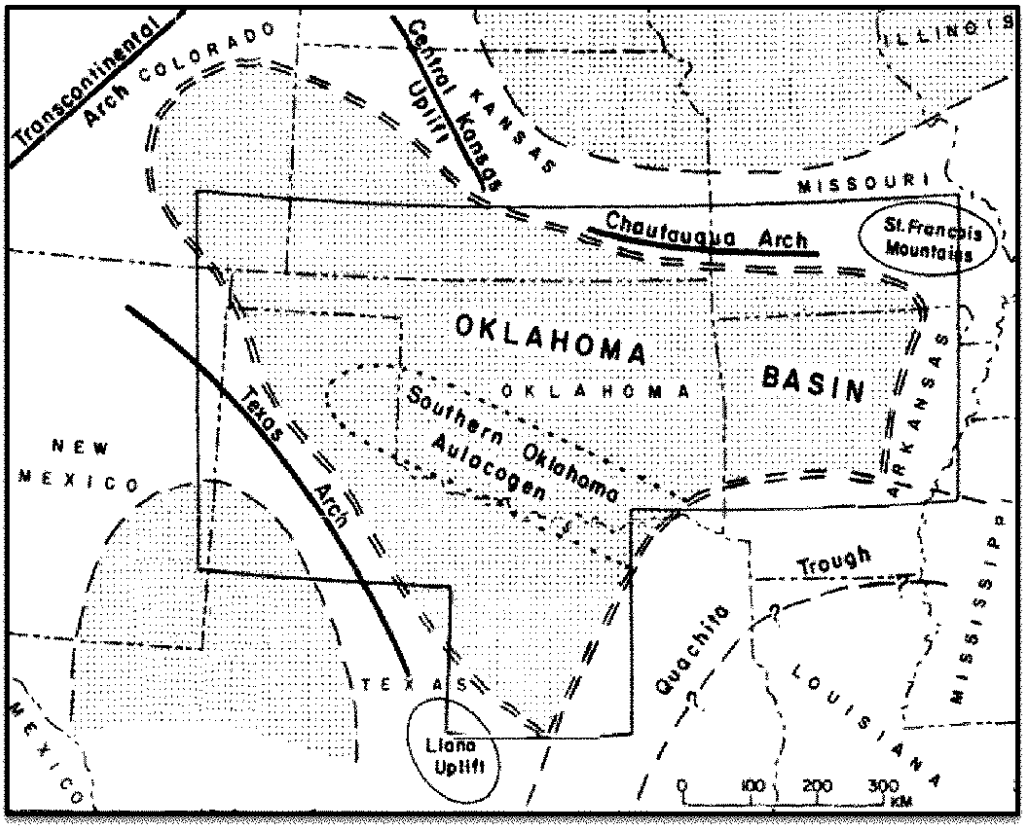

Figure 8: The Oklahoma Basin (modified from Johnson et al., 1989)

than the Goddard (Andrews, 2008). The Springer Group marked the true onset of the Ouachita Orogeny as well as the second phase of geologic history in the Phanerozoic Mid-Continent (Johnson et al., 1989; Visher, 1989).

While the first phase of Phanerozoic history was characterized by deposition, the second phase was a balance of disruptive tectonic activity, erosion, and deposition. The Ouachita Orogeny shaped and defined the various proto-basins within the expansive Oklahoma Basin (Visher, 1989). The Southern Oklahoma Aulocogen developed into the Anadarko Basin while the Ardmore Basin formed from one of the smaller proto-basins in the Oklahoma Basin (Visher, 1989). The Anadarko and Ardmore Basins are the only known locations where the Springer Group and its basal member, the Goddard Formation,

can be found today in the subsurface (Hemish and Andrews, 2001).

Major uplift and erosion across the Mississippian-Pennsylvanian boundary created a pre-Pennsylvanian unconformity across most of the North American midcontinent (Beckman and Sloss, 1965). The pre-Pennsylvanian unconformity is present above the Goddard in the Ardmore Basin as well as in the northern Anadarko Basin where the basin is relatively shallow (Wang and Philp, 2001). An exception to this unconformity is in the deep Anadarko Basin where the Goddard provides a continuous record of deposition across the Mississippian-Pennsylvanian boundary (Visher, 1989). Continued deposition during the Pennsylvanian and Permian contributed up to 18,000 and 7,000 feet of sediment, respectively, into the depocenter of the Anadarko Basin (Visher, 1989). These sediments were a mix of carbonate, evaporite, and clastic sediments (Visher, 1989).

Today, the Anadarko Basin is the deepest cratonic basin in the United States (Johnson et al., 1989). The asymmetrical Anadarko Basin is up to 40,000 feet thick along the southern margin and thins to several thousand feet towards the northwest (Johnson et al., 1989; Figure 9). The southern boundary of the Basin is defined by the Wichita and Amarillo Uplifts while the Nemaha Uplift serves as an eastern boundary (Visher, 1989). The Cimarron Arch outlines the western extent of the Basin (Visher, 1989). To the north, the Anadarko Basin shallows and transitions into a broad shelf referred to as the Hugoton Embayment (Visher, 1989).

The Goddard is present only in the deepest areas of the Anadarko Basin, and is produced as an unconventional resource in Grady, Stephens, and Garvin County in Oklahoma. Within the Anadarko Basin, the Goddard is present as a siliceous mudstone with occasional zones of expandable clays such as illite and smectite (Wang and Philp,

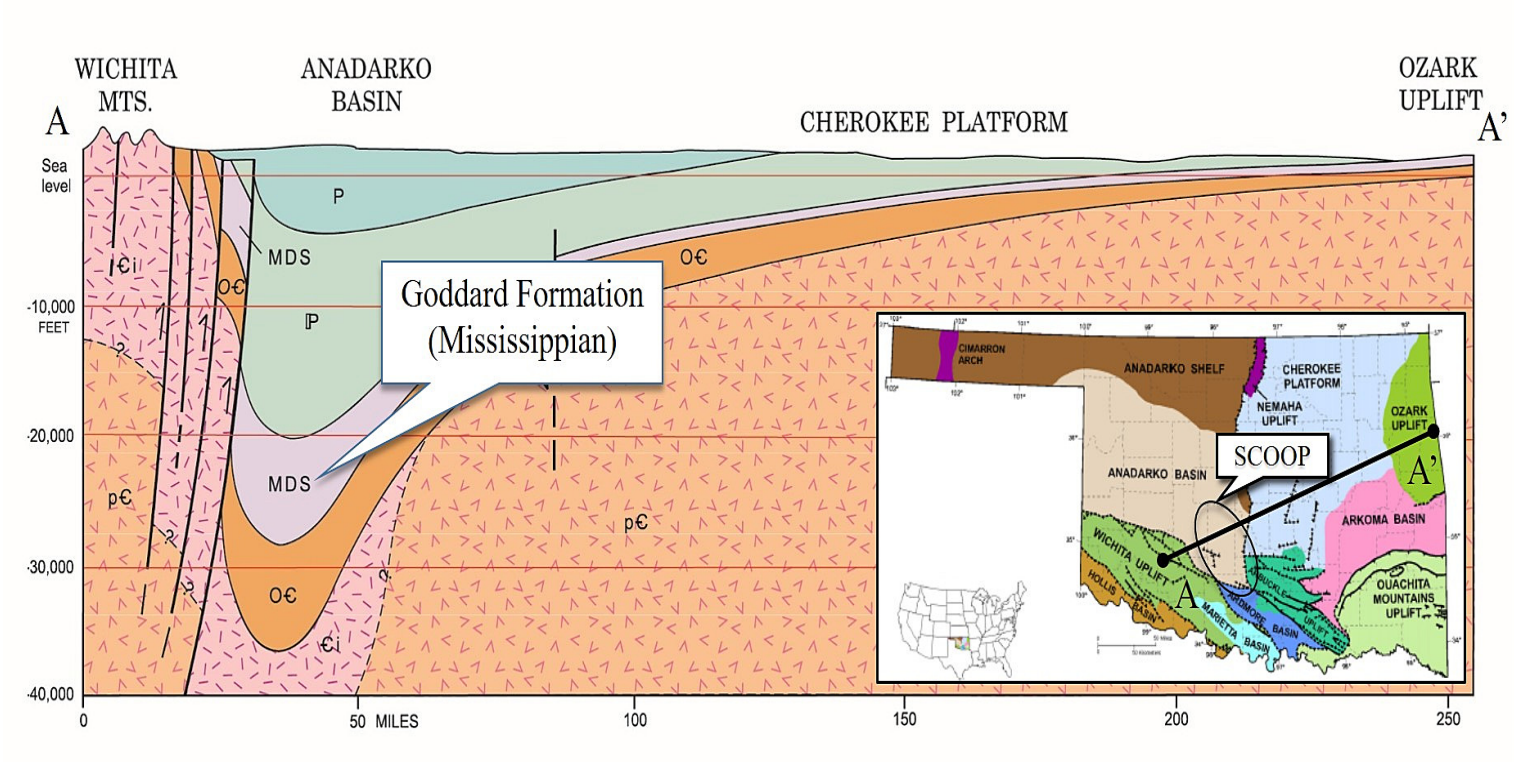

Figure 9: Cross section of the Anadarko Basin (modified from Johnson et al., 2008; modified from Cardott, 2012a)

2001; Ardmore Geological Society, 2015). Zones targeted as unconventional resources have TOC between three to four weight percent (Eagle Rock Energy Partners, 2015). The thickness of the Goddard varies from a few hundred feet thick to 2000 feet thick (Ramon et al., 1997; Hemish and Andrews, 2001). At present, there are only informally recognized zones within the Goddard Shale. Geochemical studies by Wang and Philp (2001) support an open marine depositional environment for the Goddard within the Anadarko Basin.

The Ardmore basin is southeast of the Anadarko Basin and trends along a similar northwest-southeast axis. A major fault with several thousand feet of displacement separates the Anadarko and Ardmore Basins (Hemish and Andrews, 2001). The Ardmore Basin is bounded by the Criner Hills to the southwest and the Arbuckle Mountains to the North. To the southeast, the basin is gradually buried by Cretaceous sediments rather than being defined by a structural boundary (Hemish and Andrews, 2001).

The Goddard is present in both the surface and subsurface of the Ardmore Basin. Hemish and Andrews (2001) described the Goddard in the Ardmore Basin as a fissile, non-calcareous, grey shale with intermittent sandstones. Occasional calcareous zones have also been identified in the Goddard (Peace, 1965). As in the Anadarko Basin, the thickness of the Goddard ranges from 2,500 feet in some areas to zero where it has been eroded away (Hemish and Andrews, 2001). The Goddard in the Ardmore Basin is also considered to have been deposited under normal marine conditions (Hemish and Andrews, 2001).

2.2. Paleoclimate of the Late Mississippian

The Late Mississippian Ouachita Orogeny was a result of Laurussia and Gondwana colliding to form the supercontinent of Pangaea (Rascoe and Adler, 1983; Perry, 1989). This event was concurrent with several changes in global paleoclimate, most notably the Late Paleozoic Ice Age (LPIA) and the larger shift from a global greenhouse to an icehouse state (Shi and Waterhouse, 2010). The complexity surrounding the formation of Pangaea and the onset of the LPIA (Crowell, 1978; Smith and Read, 2000; Soreghan et al., 2008; López-Gamundí et al., 2010) is beyond the scope of the study. Nonetheless, a few observations can be made regarding the effect of Pangaea's formation and the LPIA on the local paleoclimate of the Oklahoma Basin during the Late Mississippian.

One major development during the Mississippian-Pennsylvanian transition was the closing of the Rheic Seaway as Gondwana approached and collided with the Laurussian landmass (Qiao and Shen, 2014; Figure 10). This change in global oceanic and atmospheric currents is considered a primary trigger for the LPIA and the glaciation of southern Gondwanan (Smith and Read, 2000). Closure of the subequatorial Rheic Seaway would also have disrupted biologic communication between the east and western edges of the forming supercontinent (Smith and Read, 2000). The onset of major glaciation coincided with the deposition of the Goddard during the Visean (Smith and Read, 2000). While glacial ice was likely not present in the equatorial depositional environment of the Goddard, glaciation still indirectly influenced conditions during the deposition of the Goddard.

With the onset of glaciation, eustatic sea level in the Oklahoma Basin began to

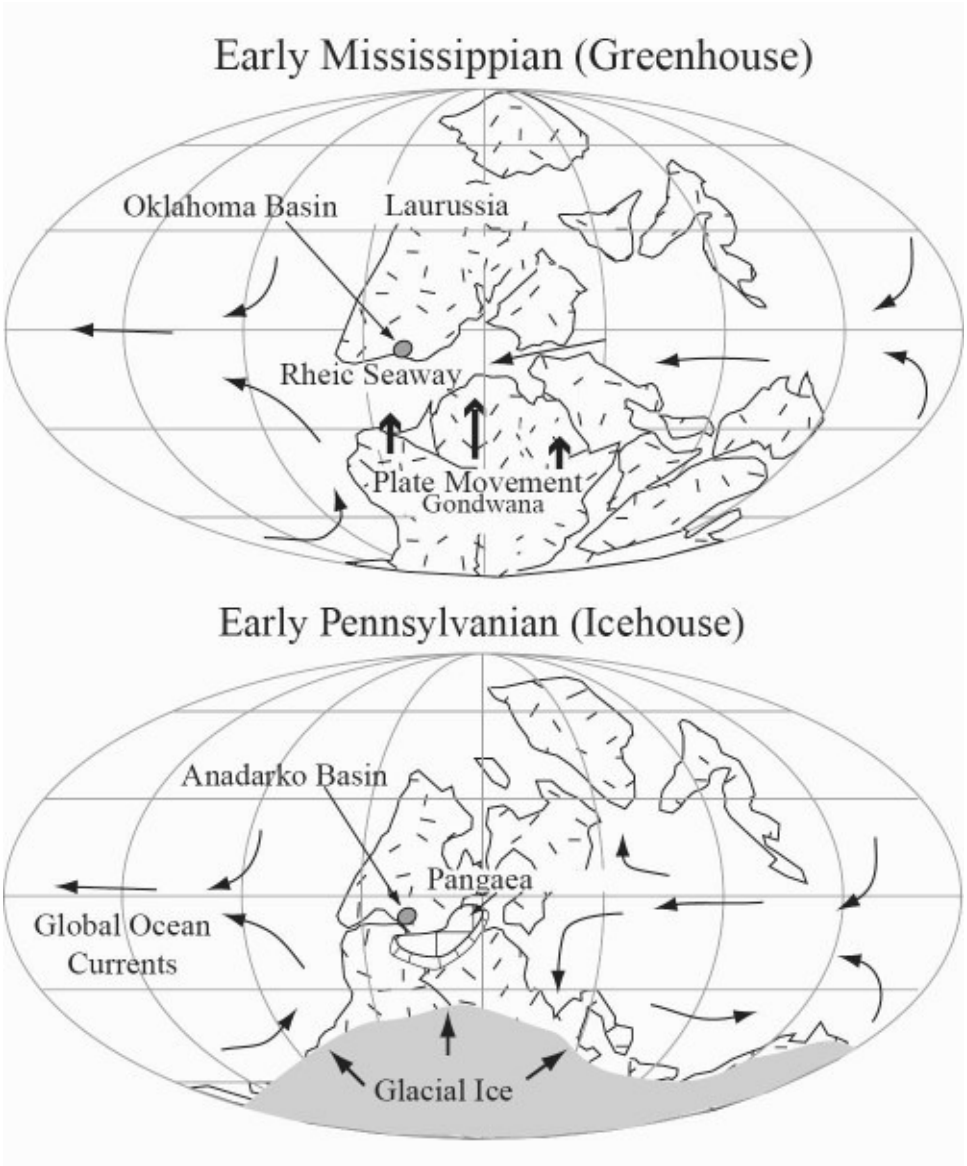

Figure 10: Closing of the Rheic Ocean (modified from Smith and Read, 2000)

regress at the end of the Late Mississippian (Rascoe and Adler, 1983). The clay-rich Goddard likely marks a high stand in sea level while the younger sand-rich units of rest of the Springer Group support a third-order regression in relative sea level (Hemish and Andrews, 2001). A more detailed description of sequence stratigraphy for the Goddard is discussed by Rush (2016). Goddard sediments are characteristic of an open marine environment dominated by mudstone with occasional pulses of sand from turbidites (Andrews, 2008) as eustatic sea level regressed. Geomorphological evidence for deltas and fluvial features is seen in the units of the Springer Group overlying the Goddard (Johnson et al., 1989).

Temperatures during the LPIA reached a global minimum which has not been surpassed in the past 600 million years (Shi and Waterhouse, 2010). As the greenhouse to icehouse transition progressed, pCO_2 levels dropped while oxygen levels rose (Shi and Waterhouse, 2010). The order of magnitude for the changes in these atmospheric gasses was large enough that this period of time is referred to as both the Late Paleozoic Carbon Dioxide Minimum and the Late Paleozoic Oxygen Pulse (Shi and Waterhouse, 2010).

Another change brought on by the LPIA was a global increase in loess (Smith and Read, 2000; Soreghan et al., 2008). The primary mechanism responsible for increased production of terrestrial eolian silt was glacial grinding (Soreghan et al., 2008). Other minor mechanisms for loess production, such as chemical weathering and fluvial processes, operate continuously throughout the geologic record but contribute minimal loess relative to glacial grinding (Soreghan et al., 2008).

Loess can increase biologic productivity by effectively seeding terrestrial and marine systems with bioavailable nutrients. A two-phase study demonstrated the response iron

seeding could produce in open ocean environments (Martin et al., 1994; Coale et al., 1996). In both studies, the addition of bioavailable iron triggered plankton blooms as well as local CO_2 drawdowns related to the increase in productivity (Coale et al., 1996). Continental dust is mentioned as a natural source for bioavailable iron (Coale et al., 1996). Increased loess production from early glaciation in the Late Mississippian could therefore have facilitated expansive, recurring plankton blooms in marine settings that would otherwise have been limited in iron.

2.3. Biology of the Late Mississippian

In addition to being a time of incipient tectonism and glaciation, the Late Mississippian was also a time of transition for the biosphere. A major mass extinction event during the Serpukhovian coincided with the forming of Pangaea and the onset of the LPIA (Powell, 2008). The Serpukhovian extinction event is outranked only by the classic Big Five (McGhee et al., 2013; Figure 11). During the Serpukhovian period, between 28 to 39 percent of marine genera are estimated to have gone extinct (Powell, 2008; McGhee et al., 2013). One characteristic that appears to have been a strong predictor for survival is latitudinal range. The preferential survival of species with larger latitudinal ranges has been observed in several regions and genera (Bonelli and Patzkowsky, 2008; Powell, 2008; Shi and Waterhouse, 2010; Qiao and Shen, 2014). An explanation for the improved survival of genera with greater range is that they were better adapted to the overall decrease in global temperature and increase in seasonality that occurred with the onset of the LPIA (Powell, 2008).

Major Phanerozoic Mass Extinctions*		
Rank		Extinction Event
Big Five	1	Changhsingian
	2	Rhaetian
	3	Hirnantian
	4	Famennian
	5	Maastrichtian, Frasnian
	6	Serpukhovian
	7	Givetian
	8	Eifelian
	9	Capitanian
	10	Ludfordian
*By Taxonomic Severity		

Figure 11: Major mass extinctions of the Phanerozoic ranked by taxonomic severity (from McGhee et al., 2013)

Another biologic response to the Serpukhovian Extinction was a decline in macro-evolution rates. Many studies focusing on the rate of origination and evolution during the Late Paleozoic focus on large, easily documented organisms such as brachiopods (Powell, 2008; Shi and Waterhouse, 2010; Qiao and Shen, 2014). In these studies, genera with wide latitudinal range tended to expand and displace species with warmer or narrower temperature ranges (Powell, 2008; Shi and Waterhouse, 2010; Qiao and Shen, 2014). Global diversity decreased as invasive, homogeneous communities increased their latitudinal extent (Shi and Waterhouse; 2010, Qiao and Shen, 2014). The rate of species origination remained low until the end of the LPIA (Powell, 2008; Shi and Waterhouse, 2010).

2.4. Defining the Goddard Formation

The Goddard Formation plays a geologically important role in Oklahoma; as the sole formation to conformably straddle the Mississippian-Pennsylvanian boundary in Oklahoma, the Goddard contains clues to a murky period in the state's geologic past. However, the stratigraphic definition of the Goddard has consistently fluctuated since the formation was first identified. The lack of consistency regarding the definition of the Goddard contributes to the difficulty of correlating and studying intervals of this formation (Hemish and Andrews, 2001).

The underlying Caney Shale and overlying Springer group were both recognized prior to the naming of the Goddard Formation (Westheimer, 1956). Taff defined the Caney Shale in 1901 (Westheimer, 1956). Taff also described the overlying unit as the Glenn, which included the modern Goddard, Springer, and additional overlying Pennsylvanian strata found in the Arbuckle mountains into a massive assemblage (Westheimer, 1956). The Springer was carved out of the basal Glenn Formation and officially named by Goldston in 1922 (Westheimer, 1956). While Goldston's Springer designation was generally accepted, the larger Glenn formation quickly fell out of use as it was criticized for being too expansive and including already named formations (Girty and Roundy, 1923; Westheimer, 1956).

Through the early 1900s, the Springer Group became fairly well delineated; the Rod Club Sandstone served as an easily identifiable boundary between the Springer and the shales below (Westheimer, 1956; Figure 2). Interest in the sandstone units of the Springer was also spurred by their role as conventional gas reservoirs in the Mid-Continent. There

are various names for each of the four main sandstone units of the Springer in both the surface and subsurface (Peace, 1965; Hemish and Andrews 2001). As noted by Hemish and Andrews (2001), the correlation between subsurface and surface names for the Springer sands is poor. Correlation of the shales within the Springer Group is even more challenging as the shales lack formal names and are typically referred to in relation to their underlying sandstone unit (Westheimer, 1956; Peace, 1965; Hemish and Andrews, 2001).

The boundaries of the Goddard Formation were defined almost by omission. The sands of the Springer served as a sharp upper boundary for the Goddard. The dark black shales of the Mississippian Caney Shale also served as a soft boundary between the true Caney and the overlying Goddard (Westheimer, 1956; Peace, 1965). Before Westheimer assigned the interval the name of Goddard in the mid-1950s, the shales of the Late Mississippian were often called the Pennsylvanian-Caney or the Penn-Caney (Bennison, 1956; Westheimer, 1956; Branson, 1957; Rascoe and Adler, 1983). This term was misleading as the Penn-Caney unit was known to be Mississippian in age as early as the 1950s (Westheimer, 1956). Other papers have also included some or all of the Springer Group in the Mississippian, although the upper units of the Springer Group are most certainly Pennsylvanian in age (Reedy and Sykes, 1959; Brown and Northcutt, 2008).

At present, the Goddard Formation is known to belong to the Chesterian Series of the Late Mississippian (Andrews, 2008). The Goddard Formation is included as the basal unit of the Springer Group, which spans the Late Mississippian and extends into the early Pennsylvanian (Andrews, 2008). The inclusion of the Goddard within the Springer Group

is due to convenience rather than a genetic relationship; the shale above the Rod Club Member of the Springer Group is almost impossible to distinguish from the Goddard in the field (Westheimer, 1956; Peace, 1965). The type section for the Goddard can be found at the Goddard Ranch in Johnston County, Oklahoma where some 2850 feet of the Goddard is exposed (Westheimer, 1956). Currently, some independent producers in Oklahoma have popularized the term Black Marker for the zone of the Goddard targeted for unconventional production in the Anadarko Basin (Eagle Rock Energy Partners, 2015).

3. Methods

3.1. Sample Selection

The objective of this study was to gain an understanding of geochemical trends in the Goddard Formation within the South Central Oklahoma Oil Province (SCOOP). Therefore, samples were selected to cover the extent of the SCOOP as thoroughly as possible (Figure 12). A total of 16 source rocks, 11 oils, and 1 oil seep asphalt were analyzed (Table 1). A flowchart for the analysis workflow used in this study is shown in Figure 13.

Fifteen of the 16 rock extracts were either whole or side-wall core. The core samples were obtained from four wells located in Stephens and Grady County, Oklahoma. Sample SR-15 was a source rock extract from a core sample studied by Jones and Philp (1990); this study identified the SR-15 sample as Springer in origin (Jones and Philp, 1990). Only the aliphatic and aromatic fractions for SR-15 were available for analysis. An additional outcrop sample, OC-1, was collected outside of the SCOOP in Pontotoc County, Oklahoma. The outcrop was located in an area mapped as Springer by the Oklahoma Geological Survey (OGS) (Ham et al., 1990). The outcrop sample was collected from a two-foot deep hole dug away from any deep root networks or standing water. The oil seep sample was also collected outside of the SCOOP in Carter County. This asphalt sample, AS-1, was sourced from an oil seep in an unnamed, abandoned quarry. The 11 oil samples were obtained from 11 different wells in Stephens and Grady County. All 11 wells were drilled horizontally and hydraulically fractured. Oils OL-8

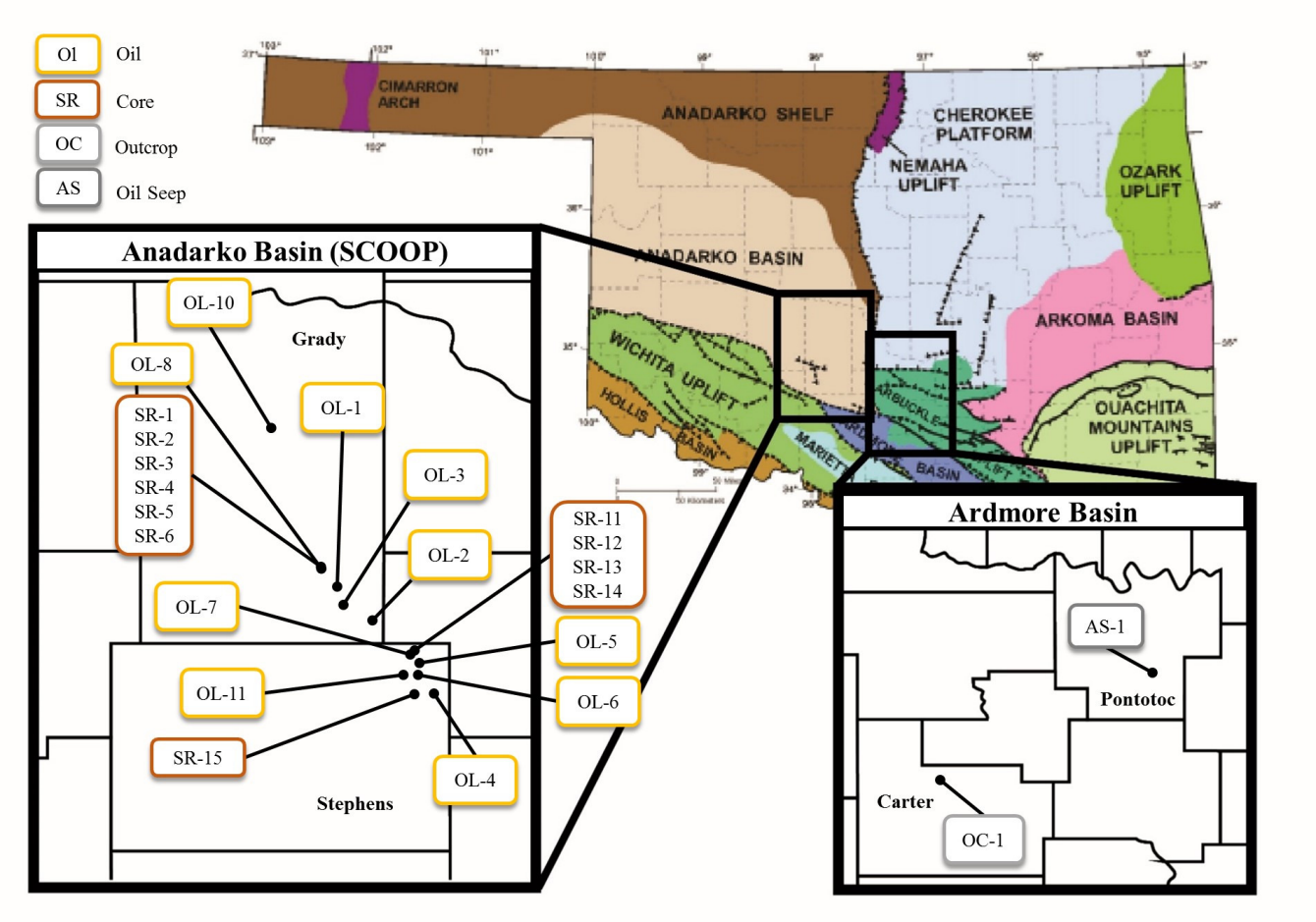

Figure 12: Map of sample locations in the Ardmore Basin and SCOOP in the Anadarko Basin. The exact locations for OL-9, SR-7, SR-8, SR-9, and SR-10 are unknown. Sample OL-9 is located in Grady County near OL-7. The SR-7, SR-8, SR-9, and SR-10 core samples all come from the same location in Grady County. (modified from Cardott, 2012b)

ID	Type	County	Section	Township	Range	Depth (ft)
OI-1	Oil	Grady	28	4N	5W	11801
OI-2	Oil	Grady	13	3N	5W	11923
OI-3	Oil	Grady	3	3N	5W	12070
OI-4	Oil	Stephens	23	2N	4W	10724
OI-5	Oil	Stephens	16	2N	4W	13264
OI-6	Oil	Stephens	21	2N	4W	13736
OI-7	Oil	Stephens	9	2N	4W	11934
OI-8	Oil	Grady	20	4N	5W	12961
OI-9*	Oil	Grady				
OI-10	Oil	Grady	26	7N	6W	11965
OI-11	Oil	Stephens	5	2N	4W	12004
SR-1	Whole Core	Grady	17	4N	5W	13045
SR-2	Whole Core	Grady	17	4N	5W	13035
SR-3	Whole Core	Grady	17	4N	5W	12965
SR-4	Whole Core	Grady	17	4N	5W	13010
SR-5	Whole Core	Grady	17	4N	5W	12945
SR-6	Whole Core	Grady	17	4N	5W	13074
SR-7**	Sidewall Core	Grady				12606
SR-8**	Sidewall Core	Grady				12549
SR-9**	Sidewall Core	Grady				12418
SR-10**	Sidewall Core	Grady				12351
SR-11	Sidewall Core	Stephens	4	2N	4W	13040
SR-12	Sidewall Core	Stephens	4	2N	4W	13067
SR-13	Sidewall Core	Stephens	4	2N	4W	13090
SR-14	Sidewall Core	Stephens	4	2N	4W	13104
SR-15	Whole Core	Stephens	7	4N	1W	7204
OC-1	Outcrop	Pontotoc	30	2N	7E	2
AS-1	Asphalt	Carter	S11	3S	R1	0

* Exact location and depth unknown. The well for OI-9 is within a mile of the well for OL-8.

** Exact location and well name for core unknown.

Table 1: Sample names and locations for Goddard oils and source rocks

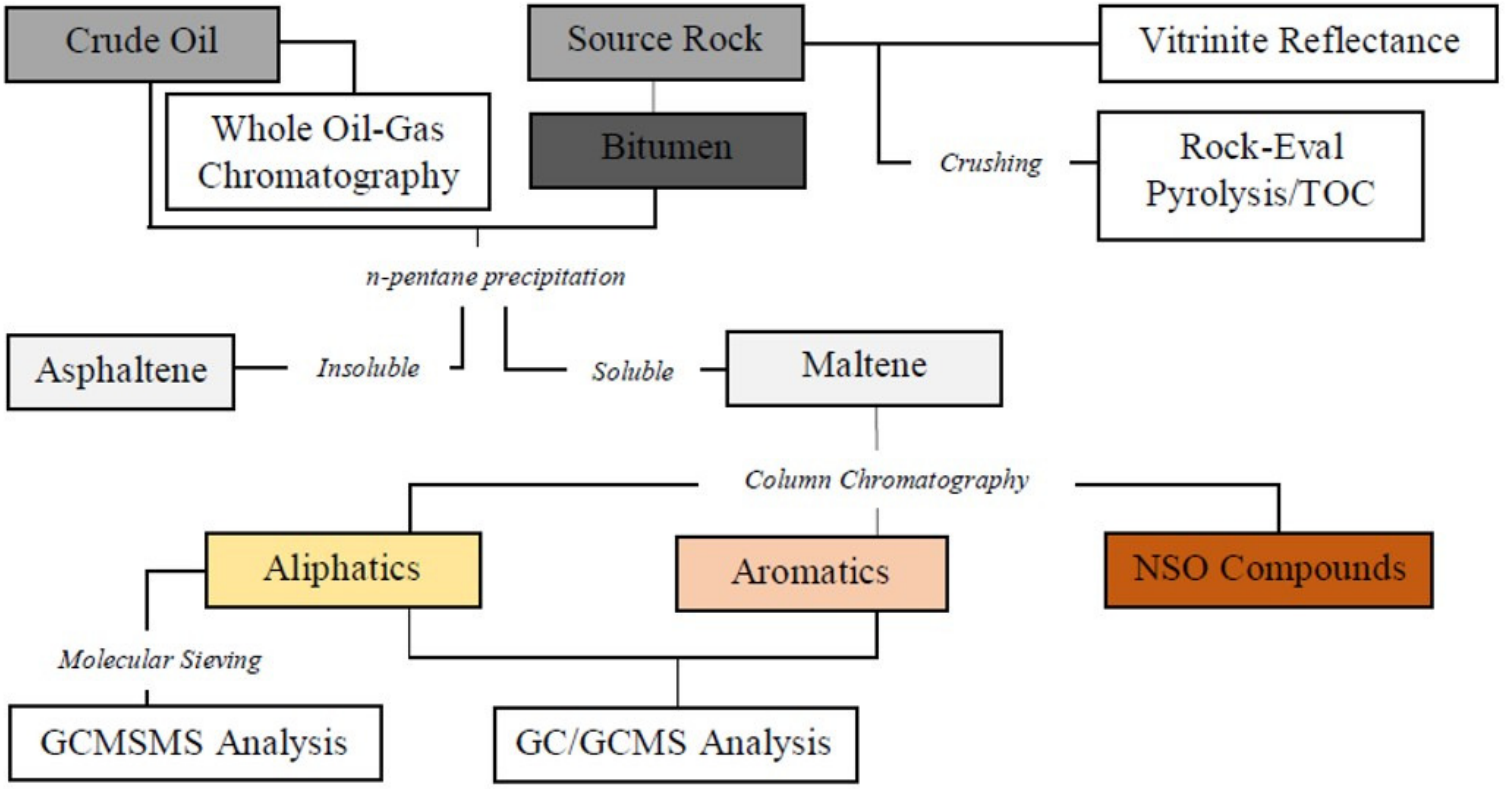

Figure 13: Schematic for methods workflow

and OL-9 were produced from two wells less than a mile apart and both wells targeted the same Goddard interval.

3.2. Experimental

3.2.1. Rock-Eval Pyrolysis

Rock-Eval pyrolysis (Rock-Eval) is a routine technique used to rapidly evaluate the generative capacity, thermal maturity, and approximate kerogen type of a source rock (Peters, 1986). The basic pyrolysis method heats a finely crushed rock sample in an inert atmosphere at a programmed rate (Peters, 1986). As the sample is heated, free hydrocarbons are released and measured, as are the subsequent products from kerogen cracking at higher temperatures (Peters, 1986). Samples thought to be contaminated by oil-based mud may be pre-extracted with an organic solvent such as dichloromethane (DCM) prior to Rock-Eval analysis. Pre-extraction however, will reduce the amount of free hydrocarbons measured in the sample. All core and outcrop samples in this study were determined to have minimal oil-based mud contamination and were analyzed either without pre-extraction or briefly rinsed in DCM followed by methanol.

Rock-Eval data were collected and interpreted in the form of pyrograms and reported data. Two methods of Rock-Eval pyrolysis were used; the difference between the results of these two methods is most pronounced when interpreting the free and sorbed hydrocarbons (Figure 14). In the traditional Rock-Eval method, the S1 peak corresponds to all liberated hydrocarbons in a source rock, both free and sorbed. The S2 peak represents the potential generative capacity of a source rock. Typically, as a source rock

matures, the S1 peak increases and the S2 peak diminishes. The S3 peak corresponds to inorganic CO_2; this peak is used to approximate the carbonate fraction of a sample. The S4 peak corresponds to the inert kerogen in a source rock; inert kerogen is unable to generate additional hydrocarbons. As with the S1 peak, the S4 peak also increases with source rock maturation (Peters, 1986). The following samples were screened by GeoMark Petroleum Services Ltd. using traditional Rock-Eval pyrolysis: SR-1, SR-2, SR-3, SR-4, SR-5, SR6, and OC-1. A Rock-Eval 6 apparatus was used to evaluate these samples. An adequate mass of the SR-15 core sample was not available, so that sample was not screened using Rock-Eval.

The remaining eight core samples were screened by IFP Energies nouvelles using a method of Rock-Eval developed in 2015 specifically for unconventional shales (Romero-Sarmiento et al., 2015a; Romero-Sarmiento et al., 2015b). This method also uses a Rock-Eval 6 device but the heating program is designed to increase the separation of certain hydrocarbons in an unconventional shale e.g. sorbed vs. free hydrocarbons (Figure 14). Specifically, the traditional S1 peak is split into an Sh0 peak for light, free hydrocarbons and a Sh1 peak which corresponds only to the heavier, free hydrocarbons in the shale (Romero-Sarmiento et al., 2015b). The sum of Sh0 and Sh1 peaks in this unconventional method are equivalent to the S1 peak obtained using traditional Rock-Eval (Romero-Sarmiento et al., 2015a; Romero-Sarmiento et al., 2015b). The sum of the S0 and S1 peaks can be used to estimate oil-in-place (Romero-Sarmiento et al., 2015b). A full description of the temperature program for this unconventional-shale method can be found in (Romero-Sarmiento et al., 2015b).

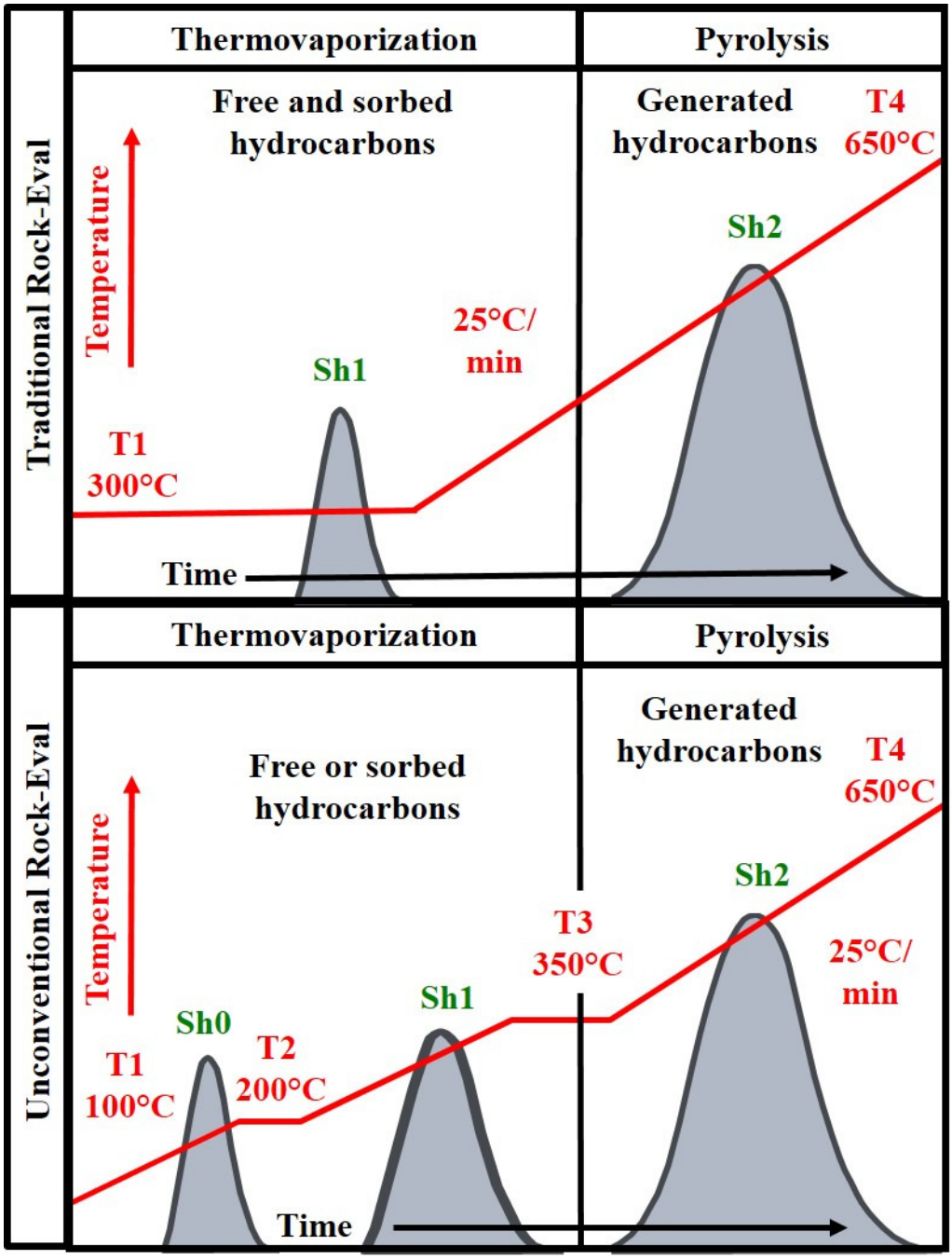

Figure 14: Comparison of idealized pyrograms and temperature profiles for traditional and unconventional Rock-Eval methods (after Peters, 1986; Romero-Sarmiento et al., 2015a)

3.2.2. Petrographic Analysis

Two samples were selected for petrographic analysis; OC-1 and SR-14. Both samples were prepared and interpreted by Brian Cardott at the OGS. The vitrinite reflectance of both samples was determined using methods outlined in ASTM, 2011 and Cardott (2012a). A description of kerogen macerals was also recorded for each sample based on the identification procedures outlined in Cardott (2012a). Thin sections of six core samples were also prepared for analysis on a scanning electron microscope (SEM). Elemental analyses and SEM images for these thin sections were provided courtesy of Will Rush at the University of Oklahoma Institute of Reservoir Characterization.

3.2.3. Source Rock Extraction

Fifteen source rock samples were extracted for this study. To prepare each source rock sample for extraction, approximately 50 g of sample were rinsed thoroughly with methanol and DCM and allowed to dry for 24 hours.

After being cleaned and dried, each sample was crushed using either a Coorstek porcelain mortar and pestle or Spex 8000 Mixer/Mill. For the Mixer/Mill, no more than eight g of rock chips were crushed at a time. Rock chips were introduced to a cylindrical, metal vessel containing several steel balls (Figure 15). The vessel was then sealed using a two-part cap and O-ring and secured in the mill. Each run of the mill lasted no longer than five minutes. After each run, the contents of the vessel were sieved. Fragments larger than 40 mesh were returned to the vessel for further crushing. For both the mortar and pestle and ball mill, the crushing process was repeated until 50 g of 40-mesh sample was

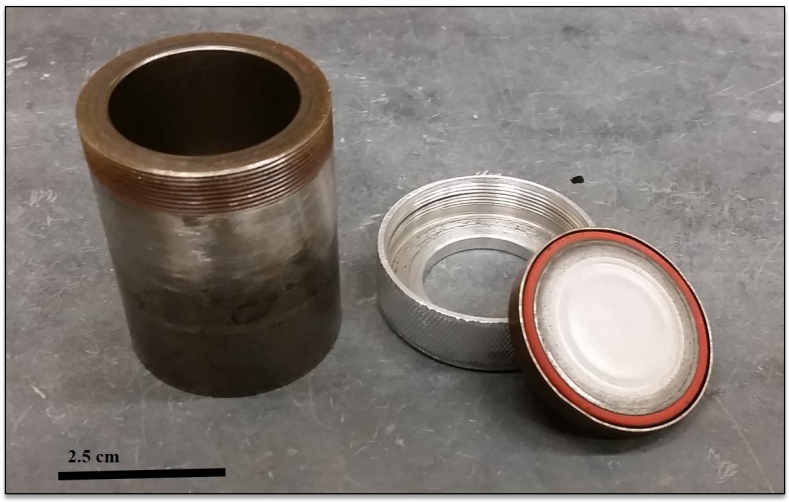

Figure 15: Vessel for Spex 8000 Mixer/Mill

obtained.

A cellulose thimble was pre-extracted in a Soxhlet apparatus for 12 hours using MeOH:DCM (v/v = 1:1). Following pre-extraction, 50 g of 40-mesh sample was then introduced into the cellulose thimble and covered with glass wool. Solvent from the pre-extraction was discarded and fresh solvent was added to the Soxhlet assembly. Activated copper was also added to the assembly to scavenge sulfur from the extract. Each sample was then extracted for 24-36 hours.

Once the Soxhlet extraction was complete, the resulting extract was dried using a Yamato HiTEC RE-51 Rotary Evaporator and a BM-51 heated bath. The water bath was heated to 37°C while the sample was rotated at a rate of 100 revolutions per minutes. The cellulose thimble containing the extracted sample was dried for 24-48 hours in a fume hood before being stored. The extract was then transferred to a 20 mL vial. After drying using an Organomation Model 112 Analytical Evaporator, the extract mass was obtained.

3.2.4. Asphaltene Precipitation

To precipitate the asphaltene fraction of both the source rock extracts and oils, 100-200 mg of sample was introduced into a centrifuge tube. With the centrifuge tube partially submerged in a Branson Model 2510 Sonicator, approximately 2mL of n-pentane was added dropwise to the sample. This dropwise addition of n-pentane was repeated four additional times, after which n-pentane was introduced continuously until solvent levels reached the shoulder of the centrifuge tube. The sample was then placed in a freezer for at least 12 hours, after which the sample was centrifuged in a Thermo Scientific IEC Model K centrifuge for 5 minutes to settle precipitated asphaltenes. The maltene fraction was filtered and weighed. Any precipitated asphaltenes were also collected.

3.2.5. Column Chromatography

A silica column was used to fractionate prepared maltenes for all samples except OC-1 and AS-1. Sample OC-1 and AS-1 were fractionated using an alumina column. Results from silica column fractionation were compared to alumina and HPLC fractionation methods. Comparison studies were conducted by Dr. Thanh X. Nguyen at the University of Oklahoma Organic Geochemistry Group; the quality of fractionation achieved in all three methods was determined to be equivalent. A silica column was prepared using a shortened Pasteur pipette with a glass wool filter. Approximately 6.1 g of silica was added to the column and agitated to facilitate settling. Before use, the silica was heated at 120°C for 24 hours. Pentane was used to flush air from the column. 8 to 10 mg of maltene was introduced to the column and allowed to completely infiltrate the surface of

the column before 2 mL of pentane was introduced to mobilize the aliphatic fraction of the maltene. To mobilize the aromatic fraction, 4 mL of C_6:DCM (v/v = 7:3) was then introduced to the column. 8 mL of $CHCl_3$:MeOH (v/v = 98:2) were used to mobilize the remaining polar nitrogen, sulfur, and oxygen (NSO) compounds. Branched and cyclic alkanes were further isolated from selected aliphatic fractions using the method described by West et al. (1990).

3.2.6. Gas Chromatography

Gas chromatography was used to analyze both whole oils and aliphatic and aromatic fractions. Whole oils were analyzed on an Agilent Technologies 6890 Gas Chromatograph using a split injection method. The column used was a J&W Scientific DB-Petro column (250um inner diameter and 25um coating). Helium was used as a carrier gas at a flow rate of 1.4mL/min. The temperature program for whole oil analysis was as follows: the initial temperature began at 40°C and was held for 1.5 minutes. Then the temperature was increased at a rate of 2°C/minute until the temperature reached 130°C. At that point, the temperature continued to increase at a rate of 4°C/minute until the 300°C. The final temperature of 300°C was held for 35 minutes.

Aliphatic and aromatic fractions were analyzed on an Agilent Technologies 6890 Gas Chromatograph using a splitless injection method. The column used was a fused silica J&W Scientific 122-5544G DB-5ms (250um inner diameter and 25um coating). The carrier gas used was helium and the flow rate was 2mL/min. Both aliphatic and aromatic fractions were diluted to concentrations of 3mg/mL hexane. The temperature program

used began at 40°C for 1.5 minutes, followed by an increase in temperature at a rate of 4°C/minute until 300°C. The final temperature of 300°C was held for 14 minutes.

3.2.7. Gas Chromatography - Mass Spectrometry

An Agilent Technologies 7890A Gas Chromatograph (GC), paired with an Agilent Technologies 5975 XL Mass Selective Detector, was used to analyze aliphatic and aromatic fractions. Selected branched and cyclic saturate fractions were also analyzed. The ionization energy for the MS was 70eV for the electron impact mode. The ion source temperature was 250°C and the quadrupole analyzer was maintained at 200°C. The interface temperature between the GC and mass spectrometer (MS) was 310°C. Single ion monitoring (SIM) and multiple ion detection (MID) modes were used to analyze selected ions for both fractions. The column used for the GC was a J&W Scientific DB-5MS 122-5562 fused silica column (250um inner diameter and 25um coating). The flow rate for the carrier gas, helium, was 1.4 mL/min. The same dilution of 3mg/mL hexane was used to prepare both fraction. Samples were run using splitless capillary injection. The temperature program for GCMS analysis began at 40°C and was held for 1.5 minutes. The temperature was then increased at a rate of 4°C/minutes until a temperature of 310°C was reached. A temperature of 310°C was maintained for another 51.5 minutes.

3.2.8. Gas Chromatography-Mass Spectrometry-Mass Spectrometry

A Thermo Scientific Trace 1310 GC coupled with a Thermo Scientific TSQ 8000 Triple Quadrupole MS was used to analyze the branched and cyclic fractions of 10 oils

and 13 extracts. Sample diluted to 6 mg/mL with hexane before injection. The column used was a J&W Scientific fused silica DB-5MS 12205562 (250um inner diameter and 25um coating). Helium was used as the carrier gas for the GC at a flow rate of 1.4 mL/min. The GC temperature program began at 40°C and was held for 1.5 minutes before the temperature was increased at a rate of 4°C /minute until a target temperature of 310°C was reached. A temperature of 310°C was then held 55.5 minutes. Argon was used as a collision gas for the second MS quadrupole. The fore line pressure was maintained at 75 mTorr and the ion gauge pressure was 1.6c10-5 Torr. Temperatures in the ion source and GC-MS interface were both held at 300°C.

4. Results

4.1. Bulk Geochemical Data

Bulk geochemical characteristics for source rock include TOC content, thermal maturity, and general kerogen characterization. Core samples were screened for these characteristics using Rock-Eval (Table 2). A range of 2-12 weight percent TOC has previously been observed within producing intervals of the Goddard Formation (Ardmore Geological Society, 2015). The TOC values obtained in this study will provide additional data to understand lateral trends in TOC for the Goddard within the Anadarko Basin. Thermal maturity trends for the Goddard Formation are less precisely mapped compared to formations such as the Woodford (Cardott, 2012b; Cardott, 2013). Thermal maturity data from this study will contribute to more accurate thermal models for the Goddard Formation. Whole oil analysis was also used to screen oils for thermal maturity, biodegradation, and mixing.

4.1.1. Total Organic Carbon Content

The TOC content for 15 source rocks was obtained using Rock-Eval (Table 2). All TOC values are listed as a percent of the total source rock weight. Rock-Eval data for SR-15 were not available. The range of TOC for samples analyzed using conventional Rock-Eval was 0.86 wt. % to 7.77 wt. %; the median total organic carbon content was 4.45 wt. %. The sample with the lowest total organic carbon, SR-5, also had the highest carbonate content at 48.26 wt. %. Although multiple samples were collected from three

Sample	TOC[1]	Sh0[2]	Sh1[3]	S1[4]	S2[5]	S3[6]	Tmax[7]	%Ro[8]*	HI[9]	OI[10]	CC[11]
OC-1	3.15			1.95	70.42	0.88	427	0.53 (0.60)	770	10	4.45
SR-1	4.45			8.73	8.25	0.65	449	0.92	185	15	2.56
SR-2	5.85			7.32	11.38	0.68	450	0.94	195	12	4.33
SR-3	6.51			13.12	14.28	0.79	445	0.85	219	12	4.85
SR-4	7.77			9.49	17.81	0.83	447	0.89	229	11	5.19
SR-5	0.86			0.75	0.75	0.50	445	0.85	88	58	48.26
SR-6	1.68			0.29	0.65	0.18	460	1.12	39	11	4.61
SR-7	0.74	0.22	0.59	0.81	1.65		457	1.08	223	9	
SR-8	1.46	1.43	0.91	2.34	1.35		461	1.15	92	5	
SR-9	3.15	0.72	1.81	2.53	4.40		460	1.13	140	3	
SR-10	3.55	0.97	2.15	3.12	4.10		460	1.13	115	3	
SR-11	5.51	3.77	6.19	9.96	10.44		445	0.86	189	1	
SR-12	6.26	6.99	6.61	13.60	9.11		452	0.99	146	2	
SR-13	7.43	5.74	7.95	13.69	12.60		450	0.95	170	2	
SR-14	5.80	5.15	7.99	13.14	10.11		450	0.95 (1.04)	174	1	

OC-1 and SR-1 to SR-6 analyzed using traditional Rock-Eval

SR-7 to SR-14 analyzed using unconventional Rock-Eval. S3 and CC data not provided by IFP Energies nouvelles

*Calculated using the formula %Ro (from Tmax) = 0.0180 x Tmax – 7.16 (Jarvie et al., 2005). Values in parentheses were manually measured.

1.Total organic carbon (wt. %), 2. Free hydrocarbons (mg HC/g rock), 3. Sorbed hydrocarbons (mg HC/g rock), 4. Free and sorbed hydrocarbons (mg HC/g rock), 5. Remaining hydrocarbon potential of kerogen (mg HC/g rock), 6. Oxygen content of sample (mg CO_2/g rock, 7. Temperature of maximum S2 evolution (°C), 8. Vitrinite Reflectance, 9. Hydrogen Index (mg HC/g TOC), 10. Oxygen Index of sample (mg CO2/g TOC), 11. Carbonate Content (wt %)

Table 2: Rock-Eval pyrolysis data

of the four sets of core, the sampling interval was determined to be too coarse in each case to provide meaningful interpretation of the vertical variation in TOC.

Eight of the core samples (SR-7 to SR-14) were analyzed using a new method for Rock-Eval developed for unconventional resource shales by IFP Energies nouvelles (Romero-Sarmiento et al., 2015b; Table 2). This method evaluates classic Rock-Eval parameters as well as hydrocarbon content (HC, mg HC/g rock). The hydrocarbon content indices (S1) for SR-5 to SR-10 and OC-1 were between 0.81 and 3.12 mg HC/g rock. These values are considered relatively low (Peters et al., 1986; Romero-Sarmiento et al., 2015b). A cross-plot modified from Jarvie (2012) of the hydrocarbon content index and TOC indicates that SR-2, SR-4 to SR-10, and OC-1 all fall into the so-called low-oil content or oil show category. (Jarvie, 2012; Romero-Sarmiento et al., 2015b; Figure 16). Samples SR-1, SR-3, and SR-11 to SR-14 all plot much higher; the range of the hydrocarbon content index for these samples is 8.73-13.69 mg HC/g rock. When the hydrocarbon content for each of these samples is plotted against their respective TOC values, these samples are predicted to freely produce oil based on the hydrocarbon content categories developed by Jarvie (2012; Figure 16). The IFP Energies nouvelles provided oxygen index data but not S3 peak data or carbonate content for samples SR-7 to SR-14 (Table 2).

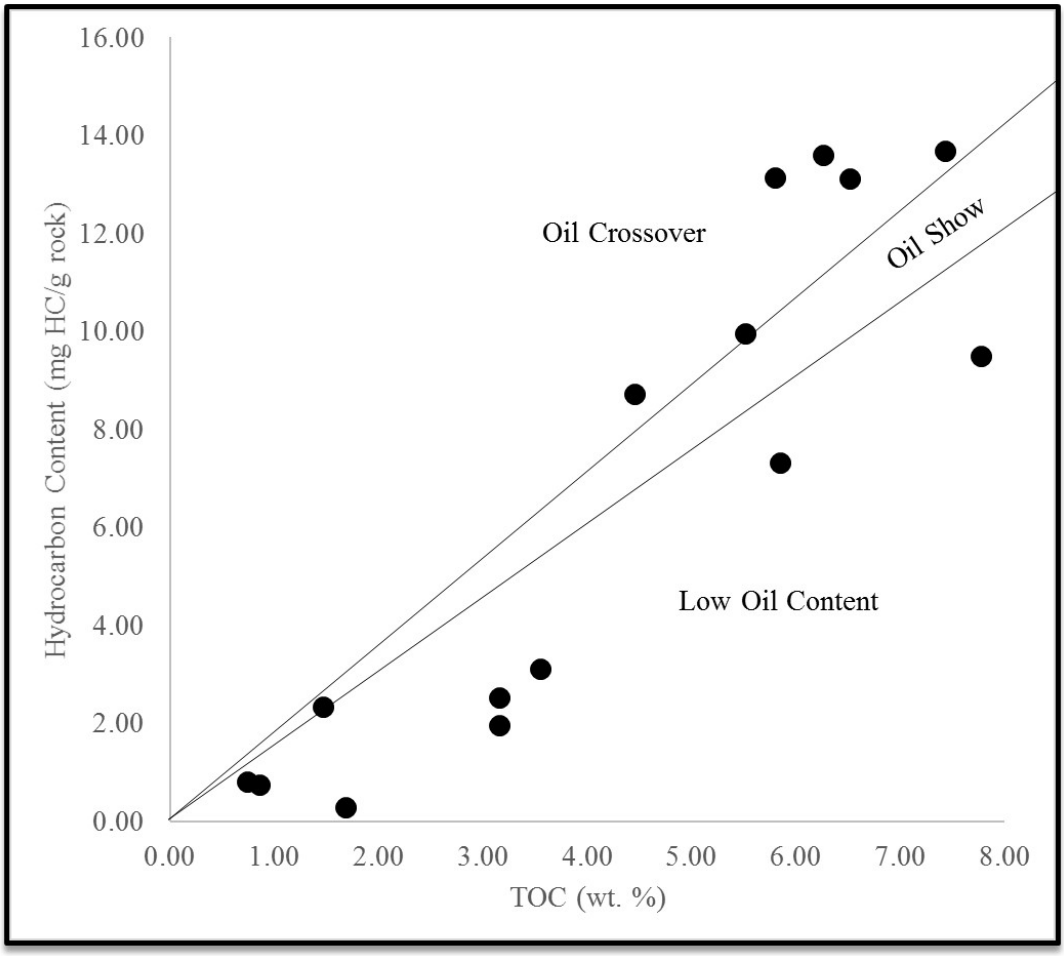

Figure 16: Cross plot of TOC (wt. %) and hydrocarbon content (mg HC/g rock) to infer oil shows in unconventional resource shales (after Jarvie 2012)

4.1.2. Thermal Maturity

Early estimates of thermal maturity for Goddard source rocks relied on vitrinite reflectance maps produced by Cardott (2012a) for the Woodford Shale. The underlying Woodford is stratigraphically proximal to the Goddard (Johnson et al., 1989) and %Ro trends for the Woodford have been thoroughly mapped (Cardott, 2012b). While thermal maturity values are likely greater for the Woodford than the Goddard, such maps provided trends and upper limits to thermal maturity during initial screening.

Rock-Eval was used to assess the thermal maturity of the Goddard core and outcrop samples in this study. The T_{max} temperatures were directly obtained from Rock-Eval pyrograms and used to calculate equivalent values for vitrinite reflectance (Table 2). Pyrograms for all samples were reviewed to assess data quality. No Rock-Eval data were available for the SR-15 sample.

A complete list of T_{max} values for all rock extracts can be found in Table 2. The T_{max} temperatures for the rock samples ranges from 427°C to 461°C. Generally, a T_{max} temperature of 435-445°C corresponds to the onset of oil generation while 470°C marks the end of the oil window (Peters, 1986). The actual onset of oil generation varies based on kerogen type (Peters, 1986; Pepper and Corvi, 1995). Calculated vitrinite values ranged from 0.53 %Ro to 1.15 %Ro. Sample OC-1 was the only sample with a vitrinite value below the early oil window. The thermal maturities of the majority of the core samples was nearing or within the late oil window.

Vitrinite reflectance for two samples, OC-1 and SR-14, was manually measured by Brian Cardott of the OGS to assess the accuracy of calculated vitrinite values (Table 2).

The measured values were within an acceptable margin of error for the calculated vitrinite reflectance. For OC-1, the measured vitrinite reflectance was 0.60 %Ro. Only three suitable vitrinite clasts were found in the sample; 20 vitrinite macerals are needed for statistical significance measurements (Cardott, 2012a). However, additional bitumen reflectance measurements and green-colored fluorescence of *Tasmanite* algae were consistent with a vitrinite reflectance of 0.60 %Ro (Figures 17).

The mean %Ro for SR-14 was 1.26 %Ro, based on 28 vitrinite measurements. This value was higher than the %Ro of 0.95 calculated from T_{max}. This discrepancy may be caused by an abundance of inertinite-like vitrinite included in the measurement. The small size of individual vitrinite macerals may also have contributed to possible errors in calculating thermal maturity from vitrinite. The calculated vitrinite reflectance may also have been inaccurate; T_{max} is influenced by organic matter input and fusinite was moderately abundant in SR-14. An adjusted bitumen reflectance of 1.04 %Ro for SR-14 was more consistent with the calculated vitrinite reflectance.

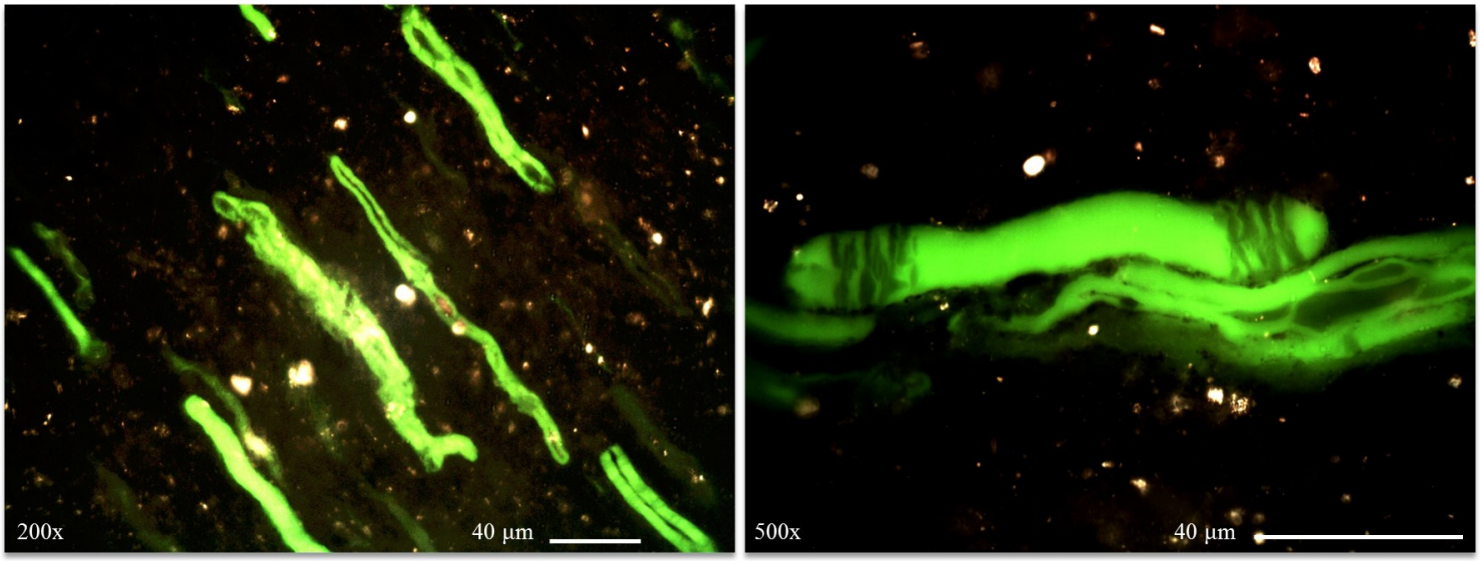

Figure 17: Fluorescing *Tasmanite* fossils in OC-1 sample (Courtesy of B. Cardott, Oklahoma Geological Survey, 2016)

4.1.3. Kerogen Characterization

As mentioned in previous chapters, initial kerogen characterization is often done using the PVK model because kerogen types can be assigned using minimal bulk geochemical data (Peters, 1986). Bulk geochemical data alone are typically insufficient to develop a meaningful organofacies interpretation. Organofacies characterization is discussed in the next chapter following a more comprehensive analysis of both bulk geochemical and biomarker data.

The original van Krevelen model was developed from empirical observations based on a subset of coals and their respective elemental hydrogen and oxygen abundance normalized to carbon (van Krevelen, 1950). The use of this model has expanded beyond coals, and elemental measurements have been replaced with oxygen and hydrogen index parameters easily obtained through routine Rock-Eval (Tissot and Welte, 1984). The modern PVK diagram is used to characterize kerogen type based on these oxygen and hydrogen indices (Peters, 1986). The four kerogen types include: Type I, very oil-prone; Type II, oil prone; Type III, gas-prone; and Type IV, inert (Peters, 1986). Type I kerogens are often associated with lacustrine conditions while Type II kerogens are typically designated as marine in origin. Type III kerogens are sourced from terrestrial plant matter. The Type IV category includes residual kerogens with no capacity for hydrocarbon generation.

The majority of core samples fell within the region of the diagram where the four kerogen type curves converge (Figure 18). This pattern is typical of samples with thermal maturities beyond the early oil window and highlights a weakness of the PVK model.

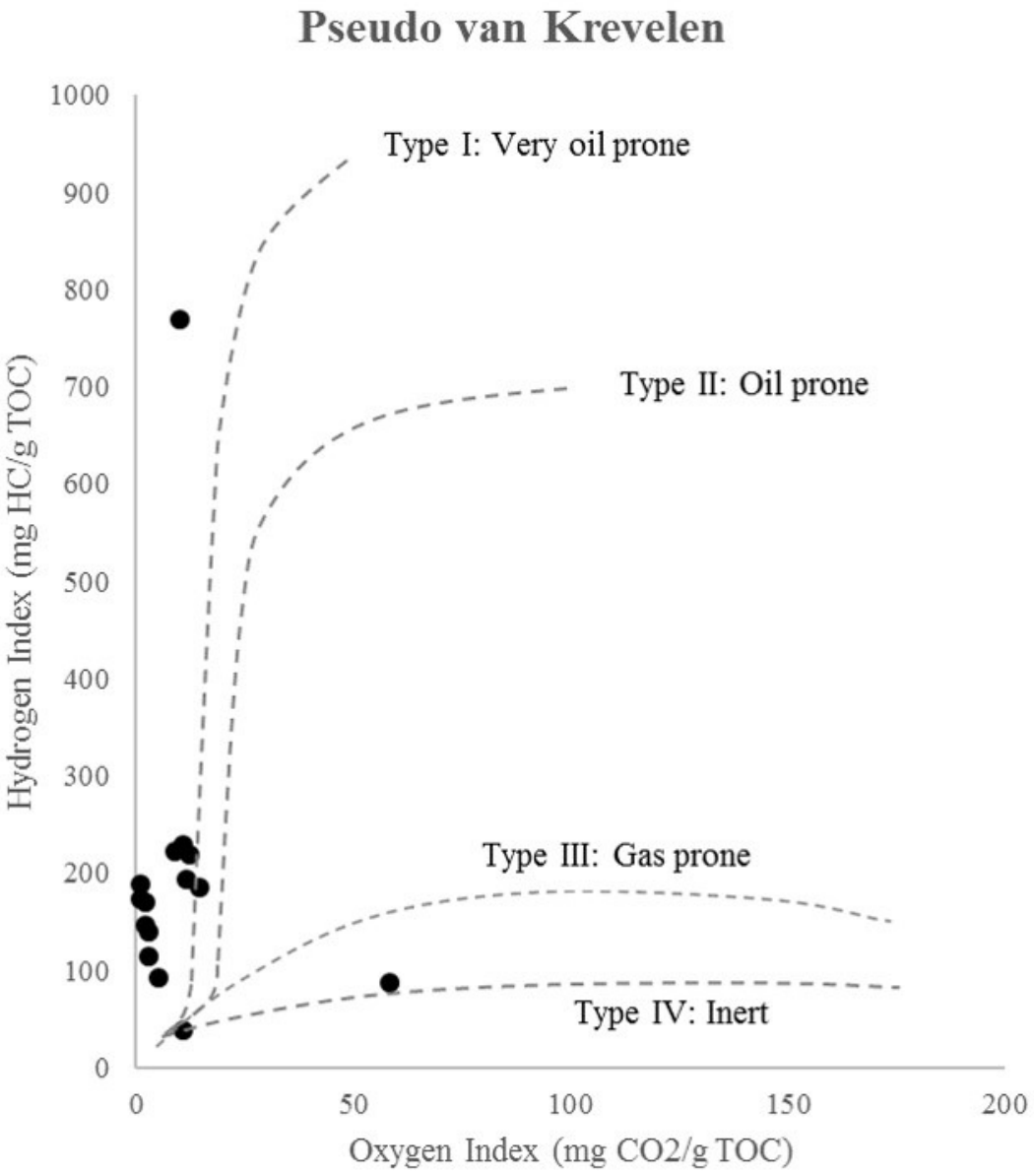

Figure 18: Pseudo van Krevelen diagram for Goddard source rocks (after Peters, 1986)

Nevertheless, most of the core samples plotted closely along the Type I and II kerogen trends and had low OI values. Sample OC-1 fell along the Type I kerogen curve with an HI of 770 and an OI of 10. As OC-1 was determined to be thermally immature, its location on the PVK diagram can more confidently be attributed to original kerogen type of OC-1.

Brian Cardott, of the Oklahoma Geological Survey, also analyzed kerogen macerals for OC-1 and SR-14. *Tasmanites* were present in both samples, but not in high abundance compared to *Tasmanite* shales or even local Oklahoma source rocks such as the Woodford Shale. Sample SR-14 also contained moderately abundant fusinite macerals (Figure 19). Fusinite is associated with the burning of woody terrestrial organic matter (Cardott, 2012a). Additional SEM analysis was conducted by Will Rush, at the University of Oklahoma Institute of Reservoir Characterization, on thin sections from SR-1, SR-2, SR-3, SR4, SR-5 and no evidence of abundant *Tasmanites* fossils was noted (W. Rush, University of Oklahoma Institute of Reservoir Characterization. Personal Communication, February 22nd, 2016).

4.1.4. Whole Oil-Gas Chromatography

Crude oils can be analyzed using gas chromatography without additional preparation. Whole oil analysis provides preliminary information regarding both thermal maturity and biodegradation. As thermal maturity increases, n-alkanes are generated through thermal cracking and increase in abundance relative to pristane and phytane (Tissot et al., 1971; Shanmugam, 1985). Biodegradation reverses this trend and increases the ratio of pristane

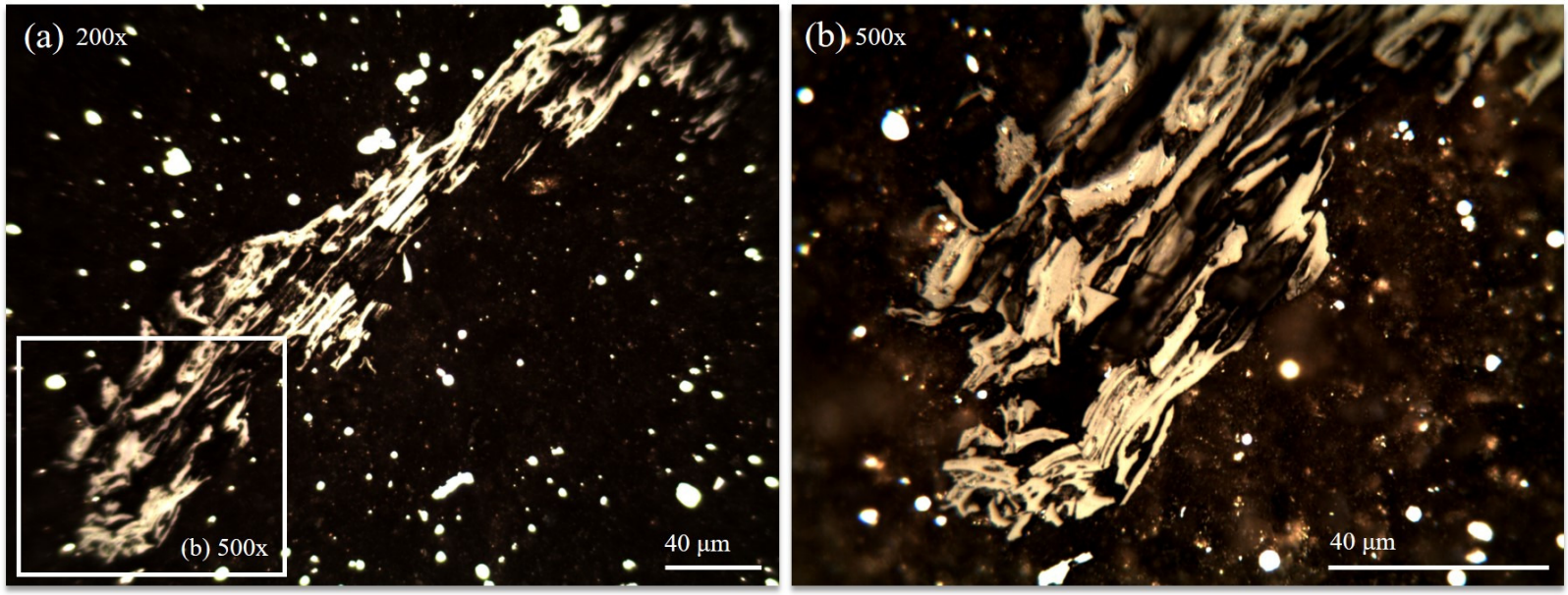

Figure 19: Fusinite maceral at (a) 200x magnification and (b) 500x magnification in SR-14 (Courtesy of B. Cardott, Oklahoma Geological Survey, 2016)

and phytane to the n-alkanes. Thermal maturity and biodegradation assessments can be confounded by organic matter input which influences the distribution of n-alkanes and isoprenoids (Didyk, 1978; Alexander et al., 1981; Shanmugam, 1985).

Whole oil analysis can also indicate mixing. When a secondary condensate mixes with a residual oil, a whole oil-gas chromatogram often displays a bimodal distribution of n-alkanes (Figure 20). Mixed organic matter inputs have also been suggested as another cause for the bimodal distribution of n-alkanes (Henry and Lewan, 1999).

Eleven Crude oils were evaluated using gas chromatography. All oils were characterized as low-wax with the n-alkanes in all samples extending out to C_{29}-C_{37}. The carbon number preference of the n-alkanes in whole oil-gas chromatograms was near one for all oils (Peters et al., 2005). Evidence of possible, but slight, biodegradation was seen in all samples. A bimodal distribution was also observed in almost all oils. Two representative whole oil-gas chromatograms are shown in Figure 21. The abundance of light hydrocarbons from C_5-C_7 was pronounced in oils such as OL-2. Oils such as OL-7 displayed more normal n-alkane distributions yet still had an abundance of light-end hydrocarbons.

Light-end hydrocarbons ($<C_9$) were also analyzed for each of the crude oils. Thermal stress, biodegradation, and evaporative fractionation each have varying influence on light-end aromatics, paraffins, naphthenes, and n-alkanes. Relative changes in the abundance of these compounds are described as changes in aromaticity and paraffinicity (Thompson, 1987). Aromaticity compares aromatic hydrocarbons to normal alkanes of the same carbon number while paraffinicity compares paraffin and naphthene abundance (Thompson, 1987). Specific aromaticity and paraffinicity ratios can be compared to one another to interpret the extent of alteration in oils. For example, Thompson compared

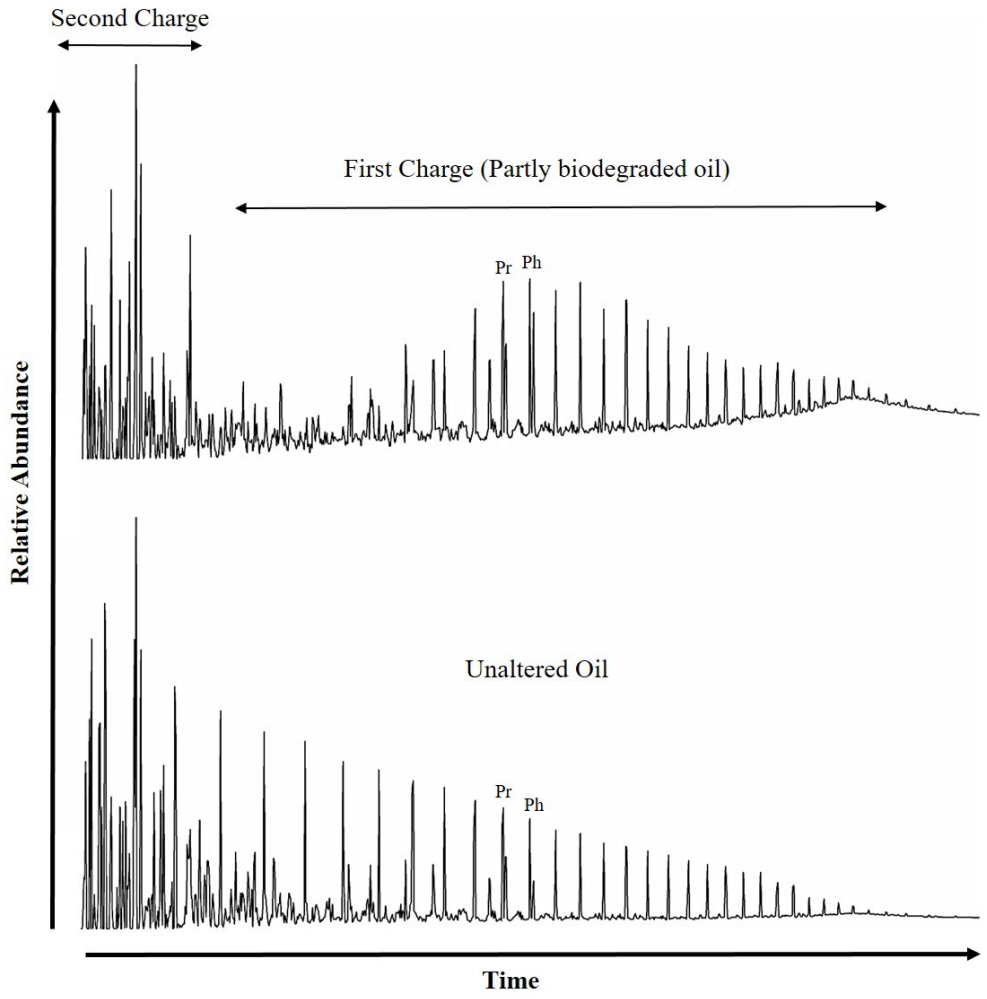

Figure 20: Whole oil-gas chromatograms of biodegraded and unaltered oils from the Magdalena Basin (Ramon et al., 1997)

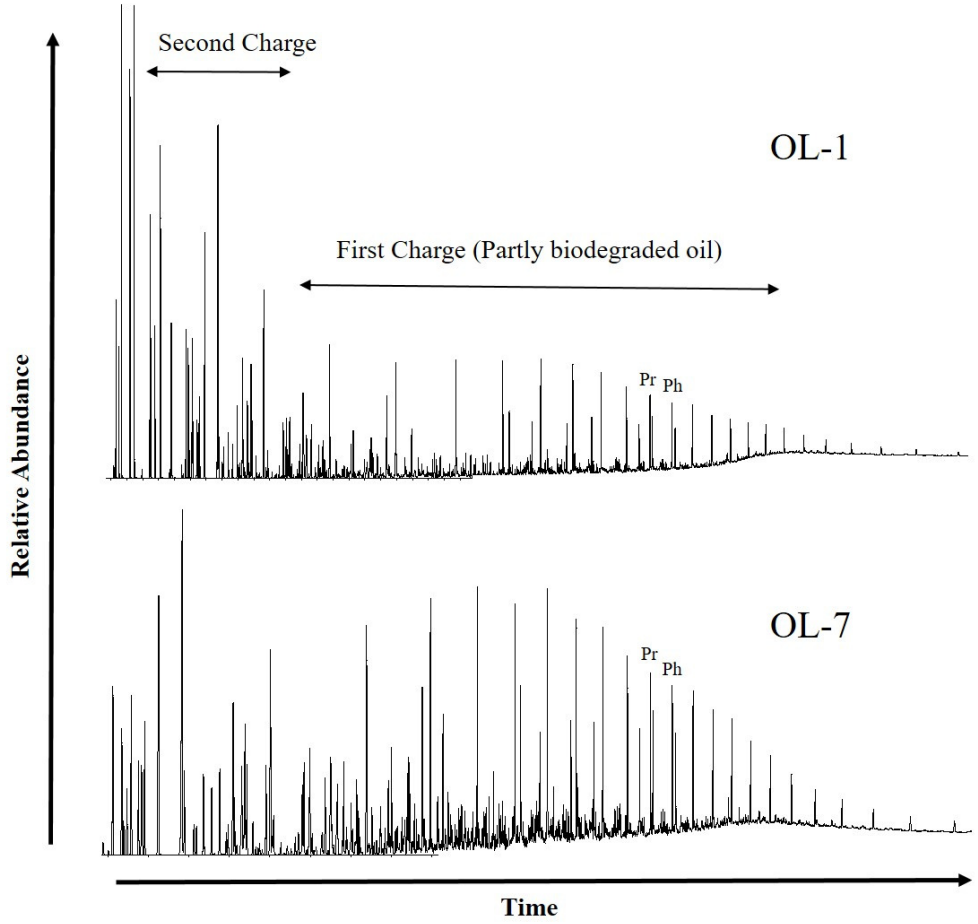

Figure 21: Representative whole oil-gas chromatograms of biodegraded oils for the Goddard

two specific aromaticity and paraffinicity ratios in his B-F diagram (Thompson, 1987). All Goddard oils cluster together on the B-F diagram (Figure 22). Sample OL-9 has a slightly higher aromaticity ratio that causes it to plot outside the main cluster. Sample OL-10 has the highest paraffinity ratio and also plots slightly apart from the main cluster. Overall, the most notable observation for these oils is their similarity.

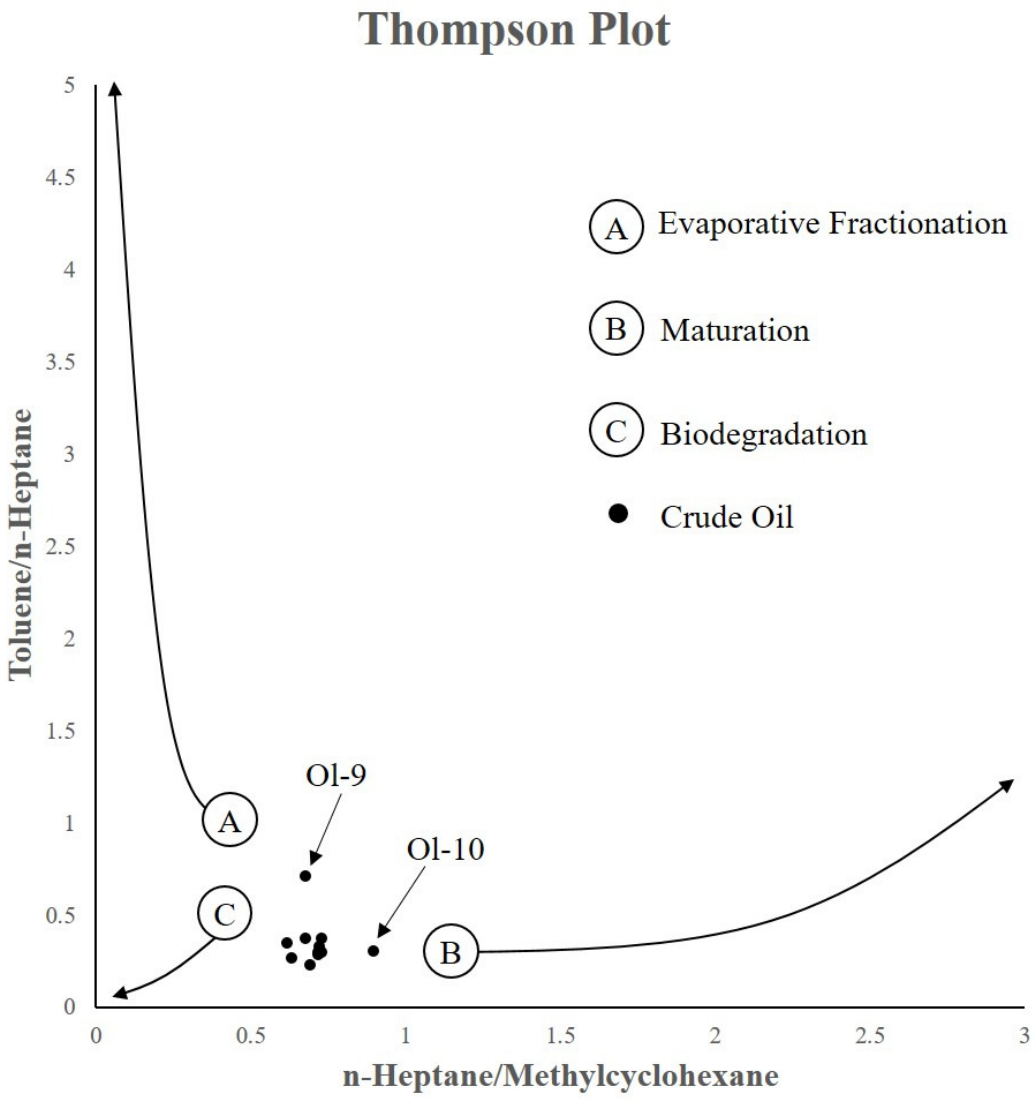

Figure 22: B-F Plot of Goddard crude oils (after Thompson, 1987)

4.2. Fraction Yields

Only two source rock samples, SR-6 and SR-7, were determined to be insufficiently rich in bitumen for further analysis. The remaining 13 source rock samples yielded 83.78 to 706.20 mg of bitumen. The bitumen component was precipitated to yield an asphaltene and maltene fraction (Table 3). A summary of the aliphatic, aromatic, and NSO fraction data is included in Table 4 and a ternary diagram showing the relative abundance of the aliphatic, aromatic, and NSO fractions for the oils and extracts is shown in Figure 23. For the oils, the aliphatic fraction ranged from 79-90 percent of the total recovered fraction. As would be expected (Hunt, 1996), the relative abundance of the aliphatic fraction was less for the extracts than the oils; the relative percentage for the aliphatic fractions was between 56-75 percent. Sample OC-1 had a minor aliphatic fraction and approximately equal aromatic and polar fractions.

Sample	Extract (mg)	Maltene (mg)	Asphaltene (mg)
OC-1	224.14	75.44	22.86
SR-1	146.42	140.27	4.16
SR-2	456.40	189.17	7.83
SR-3	653.97	194.54	8.86
SR-4	597.76	197.07	6.83
SR-5	214.25	106.14	1.96
SR-6*	11.17		
SR-7*	43.04		
SR-8	83.78	10.95	1.89
SR-9	176.81	94.93	8.52
SR-10	146.82	106.09	5.40
SR-11	706.20	193.47	3.68
SR-12	734.24	194.76	4.10
SR-13	621.53	201.39	1.81
SR-14	657.62	200.45	4.86
Approximately 50 g extracted for each sample *No maltene data avialable			

Table 3: Extraction data for Goddard source rocks

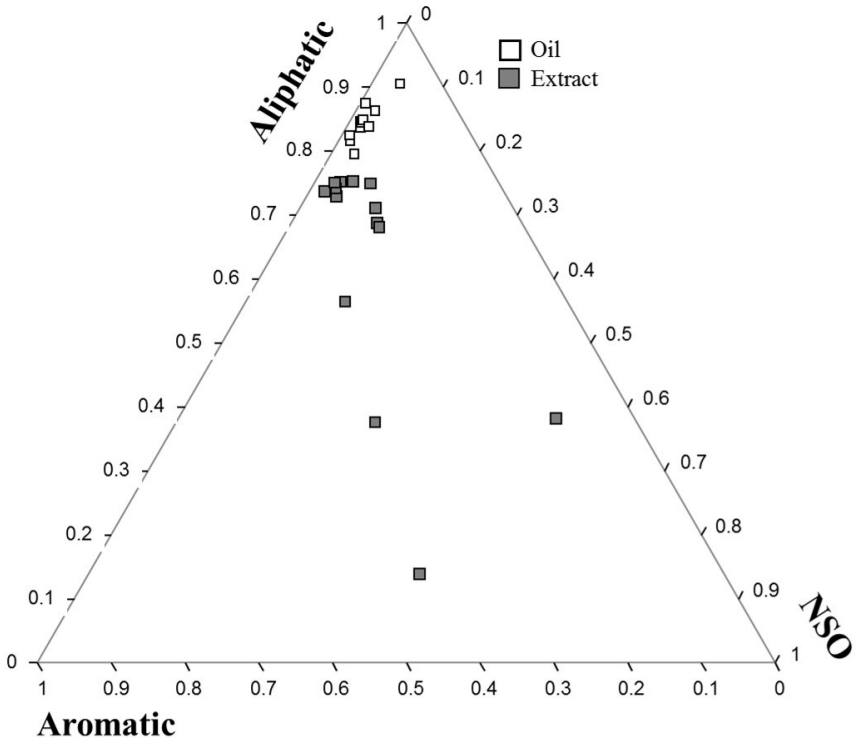

Figure 23: Ternary diagram of fraction data for Goddard source rocks and oils

4.3. Biomarker Analysis

4.3.1. n-Alkanes and Isoprenoids

The distribution of n-alkanes and isoprenoids in chromatograms of aliphatic fractions from source rocks and oils can be used to interpret the approximate thermal maturity and extent of biodegradation, (Tissot et al., 1971; Shanmugam, 1985). As thermal maturity increases, n-alkanes are generated through thermal cracking of kerogen or already generated n-alkanes; this process increases the abundance of short-chain n-alkanes as well as relative abundance of n-alkanes to isoprenoids such as pristane and phytane (Shanmugam, 1985). Biodegradation reverses this trend and preferentially removes the n-alkanes over isoprenoids (Tissot et al., 1971; Shanmugam, 1985). The effects of biodegra-

Sample	Type	Aliphatic (mg)	Aromatic (mg)	NSO (mg)
Ol-1	Oil	5.83	0.96	0.10
Ol-2	Oil	6.37	0.82	0.19
Ol-3	Oil	6.22	1.07	0.14
Ol-4	Oil	5.77	1.19	0.11
Ol-5	Oil	5.73	0.95	0.11
Ol-6	Oil	6.02	0.81	0.05
Ol-7	Oil	5.06	0.8	0.10
Ol-8	Oil	6.07	1.21	0.08
Ol-9	Oil	6.31	0.39	0.27
Ol-10	Oil	5.48	1.19	0.22
Ol-11	Oil	6.48	1.02	0.23
SR-1	Whole Core	5.20	1.21	0.53
SR-2	Whole Core	5.79	1.65	0.98
SR-3	Whole Core	6.32	1.66	0.91
SR-4	Whole Core	5.82	1.68	1.05
SR-5	Whole Core	4.41	2.35	1.05
SR-6*	Whole Core			
SR-7*	Sidewall Core			
SR-8	Sidewall Core	5.40	1.41	0.37
SR-9	Sidewall Core	5.60	1.77	0.31
SR-10	Sidewall Core	5.23	1.46	7.02
SR-11	Sidewall Core	5.72	1.88	0.16
SR-12	Sidewall Core	5.91	1.68	0.27
SR-13	Sidewall Core	5.48	1.66	0.25
SR-14	Sidewall Core	5.57	1.65	0.20
OC-1	Outcrop	1.43	4.24	4.60
AS-1	Asphalt	12.22	11.51	8.75

*No fraction data avialable

Table 4: Fraction data for Goddard oils and source rocks

dation and thermal alteration are most commonly observed using the ratios of pristane/C_{17} and phytane/C_{18} (Shanmugam, 1985). In addition to biodegradation and thermal stress, depositional conditions can also influence the distribution of isoprenoids. The relative abundance of pristane and phytane are closely linked to redox conditions of the initial depositional environment (Didyk et al., 1978; Bylinkin, 1987). For the oils and source rocks in this study, Pr/Ph values range from 0.77 to 1.86. Selected n-alkane and isoprenoid ratios are included in Table 5 and plotted in Figure 24.

Sample	Type	Pr/Ph	Pr/C_{17}	Ph/C_{18}
OI-1	Oil	1.3	1.1	0.8
OI-2	Oil	1.4	1.1	0.8
OI-3	Oil	1.9	1.1	0.8
OI-4	Oil	1.3	1.1	0.8
OI-5	Oil	1.4	1.0	0.8
OI-6	Oil	1.4	1.0	0.8
OI-7	Oil	1.4	1.1	0.8
OI-8	Oil	1.3	1.1	0.8
OI-9	Oil	1.4	1.0	0.8
OI-10	Oil	1.2	0.6	0.6
OI-11	Oil	1.3	0.7	0.7
SR-1	Whole Core	1.2	0.8	0.7
SR-2	Whole Core	0.9	0.6	0.9
SR-3	Whole Core	1.5	0.4	0.4
SR-4	Whole Core	1.0	0.7	0.9
SR-5	Whole Core	1.3	0.9	0.8
SR-6*	Whole Core			
SR-7*	Sidewall Core			
SR-8	Sidewall Core	0.8	0.4	0.7
SR-9	Sidewall Core	0.9	0.5	0.8
SR-10	Sidewall Core	1.0	0.7	0.9
SR-11	Sidewall Core	0.9	0.6	0.8
SR-12	Sidewall Core	0.9	0.5	0.8
SR-13	Sidewall Core	0.9	0.5	0.8
SR-14	Sidewall Core	0.9	0.5	0.7
SR-15	Whole Core	1.8	0.5	0.5
OC-1	Outcrop	1.3	1.0	1.0
AS-1*	Asphalt			
*Data not available				

Table 5: n-Alkane and isoprenoid ratios for Goddard oils and source rock extracts

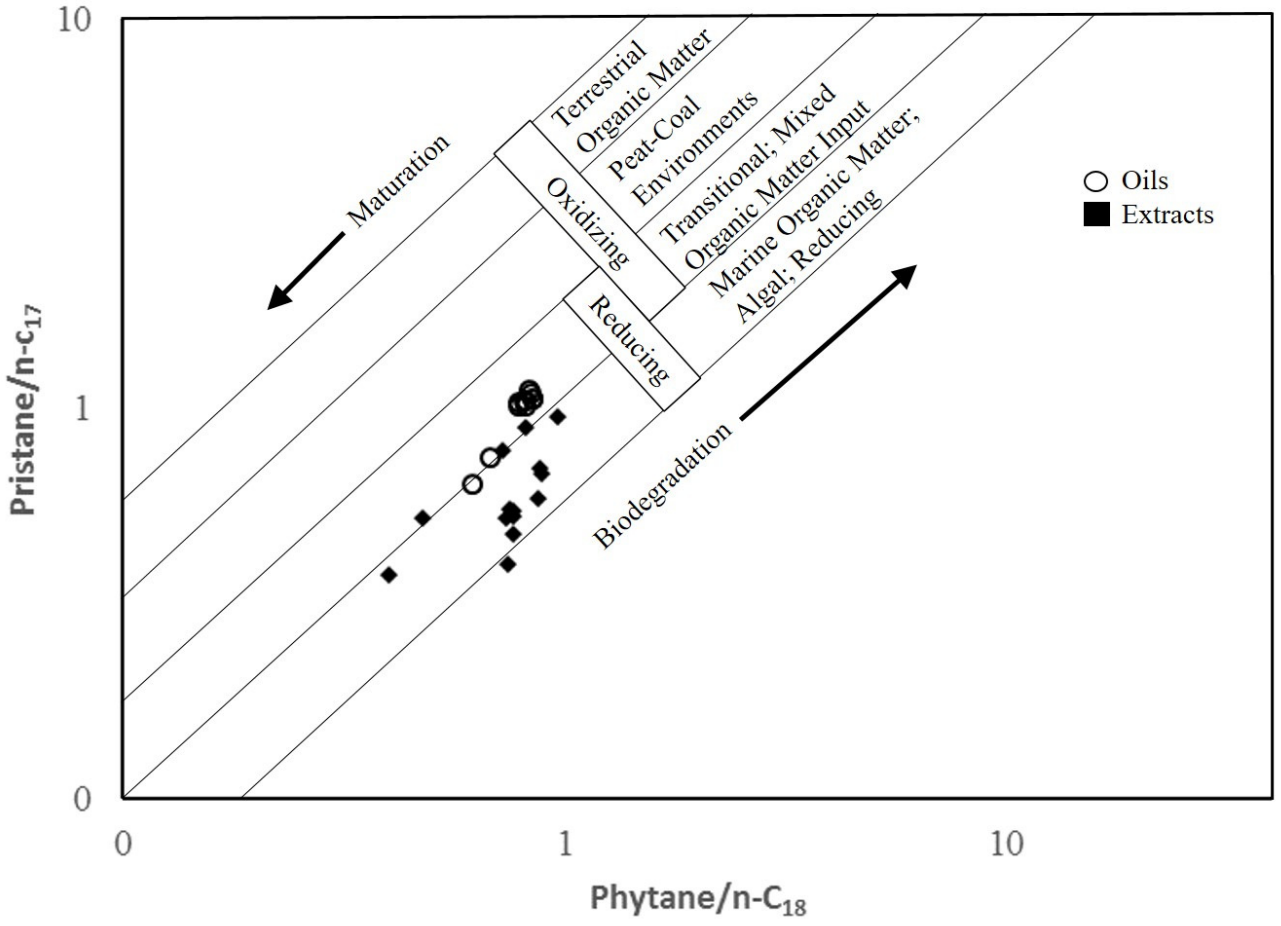

Figure 24: Plot of n-alkane and isoprenoid ratios for Goddard oils and source rock extracts (After Shanmugam, 1985)

Almost all the aliphatic chromatograms for both the oils and source rock extracts shared a similar distribution of n-alkanes as shown in Figure 25a. Most of the aliphatic fractions were dominated by the short-chain C_{12}-C_{18} n-alkanes. The longest-chain n-alkane identified was C_{37}.

The two samples that differed from the distribution described above were OL-3 and SR-15. In OL-3, the aliphatic fraction was dominated by the C_{10}-C_{21} n-alkanes (Figure 25b). The aliphatic fraction of SR-15 was dominated by the C_{14}-C_{33} n-alkanes. Sample SR-15 was also the only sample that had a bimodal distribution of the longer chain n-alkanes; the C_{18}-C_{21} n-alkanes were diminished in SR-15 (Figure 25c).

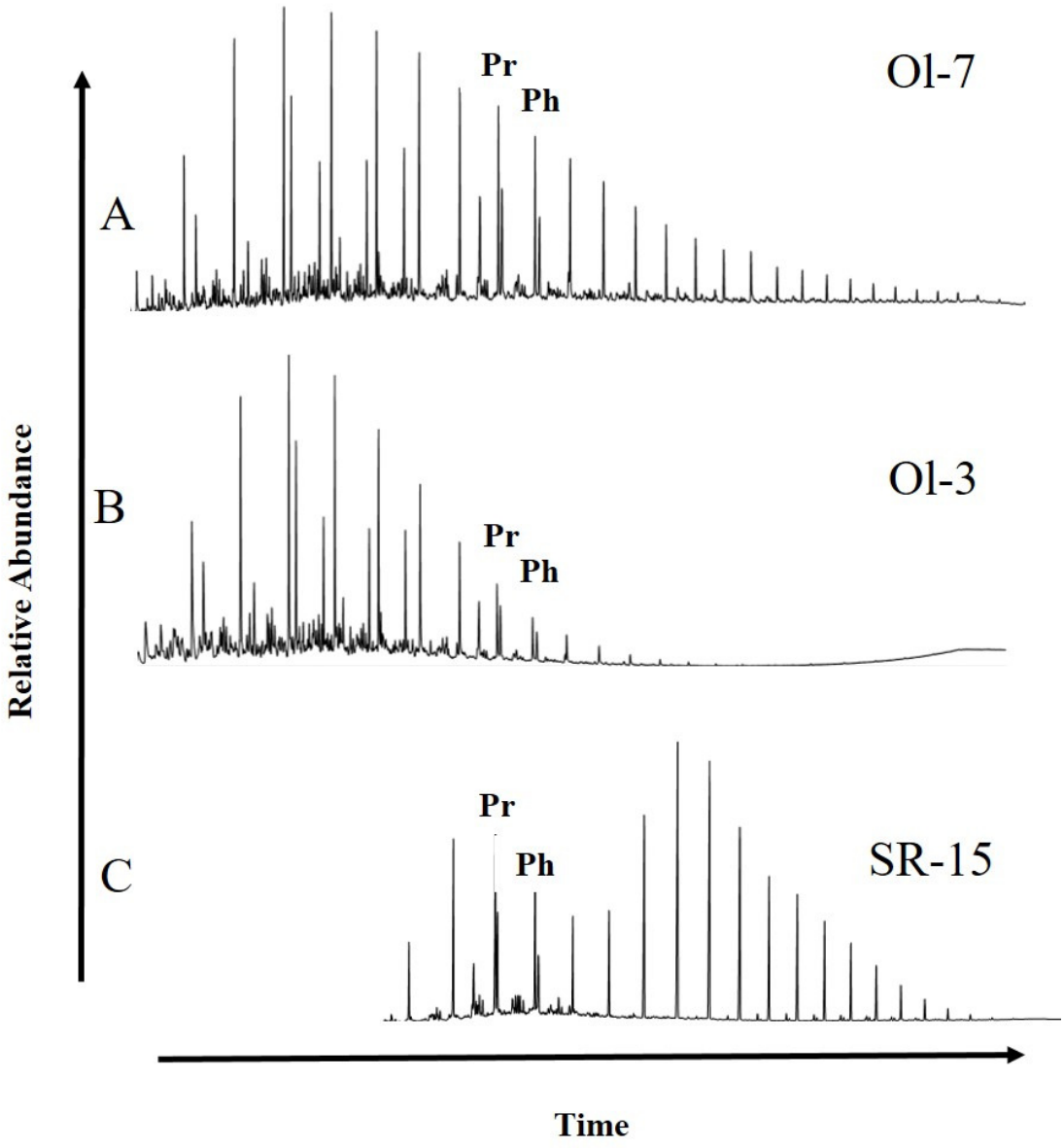

Figure 25: Chromatograms of (a) Ol-7 oil, (b) Ol-3 oil, and (c) SR-15 source rock extract aliphatic fractions. Pristane (Pr) and Phytane (Ph) are labeled

4.3.2. Tricyclic Terpanes

With the exception of AS-1, OC-1, SR-5, and SR-15, the tricyclic terpanes dominated the *m/z* 191 aliphatic chromatograms (Figure 26; Table 6). Sample AS-1, OC-1, and SR-15 all had a more typical distribution of tricyclic terpanes relative to the pentacyclic terpanes (Figure 27; Table 7). The signal intensity in the *m/z* 191 chromatogram for SR-5 was too low to clearly distinguish any hopanes or tricyclic terpanes. Extended tricyclic terpanes were identified out to C_{45} in SR-1. In the majority of oils and rock extracts, the tricyclic terpane series extended to C_{41}. In OC-1, SR-5, and SR-15, the longest extended tricyclic terpanes identified were C_{25}, C_{29}, and C_{23}, respectively.

For the majority of oil and source rock extracts that had an abundant tricyclic terpane signature, the most abundant peak on the *m/z* 191 chromatogram was the C_{23} tricyclic terpane. A smaller number of samples had either the C_{28} or C_{29} tricyclic terpane as their most abundant peak; for these samples, the C_{23} was typically almost equal in abundance to the highest peak. The C_{19} and C_{20} tricyclic terpanes were present in extremely low abundance for all oil and extract samples. The C_{26} tricyclic terpanes co-eluted with the C_{24} tetracyclic terpane. The ratio of the C_{24} to C_{23} tricyclic terpane was calculated for all samples except OC-1, SR-5, and SR-15. In these three rock extracts, the C_{24} and C_{23} tricyclic terpanes were either absent or unable to be clearly quantified. The ratio of the C_{24} to C_{23} tricyclic terpanes for the remaining samples ranged from 0.61 to 1.26. The lowest values were most often associated with rock extracts while the higher values were generally associated with oils.

The tricyclic terpanes have their first chiral center at the C_{22} carbon beginning with

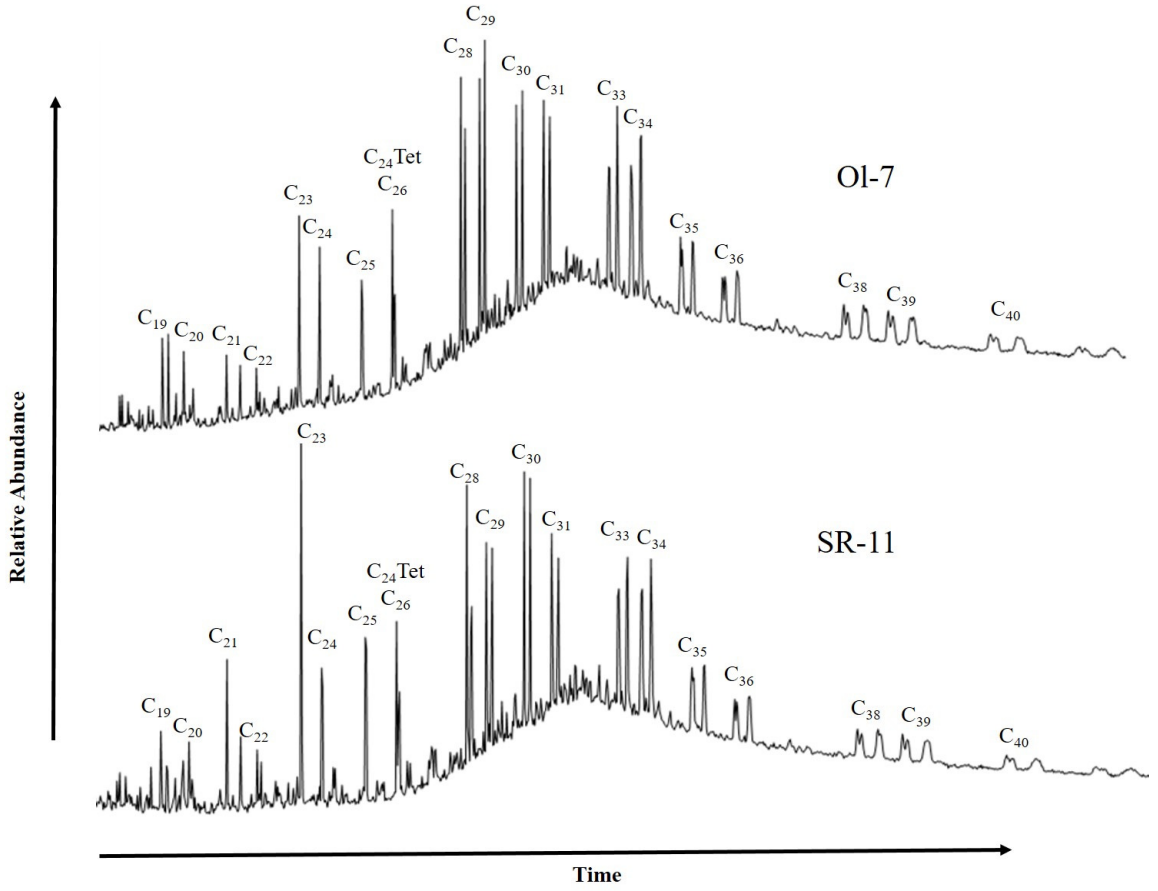

Figure 26: Representative *m/z* 191 chromatograms for Goddard oils and source rocks with abundant tricyclic terpanes. Individual S/R epimers have not been identified for the C_{25} to C_{40} tricyclic terpanes

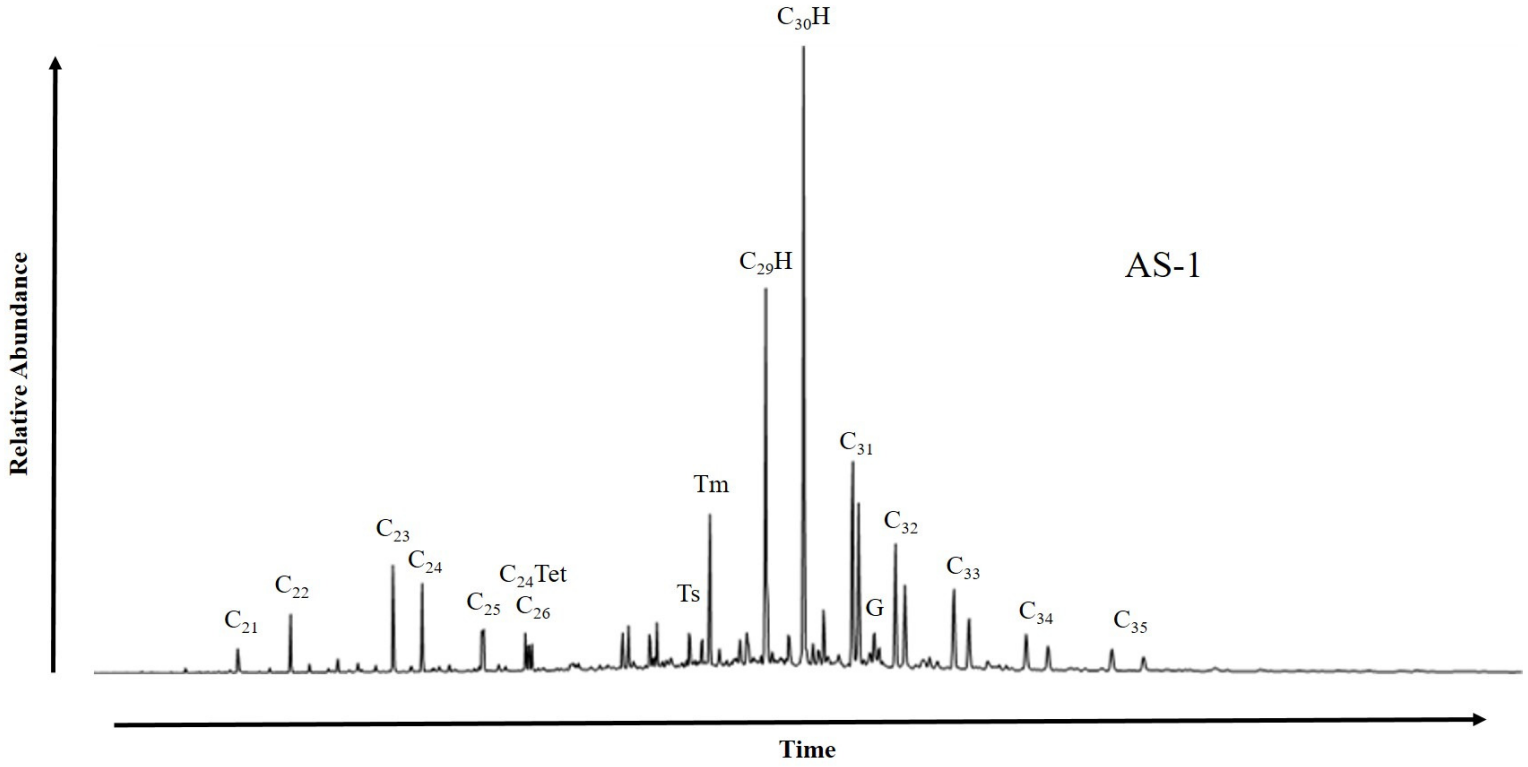

Figure 27: *m/z* 191 chromatogram for sample AS-1 with regular hopane distribution

Peak Label	Compound
C_{19}	C_{19} 13β(H),14α(H)-tricyclic terpane
C_{20}	C_{20} 13β(H),14α(H)-tricyclic terpane
C_{21}	C_{21} 13β(H),14α(H)-tricyclic terpane
C_{22}	C_{22} 13β(H),14α(H)-tricyclic terpane
C_{23}	C_{23} 13β(H),14α(H)-tricyclic terpane
C_{24}	C_{24} 13β(H),14α(H)-tricyclic terpane
C_{25}	C_{25} 13β(H),14α(H)-tricyclic terpane
C_{24} Tet	C_{24} tetracyclic terpane
C_{26}	C_{26} 13β(H),14α(H)-tricyclic terpane
C_{28}	C_{28} 13β(H),14α(H)-tricyclic terpane
C_{29}	C_{29} 13β(H),14α(H)-tricyclic terpane
C_{30}	C_{30} 13β(H),14α(H)-tricyclic terpane
C_{31}	C_{31} 13β(H),14α(H)-tricyclic terpane
C_{33}	C_{33} 13β(H),14α(H)-tricyclic terpane
C_{34}	C_{34} 13β(H),14α(H)-tricyclic terpane
C_{35}	C_{35} 13β(H),14α(H)-tricyclic terpane
C_{36}	C_{36} 13β(H),14α(H)-tricyclic terpane
C_{38}	C_{38} 13β(H),14α(H)-tricyclic terpane
C_{39}	C_{39} 13β(H),14α(H)-tricyclic terpane
C_{40}	C_{40} 13β(H),14α(H)-tricyclic terpane

Table 6: Peak Identification for compounds labeled in the *m/z* 191 aliphatic chromatogram for the tricyclic terpane-rich samples. Individual S/R epimers are not labeled

Peak Label	Compound
C21 T	C_{21} 13β(H),14α(H)-tricyclic terpane
C22 T	C_{22} 13β(H),14α(H)-tricyclic terpane
C23 T	C_{23} 13β(H),14α(H)-tricyclic terpane
C24 T	C_{24} 13β(H),14α(H)-tricyclic terpane
C25 T	C_{25} 13β(H),14α(H)-tricyclic terpane
C_{24} Tet	C_{24} tetracyclic terpane
C_{26}	C_{26} 13β(H),14α(H)-tricyclic terpane
Ts	C_{27} 18β(H)-22,29,30-trisnorneohopane
Tm	C_{27} 17α(H)-22,29,30-trisnorneohopane
C_{29} H	C_{29} 17α(H),21β(H)-norhopane
C_{30} H	C_{30} 17α(H),21β(H)-hopane
C_{31}	C_{31} (22S+22R) 17α(H),21β(H)-homohopane
C_{32}	C_{32} (22S+22R) 17α(H),21β(H)-bishomohopane
C_{33}	C_{33} (22S+22R) 17α(H),21β(H)-bishomohopane
C_{34}	C_{34} (22S+22R) 17α(H),21β(H)-trishomohopane
C_{35}	C_{35} (22S+22R) 17α(H),21β(H)-pentakishomohopane
G	Gammacerane

Table 7: Peak Identification for compounds labeled in the *m/z* 191 aliphatic chromatogram for sample with normal distributions of tricyclic and pentacyclic terpanes

the C_{25} tricyclic terpane (Farrimond et al., 1999; Peters, 2000). The 22S epimer is thought to elute before the 22R epimer because the second eluting isomer appear to be more susceptible to biodegradation (Peters, 2000). For unaltered samples with thermal maturities at or beyond the oil window, the 22S/R ratio for the C_{25}-C_{29} tricyclic terpanes epimers approaches parity.

4.3.3. Pentacyclic Terpanes

Pentacyclic terpanes, or hopanes, are derived from the membrane lipids of prokaryotic organisms (Ourisson et al., 1982). The ubiquity of prokaryotic organisms is reflected in the near universal presence of hopanes in oils and sediments associated with all types of organofacies. As Ourisson and Albrecht (1992) described them, the hopanes are the "most abundant family of complex organic substances on earth."

Hopanes were evaluated using both SIM GCMS (*m/z* 191) and GCMSMS. For the *m/z* 191 chromatograms, only samples OC-1, AS-1, and SR-15 had any detectable hopanes. The OC-1 extract had abundant hopanes from C_{30} to C_{35}. The AS-1 asphalt extract had particularly well preserved hopanes (Figure 27). In both OC-1 and AS-1, the abundance of the homohopanes decreased incrementally from C_{31} to C_{35} (Table 7). For SR-15 , the C_{29} to C_{35} hopanes were detected although the C_{34} and C_{35} homohopanes were only present in low abundance. The *m/z* 191 chromatograms for all other samples were dominated by the tricyclic terpanes. For these tricyclic terpane-rich samples, additional GCMSMS analyses revealed only trace amounts of the C_{30} hopane and the homohopanes.

While hopanes are mainly used for correlation of oils and source rocks, they can also

be used as biodegradation proxies (Ourisson and Albrecht, 1992). The 25-norhopanes, also known as the demethylated hopanes, are a series of compounds derived from the regular hopanes (McCaffrey et al., 1996; Peters et al., 1996). These demethylated hopanes appear once biodegradation has reached heavy to severe levels (Wenger et al., 2002). When present, the C_{29} 25-norhopane can be observed using SIM GCMS (*m/z* 191 and *m/z* 177). No 25-norhopanes were observed in any of the Goddard samples.

Hopanes are also affected by thermal stress (Peters and Moldowan, 1991; Ourisson and Albrecht, 1992). For example, with increasing thermal stress, the relative abundance of hopanes to tricyclic terpanes decreases (Seifert and Moldowan, 1978). After thermal maturity has reached the condensate window, it is possible for hopanes to be entirely obscured by more resilient biomarkers such as the tricyclic terpanes.

Specific terpanes can also be used to infer depositional conditions. For example, gammacerane is a C_{30} pentacyclic triterpane associated with stratified water columns (Sinninghe Damasté et al., 1995). Conditions that favor stratified waters also tend to favor increased salinity; therefore, gammacerane is loosely associated with hypersaline depositional conditions (Sinninghe Damasté et al., 1995). A possible gammacerane peak was observed in the *m/z* 191 chromatogram of AS-1. Gammacerane was not observed in any samples with abundant tricyclic terpanes.

4.3.4. Steranes

Steranes were determined using SIM GCMS (*m/z* 217 and *m/z* 218). These compounds have a variety of precursors. Each of the regular steranes is believed to be at least

partially derived from algae (Huang and Meinschein, 1979). Cholestane (C_{27}) is specifically sourced from red algae as well as phytoplankton (Huang and Meinschein, 1979). Ergostane (C_{28}) is strongly associated with various fungal precursors as well as diatoms and phytoplankton (Huang and Meinschein, 1979; Volkman, 1986; Weete et al., 2010). Stigmastane (C_{29}) is associated with higher land plants as well as green algae (Huang and Meinschein, 1979; Volkman, 1986). There is increasing evidence that bacteria may also be able to biosynthesize sterols (Pearson et al., 2003).

The variety and overlap of regular sterane precursors is the primary reason that steranes are poor indicators of depositional environment (Moldowan et al., 1985). One exception is 24-n-propylcholestane, which is derived from 24-n-propylsterols synthesized by the modern marine algae order *Sarcinochrysidales* (Moldowan et al., 1990). The relationship between 24-n-propylcholestanes and marine oils and source rocks has been well demonstrated (Peters et al., 1986; Moldowan et al., 1990). The presence of 24-n-propylcholestanes was confirmed in all Goddard samples.

While the utility of steranes for organofacies interpretation is variable, the relative abundances of the regular steranes is useful for correlation (Moldowan et al., 1985). For all the Goddard samples, the dominant regular sterane was C_{27}; the C_{29} regular sterane was the next most abundant. The C_{28} regular steranes were typically present in low abundance. A representative *m/z* 218 chromatogram is shown in Figure 28. For OC-1, SR-15, and AS-1, the C_{29} sterane was most abundant followed by C_{27} and C_{28} (Figure 29). The overall abundance of steranes was very low in both oil and source rocks extracts.

Regular steranes are also used as thermal maturity proxies. Thermal stress is primarily reflected in the isomerization of the steranes. Thermal stress causes isomerization at C_{14}

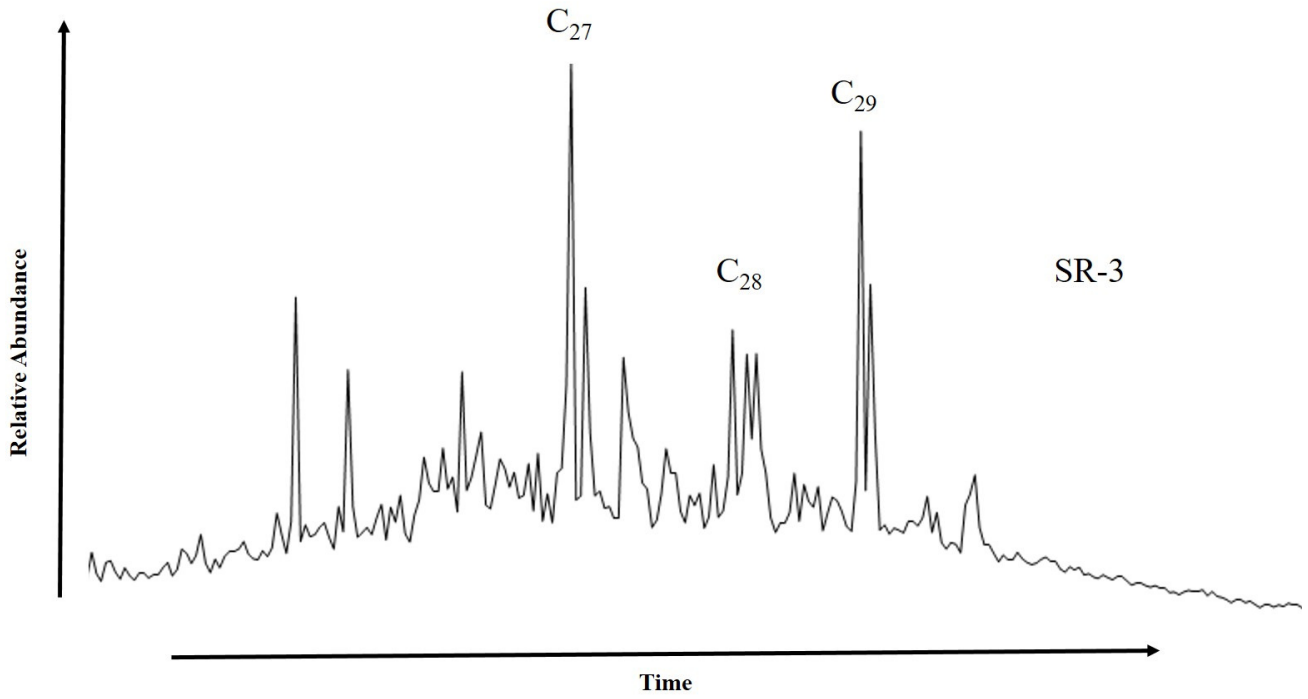

Figure 28: *m/z* 218 chromatogram for SR-3. Peaks for the C_{27}, C_{28}, and C_{29} 5α(H),14β(H),17β(H) 20S and 20R steranes are labeled

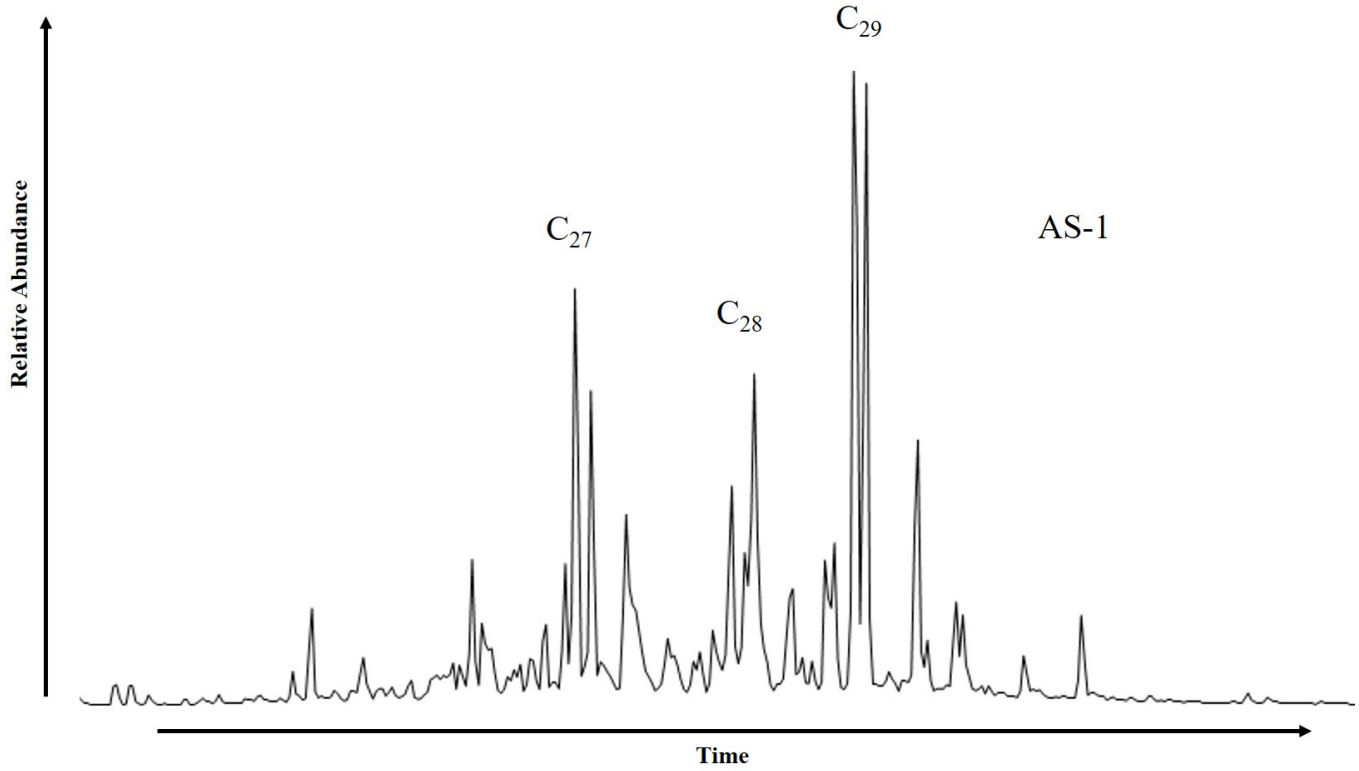

Figure 29: *m/z* 218 chromatogram for AS-1. Peaks for the C_{27}, C_{28}, and C_{29} 5α(H),14β(H),17β(H) 20S and 20R steranes are labeled

and C_{17} for regular steranes; in thermally immature samples, the ratio of $\beta\ \beta$/($\alpha\ \alpha$+$\beta\ \beta$) isomers hovers around 0.25 and increases to 0.7 by the late oil window (Seifert and Moldowan, 1986). The ratio of $\beta\ \beta$/($\alpha\ \alpha$+$\beta\ \beta$) isomers for the C_{27}, C_{28}, and C_{29} regular steranes appeared to have reached the equilibrium point in all samples except OC-1.

Unlike the regular steranes, the monoaromatic steranes (MAS) may be used to classify depositional environment as well as thermal stress (Moldowan et al., 1985). There is less overlap in the distributions of the C_{27}-C_{29} MAS relative to the regular steranes (Moldowan et al., 1985). The difference in distribution is attributed to MAS being preferentially derived from a more limited set of sterol precursors than the regular steranes (Mackenzie, 1982; Moldowan et al., 1985). The MAS were observed using SIM GCMS (*m/z* 253) but were absent from all samples except the OC-1. In OC-1, MAS appeared to be present but were too highly degraded to be interpreted. Triaromatic steranes (TAS), observed using SIM GCMS (*m/z* 231), were present in all samples. Two representative chromatograms are shown in Figure 30. The TAS are thought to be form from thermally degraded MAS (Moldowan et al., 1985). The ratio of TAS relative to the sum of both TAS and MAS reaches one by the late oil window (Mackenzie et al., 1981; Mackenzie et al., 1982). Short-chain homologs (C_{20}-C_{22}) of both the MAS and TAS were present only in low abundance.

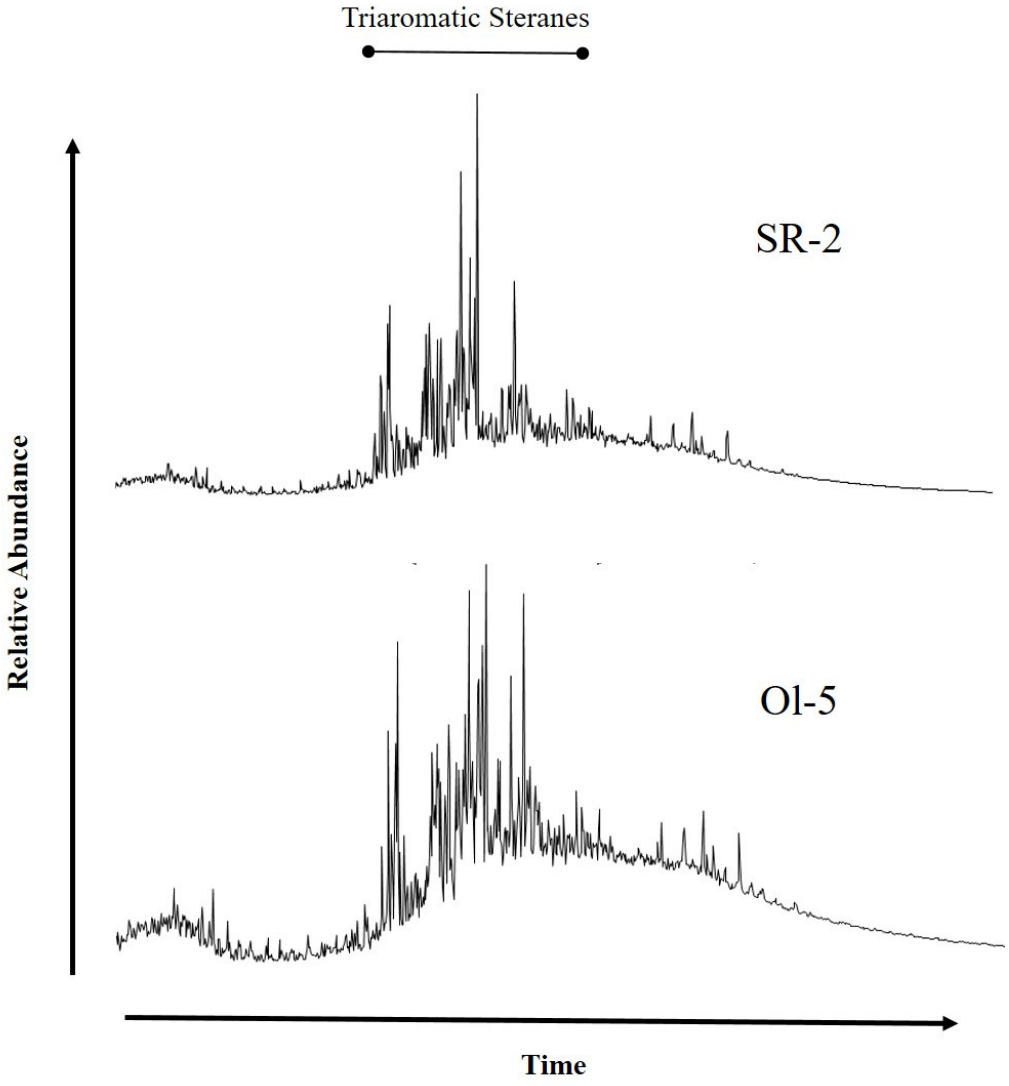

Figure 30: *m/z* 231 chromatogram for abundant TAS in SR-2 and Ol-5

4.3.5. Sesquiterpenoids

Bicyclic sesquiterpanes such as drimane and homodrimane are used as alteration proxies. Both compounds are less resistant to biodegradation than steranes and hopanes (Williams at al., 1986; Wenger et al., 2002). The presence of either drimane or homodrimane in all of the Goddard samples indicates that only slight biodegradation has occurred (Williams et al., 1986; Wenger et al., 2002).

Bicyclic sesquiterpanes can also be used for correlation. All samples contained low to moderate amounts of drimane (Figure 31a). Drimane was always present in greater abundance relative to homodrimane in the Goddard samples. The slight variation in the abundance of drimane for the Goddard samples is worth noting as other biomarker parameters, such as the regular steranes and tricyclic terpanes, do not vary much within the Goddard. The precursor for drimane is unknown but the ubiquity of drimane supports a microbial source (Alexander et al., 1983). Variation in the abundance of drimane may be related to variation in microbial organic matter input. Homodrimane was present in low abundance in all samples except AS-1 (Figure 31b). Homodrimane was also present in greater abundance relative to drimane in AS-1.

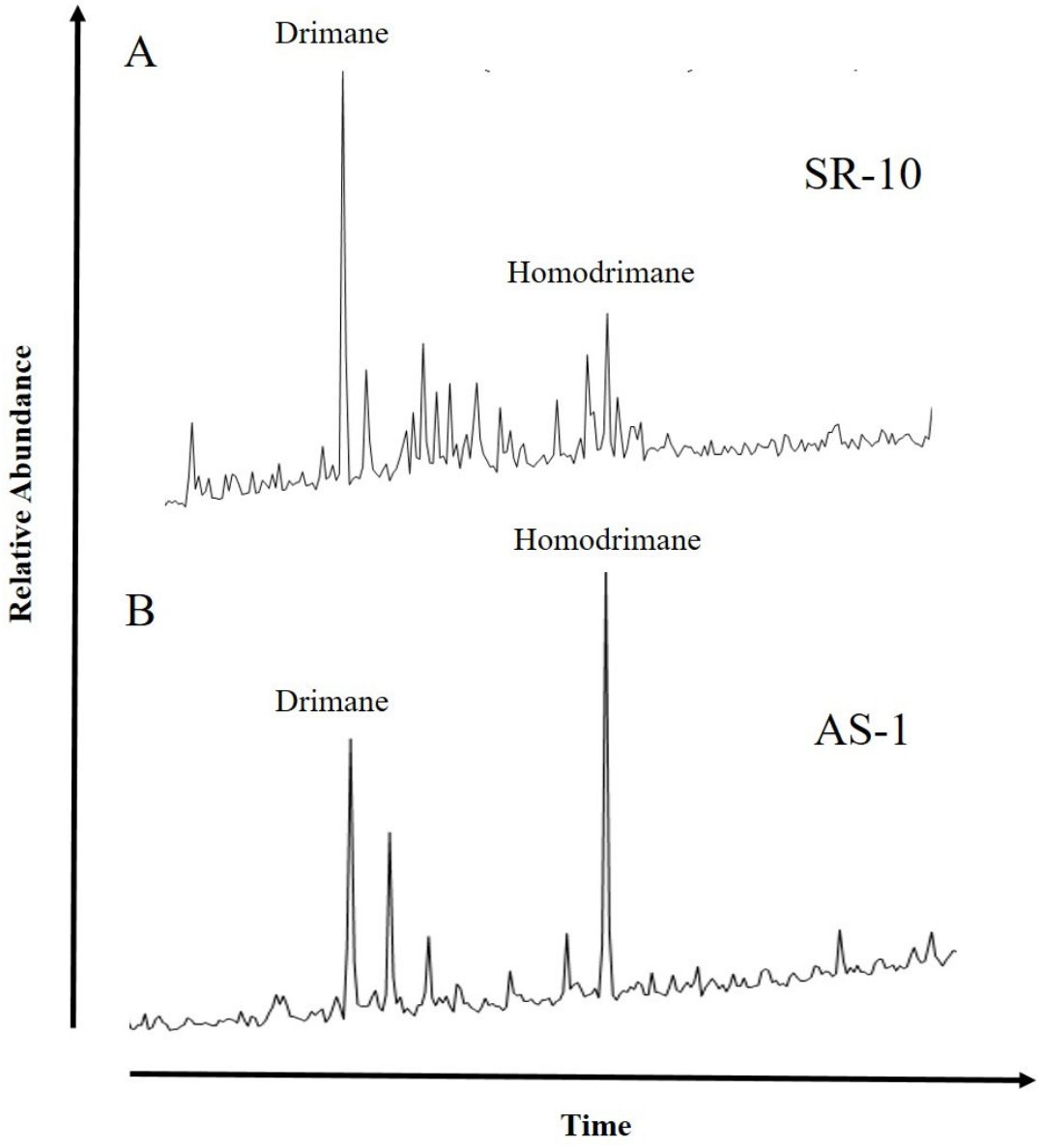

Figure 31: *m/z* 123 chromatogram for (a) SR-10 and (b) AS-1

4.3.6. Aryl Isoprenoids

Aryl isoprenoids are derived from biomarkers whose precursors are sulphur bacteria (Summons and Powell, 1987). These bacteria thrive under conditions of photic zone anoxia (Connock, 2015) and are associated with hypersaline depositional conditions (Summons and Powell, 1987). Aryl isoprenoids can be observed in both the *m/z* 133 and *m/z* 134 ion chromatograms using GCMS SIM. Aryl isoprenoids were absent in all samples except OC-1, SR-15, and AS-1. In both the OC-1 and SR-15, a series of aryl isoprenoids was easily identified (Figure 32a). The AS-1 asphalt extract appeared to have a less evident series of aryl isoprenoids. For all other samples lacking aryl isoprenoids, abundant alkyl and methyl benzenes were observed (Figure 32b). The three samples that contained aryl isoprenoids were also the only samples that has abundant hopanes rather than tricyclic terpanes.

4.3.7. Pyrogenic Polycyclic Aromatic Hydrocarbons (PAHs)

Highly peri-condensed PAHs, such as benzo(a)pyrene (B(a)P), benzo(e)pyrene (B(e)P), benzo(ghi)perylene (B(ghi)Per), and perylene (Pe) are considered to be indicators of high-temperature, organic matter alteration (Arinobu et al., 1999; Kaiho et al., 2013). As environmental indicators, the pyrogenic PAHs are therefore associated with wildfires and the combustion of higher plants (Arinobu et al., 1999; Hasegawa, 2001; Kaiho et al., 2013; Marynowski et al., 2015). Some of the pyrogenic PAHs are known to have additional sources unrelated to forest fires. For example, a biologic precursor for perylene is thought to be present in fungi (Grice et al., 2009) while benzo(e)pyrene is

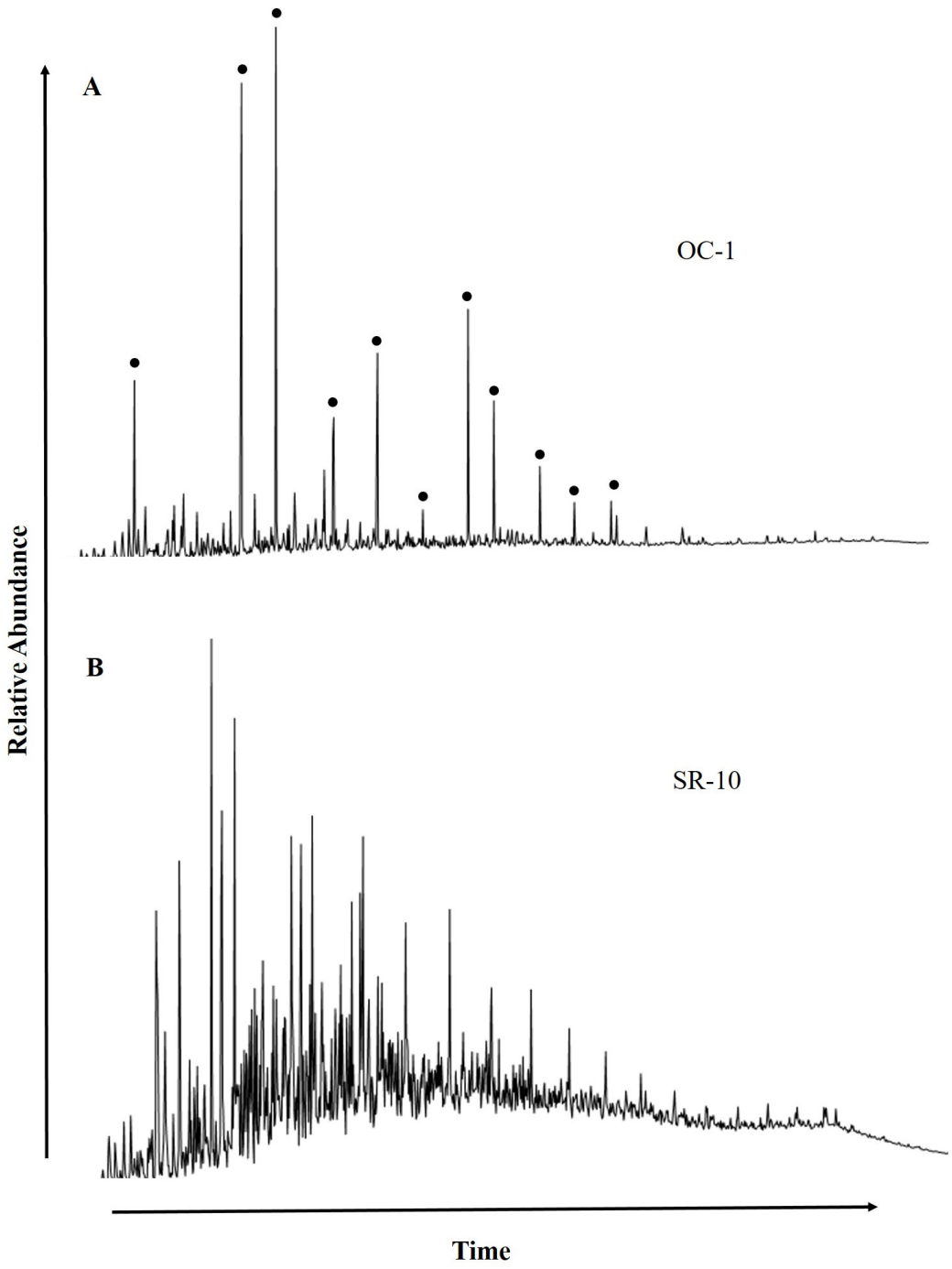

Figure 32: *m/z* 133 chromatogram for (a) OC-1 and (b) SR-10. Filled circles indicate the aryl isoprenoids present in OC-1. Note the absence of the aryl isoprenoids in SR-10

thought to be sourced from algae when found in source rocks deposited under euxinic marine conditions (Grice et al., 2007). The presence of pyrogenic PAHs in marine source rocks is also associated with erosion following forest fires (Kaiho et al., 2013). The abundance of pyrogenic PAHs can be compared with higher plant biomarkers to distinguish unaltered plant matter input from oxidized plant matter associated with wildfire events (Kaiho et al., 2013). Thermal stress can rapidly degrade pyrogenic PAHs. Perylene is completely degraded by 0.7 %Ro and only trace amounts of benzo(a)pyrene remain by 0.8 %Ro (Marynowski et al., 2015). Laboratory experiments have demonstrated that benzo(e)pyrene and benzo(ghi)perylene likely form from thermally degraded perylene (Marynowski et al., 2015).

Pyrogenic PAHs were observed using GCMS SIM (*m/z* 252 and *m/z* 276). In the oils and source rocks of the Goddard, the only pyrogenic PAHs observed were B(e)P and B(ghi)P. Figure 33 displays several *m/z* 252 chromatograms that are representative of the distribution of B(e)P for the Goddard samples. The B(e)P was observed in moderate abundance in SR-8, SR-9, SR-10, SR-11, SR-12, SR-13, and SR-14 and low relative abundance in SR-1, SR-2, SR-3, SR-4, and SR-5. The B(ghi)P was observed in trace abundances only in SR-8, SR-9, SR-10, SR-11, SR-12, SR-13, and SR-14.

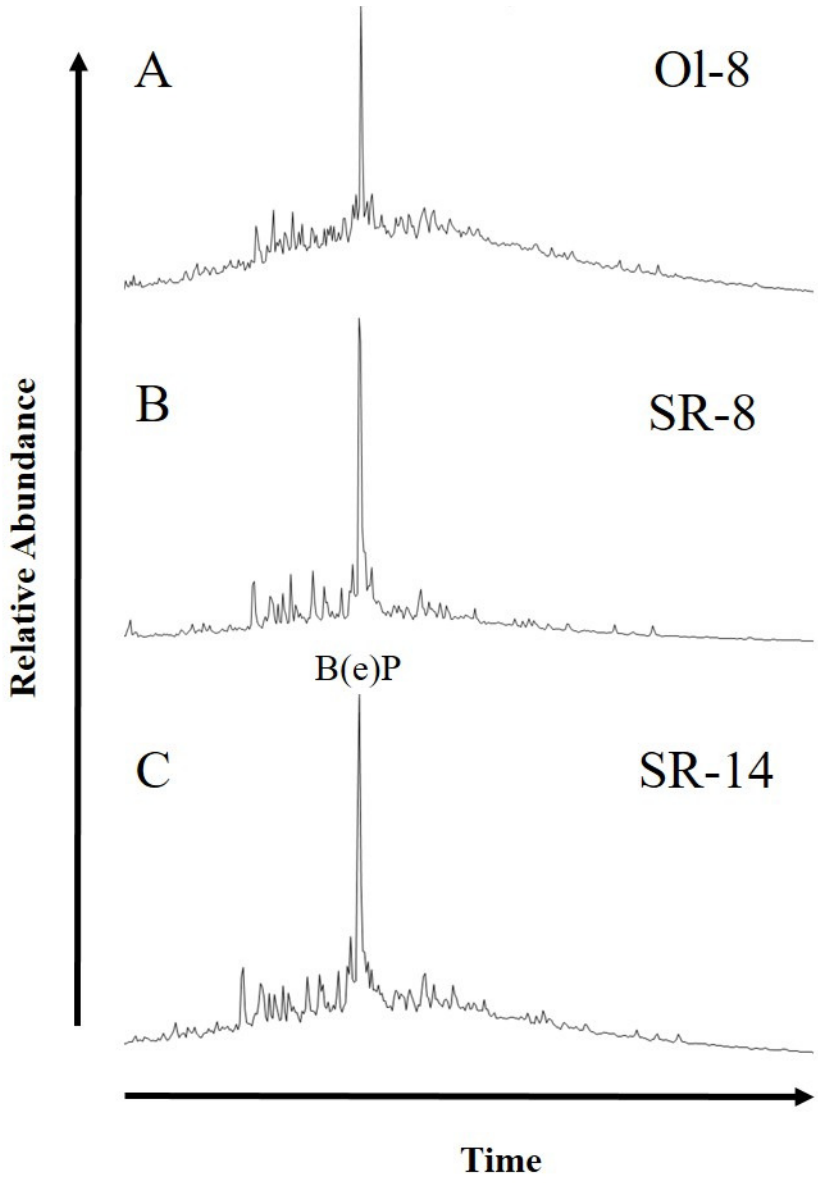

Figure 33: *m/z* 252 chromatogram for (a) Ol-8, (b) SR-8, and (c) SR-14. The peak for benzo(e)pyrene (B(e)P) is labeled

5. Discussion

The objective of this study was to characterize regional trends in the organic geochemistry. Prior to this study, geochemical interpretations for the Goddard Formation were limited to a handful of samples from surveys of source rocks and oils in the Anadarko Basin (Jones and Philp, 1990; Kim and Philp, 2001; Wang and Philp, 2001). While thorough geochemical analyses were conducted for these samples, interpretations were geographically limited and not truly applicable to a regional interpretation of the Goddard Formation.

Results from this study were used to develop an organofacies interpretation for the Goddard based on the model established by Pepper and Corvi (1995). Regional trends in thermal maturity and biodegradation for Goddard samples within the SCOOP were also observed. These interpretations were in turn used to evaluate the feasibility of various mechanisms for tricyclic terpane enrichment. Finally, a signature assemblage of biomarkers was identified and applied to oil and source rock correlation.

5.1. Organofacies

Characteristics of the organofacies defined by Pepper and Corvi (1995) are reviewed in Section 1.3 (Figure 3). Bulk geochemical and biomarker data from this study support that the Goddard most closely aligns with the Type B organofacies. The Type B organofacies is associated with marine environments, siliciclastic sedimentation, and algal and bacterial organic matter. The equivalent kerogen classification would be a Type II marine kerogen (Pepper and Corvi, 1995).

The abundance of the aliphatic fraction relative to the aromatic is loosely correlated with depositional environment. For the majority of Goddard oils and extracts, the aliphatic fraction is 75-90% of the extract. The abundant aliphatic fraction relative to the aromatic fraction suggests a clastic-rich depositional environment equivalent to a Type B organofacies (Peters et al., 2005). High thermal maturity also contributes to a relatively abundant aliphatic fraction. The SEM analysis confirms the clay-rich lithology of the Goddard. The low wax content of the n-alkanes for the oils and source rocks also supports a normal marine, Type B organofacies over a lacustrine Type C organofacies. Precursors associated with freshwater algae are also associated with waxier lipids than marine algae (Pepper and Corvi, 1995; Waples and Curiale, 1999).

Pristane and phytane are both isoprenoid hydrocarbons derived primarily from phytol, a component of chlorophyll a (Bendoraitis et al., 1962; Brooks et al., 1969; Didyk et al., 1978). Bacterial lipids and zooplankton may also be minor sources of pristane, phytane, phytol, and other intermediate precursors (Blumer and Thomas, 1965; Maxwell et al., 1971; Didyk et al., 1978). Organic matter input can also influence the abundance of pristane to phytane; greater abundances of pristane are often seen in source rocks associated with waxy, terrestrial plant matter (Brooks et al., 1969).

The relative abundance of pristane to phytane is correlated with redox conditions. Anoxic deposition conditions are thought to favor the preservation of phytane while oxic conditions hasten the degradation of phytane (Didyk et al., 1978). Therefore, Pr/Ph values below 0.8 are associated with anoxic depositional conditions while values greater than 3.0 are associated with oxic conditions (Didyk et al., 1978). The Pr/Ph values between 0.8-3.0 are not considered highly specific on their own. The Pr/Ph values for the oils and

source rocks in this study range from 0.77 to 1.86. The value at .77 is still considered to be within the non-specific range for the Pr/Ph value.

Although the Pr/Ph values for the Goddard are not within the diagnostic ranges, Pr/Ph values for the Goddard samples are still consistent with siliciclastic lithology and marine depositional environments (Moldowan et al., 1985; Peters and Moldowan, 1993). The Pr/Ph values between 0.8 and 3.0 can also be corroborated with additional biomarker parameters for more specific interpretations. For example, low abundances of C_{27} diasteranes with low Pr/Ph values have been correlated to anoxic redox conditions (Moldowan et al., 1986). Abundant diasteranes in most of the Goddard samples supports suboxic to normal rather than anoxic redox conditions (Moldowan et al., 1986).

The methyltrimethyltridecylchroman (MTTC) ratio is another parameter that can be compared to the Pr/Ph (Sinninghe Damasté et al., 1993). The MTTC ratio compares the trimethyl chroman isomer to the abundance of all the methyl chromans (Sinninghe Damasté et al., 1993). This ratio is used as a paleosalinity indicator; under normal marine conditions, the trimethyl isomer is by far the most abundant of the chromans (Sinninghe Damasté et al., 1987; Sinninghe Damasté et al., 1993). The trimethyl isomer was the only chroman detected in both the extracts and oils (Figure 34). The MTTC ratios was therefore approximately one for all samples. Correlation with Pr/Ph values suggests a normal saline depositional environment for the Goddard (Sinninghe Damasté et al., 1993).

The presence of the 24-n-propylcholestanes in all oils and source rocks is a high-confidence indicator of marine algae and therefore an open marine environment. The C_{24}/C_{23} tricyclic terpane ratio helps distinguish the Type A marine carbonate organofacies from Type B marine siliciclastic organofacies (Zumberge et al., 2000). The ratio of

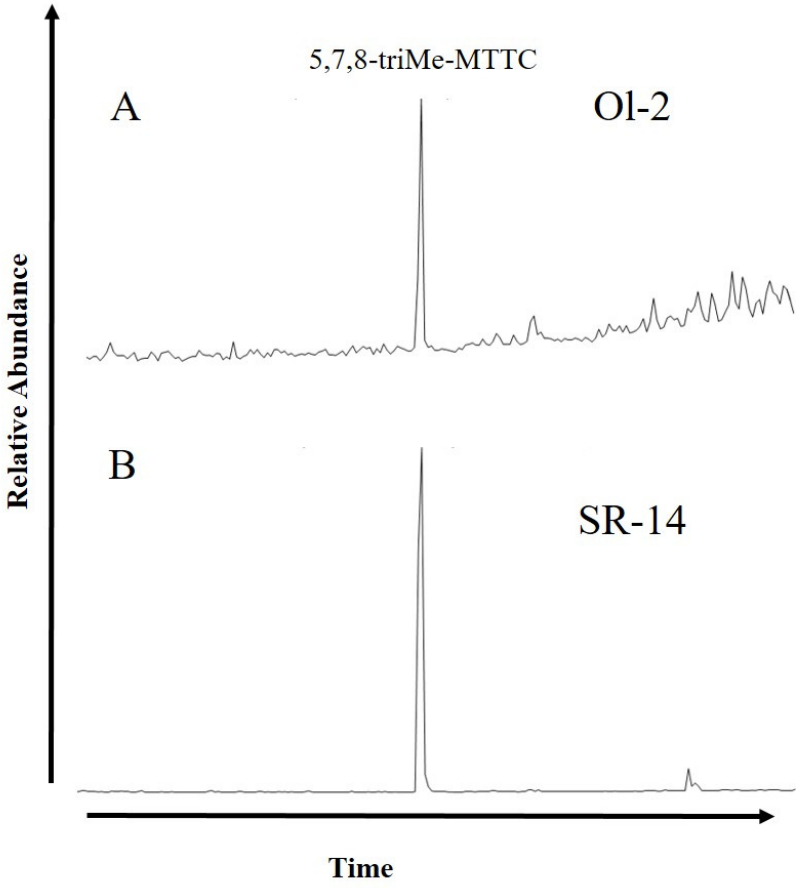

Figure 34: m/ *m/z* 149 chromatogram for (a) Ol-2 and (b) SR-14. The trimethyl isomer is labeled (5,7,8-triMe-MTTC)

C_{24}/C_{23} is greater than 0.6 for all Goddard oils and extracts, which is consistent with marine and paralic shales rather than carbonate or marl source rocks (Zumberge et al., 2000). The C_{25}/C_{26} tricyclic terpane ratio distinguishes the Type B marine from Type C lacustrine organofacies (Zumberge et al., 2000). The dominance of C_{25} relative to C_{26} also supports a Type B marine organofacies over a Type C lacustrine organofacies. The low abundance of both the C_{19} and C_{20} tricyclic terpanes in the oils and source rock extracts terpanes implies that the source rock is neither a freshwater, lacustrine organofacies nor one of the terrestrial organofacies (Tao et al., 2015).

The low abundance of gammacerane and the absence of aryl isoprenoids in the Goddard source rocks and oils has several potential explanations. It is possible that the precursor organisms for gammacerane and the aryl isoprenoids were simply not present during the deposition of the Goddard. As a result of the Ouachita Orogeny, the Anadarko Basin was increasingly isolated during the Late Mississippian. The Serpukhovian mass extinction also caused a decrease in biodiversity across the globe (Shi and Waterhouse, 2010; Qiao and Shen, 2014). These circumstances could have led to a homogeneous and slowly-changing biologic community in the Anadarko Basin that lacked the precursor organisms for gammacerane and the carotenoid-derived aryl isoprenoids. A simpler explanation is that water column stratification and photic zone anoxia did not occur during deposition of the Goddard Formation as aryl isoprenoids are indicative of such conditions. For example, aryl isoprenoids are highly specific for the Woodford Shale; this formation was deposited during a global anoxic event when photic zone anoxia was well established (Connock, 2016). The moderately high Pr/Ph values already suggest that anoxic and euxinic conditions were absent during the deposition of the Goddard. Gammacerane and

aryl isoprenoids are also loosely correlated with hypersaline conditions. The presence of extended tricyclics in all samples but OC-1, AS-1, and SR-15 suggests that salinity levels were only normal to slightly elevated during the deposition of the Goddard (Mello et al., 1988). Extended tricyclic terpanes are typically reduced or absent in in the oils and source rocks associated with hypersaline depositional environments (Philp et al., 1989; de Grande et al., 1993). Normal salinity is consistent with the high MTTC ratios mentioned previously. Abundant aryl isoprenoids and relatively low tricyclic terpanes in OC-1, AS-1, and SR-15 suggest that these three source rocks were deposited under different conditions than the Goddard samples described above. These three source rocks may even be from a different formation; the presence of aryl isoprenoids in source rocks in Oklahoma is closely associated with the Woodford Shale (Connock, 2015). Aryl isoprenoids and additional biomarker parameters for the Woodford Shale suggest photic zone anoxia and a highly stratified water column (Connock, 2015).

The presence of fusinite macerals in SR-14 and moderately abundant B(e)P in many of the extracts suggest a contribution of organic matter from wild fires to Goddard sediments (Arinobu et al., 1999; Hasegawa, 2001; Kaiho et al., 2013; Marynowski et al., 2015). The Pr/Ph values above 0.8 and a lack of aryl isoprenoids support that B(e)P originates from higher plants rather than algal organic matter deposited in euxinic conditions (Grice et al., 2007.) The absence of PAHs such as Pe and B(a)P can be attributed to the high thermal maturity of the source rocks samples; if either Pe or B(a)P were present in the Goddard, they would have been completely thermally degraded by 0.8 %Ro (Marynowski et al., 2015). Increased seasonality during the LPIA would have favored seasonal wildfires and continual input of burnt organic matter (Shi and Waterhouse, 2010). Atmospheric

oxygen levels above 30% during the Late Mississippian would also have been conducive to wildfires (Graham et al., 1995; Shi and Waterhouse, 2010). A minor contribution of terrestrial organic matter is still compatible with the characterization of the Goddard Formation as a Type B organofacies. Erosion following wildfires could have dispersed burnt plant matter into paralic and marine settings, although fusinite deposition is likely limited to proximal, rather than deep marine, depositional environments (Scott and Jones, 1994).

5.2. Thermal Maturity

Trends in T_{max} and calculated vitrinite reflectance for the Goddard source rocks (Table 2) are consistent with overall trends in thermal maturity for the Anadarko Basin (Carter et al., 1998). Maturity values are similar to the stratigraphically proximal Woodford Shale (Cardott, 2012b). A comparison of n-alkanes to isoprenoid shows that the Goddard samples are thermally mature and have not been greatly affected by biodegradation (Shanmugam, 1985). Sample OC-1 is the only immature sample in this study. The thermal maturities of the remaining extracts fall within late oil window. This assessment is consistent with the reports that unconventional Goddard production in the SCOOP is approximately 50% oil and 75% liquid overall (Continental Resources, 2014).

The low abundance of hopanes in both oils and extracts rendered many of the hopane-based thermal maturity parameters unusable. The overall scarcity of hopanes would seem to indicate severe thermal alteration. However, the level of thermal stress required to completely degrade the hopanes would also severely degrade the n-alkanes, isoprenoids,

tricyclic terpanes, and steranes. No such alteration was observed in any samples lacking hopanes. The use of tricyclic terpanes for thermal maturity proxies was also avoided, as the general abundance of tricyclic terpanes did not appear to be related to thermal stress.

The equilibrium value of the $\beta\ \beta$/($\alpha\ \alpha$+$\beta\ \beta$) ratio for regular sterane isomers appears to have been reached for all oils and extracts except OC-1. The equilibrium value for this ratio is typically reached around the end of the late oil window (Seifert and Moldowan, 1986) which is consistent with the calculated vitrinite reflectance for the source rocks and the condensate-like appearance of many of the oils.

The ratio of TAS/(TAS+MAS) in both oil and source rocks samples appears to have reached the equilibrium value of one. This parameter indicates that the maturity of these samples has at least reached the late oil window (Mackenzie et al., 1982). The relative abundance of short-chain (C_{21}-C_{22}) homologs for both the MAS and TAS serves as a maturity parameter for highly mature samples and is applicable from the late oil window into the condensate window (Mackenzie et al., 1981; Riolo et al., 1986). With increasing maturity, these short-chain homologs become more abundant relative to the regular MAS and TAS (Mackenzie et al., 1981; Riolo et al., 1986). The low abundance of these short-chain homologs indicates that the maturities for both oil and source rocks samples have not progressed much farther than the beginning of the late oil window (Mackenzie et al., 1981; Riolo et al., 1986). These observations are consistent with the vitrinite reflectance values for the source rock extracts (Mean %Ro=1.0) as well as the inferred thermal maturity for the oils.

5.3. Biodegradation

An initial review of the n-alkane and isoprenoid distributions for Goddard oils suggests that the extent of biodegradation for all samples is slight at most. The overall distribution of the n-alkanes conforms to the typical distribution for a mature, nondegraded oil. Exceptions include AS-1 where n-alkanes have been entirely degraded and SR-15 which lacks n-alkanes below C_{15} and also displays reduced C_{18}-C_{21} n-alkanes. A relative comparison of n-alkanes and isoprenoids suggests only slight biodegradation for the Goddard oils (Shanmugam, 1985; Figure 24). A B-F plot also supports that most of the oils group are only slightly biodegraded (Thompson, 1987; Figure 22).

Whole oil-gas chromatograms for the Goddard oils indicate the possibility mixing, such that a later charge of either oil or condensate may have obscured evidence of early biodegradation. However, mechanisms for mixing in an unconventional mudstone reservoir are uncertain. Evidence for mixing or multiple episodes of generation is insufficient to assert that any heavy or severe biodegradation could have been masked by mixing of biodegraded and fresh oil.

The presence of regular steranes, TAS, and tricyclic terpanes also supports that biodegradation has at most been slight (Wenger, 2002). The low abundance of hopanes and MAS might be assumed as an indicator of heavy to severe biodegradation. However, as previously discussed, the low abundance of MAS is likely caused by the high thermal maturity of both oils and source rocks. The severe levels of biodegradation required to affect the MAS would also degrade the tricyclic terpanes, TAS, and n-alkanes (Wenger, 2002), and these biomarkers are all abundant in the Goddard oils and source rocks. The

low abundance of hopanes is likely related to the Goddard's organofacies and not severe levels of biodegradation.

No 25-norhopanes were observed in any of the oils. The 25-norhopanes are thought to form during microbial methylation of hopanes (McCaffrey et al., 1996; Peters et al., 1996). Production of the 25-norhopanes is thought to possible only under anaerobic conditions (Bennett et al., 2007). The absence of 25-norhopanes may indicate that anaerobic conditions were not achieved during the biodegradation of the Goddard oils. Additional biomarker parameters only suggest that slight to moderate biodegradation has affected the Goddard oils. If the Goddard oils were mixtures of heavily biodegraded and unaltered oils, then the addition of fresh oil would also have replenished some of the more conspicuously absent biomarkers such as the hopanes and steranes. Therefore, it is proposed that the level of biodegradation affecting the Goddard oil is at most slight.

5.4. Tricyclic Terpane Signature

Abundant tricyclic terpanes are often explained by thermal maturity, biodegradation, and the presence of *Tasmanite* fossils (Zhusheng et al., 1988; Kruge et al., 1990a; Kruge et al., 1990b; Philp et al., 1992; Simoneit et al., 2005). Occasionally, fractionation mechanisms related to expulsion and migration are invoked (Kruge et al., 1990a; Kruge et al., 1990b). Fractionation is difficult to support, however, as the complexities of this process are still poorly understood.

As previously discussed, biodegradation cannot explain the dominance of the tricyclic terpanes in the oils and extracts of the Goddard Formation. Severe levels of biodegrada-

tion would be needed to entirely degrade the hopanes (Wenger et al., 2002), but there is no evidence of such extreme biodegradation in any of the Goddard samples. Sample SR-15 is excluded from this last statement, as it likely originates from a non-Goddard source rock. Severe thermal stress also fails to explain the relative abundance of tricyclic terpanes in the Goddard. All of the Goddard samples were within the beginning of the late oil window based on multiple maturity proxies (Mackenzie et al., 1981; Riolo et al., 1986; Seifert and Moldowan, 1986). Such levels of thermal stress would be insufficient to entirely degrade the hopanes. Thermal stress sufficient to affect the hopanes would certainly affect additional biomarkers including the steranes, bicyclic terpanes, and n-alkanes (Tissot et al., 1971; Shanmugam, 1985; Seifert and Moldowan, 1986). Again, there is no evidence for such severe alteration in the Goddard. At most, slight to moderate biodegradation and thermal stress may have enhanced an existing abundance of tricyclic terpanes.

Petrographic analyses of Goddard core samples only indicate a low abundance *Tasmanite* fossils for SR-14. Sample OC-1 contained moderate amounts of *Tasmanite* fossils, but as discussed in the next section, this sample was determined not to be sourced from the Goddard. No *Tasmanite* fossils were definitively identified in SEM analyses.

The absence of classic, spherical *Tasmanite* fossils does not entirely preclude other forms of *Tasmanites* from being present in the Goddard. As mentioned previously, the *Tasmanite* fossil is thought to be similar to the marine, Pachysphaera algae (Simoneit et al., 1990). These algae have a two-phase life cycle that consists of a spherical, non-motile phase and a non-spherical, motile phase (Guy-Ohlson and Boalch, 1992). It is possible that *Tasmanites* may be abundant in the Goddard but in a form that has not yet been recognized. However, it is unlikely that only one life-cycle phase of the *Tasmanite* would

be present to the exclusion of all other phases over any length of geologic time.

If the Goddard truly lacks *Tasmanite* fossils, that would support the existence of a non-*Tasmanite* precursor for the tricyclic terpanes (Simoneit, 1990; Aquino Neto et al., 1992; Azevedo, 1992; Dutta et al., 2006). Non-*Tasmanite* sources would still likely be algal-like precursors that would thrive within a Type B, marine organofacies. The consistent tricyclic terpane signature of the Goddard supports a precursor organism prone to widespread blooms that would produce a homogeneous source of organic matter.

5.5. The Goddard Fingerprint

5.5.1. Goddard Oil-Source Rock Correlation

The overall geochemical characteristics for both the Goddard oils and source rocks in this study were strikingly consistent. As the source rock and oil samples were collected from locations throughout the SCOOP, the geochemical fingerprint for the Goddard is highly applicable for oil and source rock correlation in this region of the Anadarko Basin.

The most diagnostic biomarker family for both the oils and source rocks of the Goddard Formation is the tricyclic terpanes (Figure 26). To date, no other source rock in Oklahoma has been observed to have such an abundance of these biomarkers. Globally, the Goddard is one of only a few source rocks that has a greater abundance of tricyclic terpanes relative to hopanes yet is not characterized as a *Tasmanite* source rock (Zhusheng et al., 1988; Kruge et al., 1990a; de Grande et al., 1993). The distribution of tricyclic terpanes is virtually identical in both oils and source rock extracts. The most abundant tricyclic terpane peak for source rocks was C_{23}. The C_{28} and C_{29} tricyclic terpanes were

present in equal or greater abundance relative to the C_{23} peak for most of the oils.

Cholestane (C_{27}) was the most abundant regular sterane in all of the Goddard oils and source rocks. Ergostane (C_{28}) was the least abundant peak for all of the oils and source rocks. In comparison, the Woodford Shale tends to have a lower abundance of both cholestane (C_{27}) and ergostane (C_{28}) relative to stigmastane (C_{29}).

The low abundance of MAS and high abundance of TAS in the oils and source rocks Goddard may have applications for correlation. The low abundance of MAS is mostly explained by the high maturity of both the oils and source rocks in this study (Mackenzie et al., 1982). However, the absolute absence of MAS in the majority of samples is unusual, even for source rocks and oils that have reached the late oil window in terms of thermal maturity. Other thermally mature source rocks in the Anadarko Basin, such as the Woodford, appear to retain at least a moderate abundance of MAS at similar maturities.

Goddard oils and source rocks also contain distinct distributions of bicyclic sesquiterpanoids. Homodrimane is essentially absent from both source rock and oils while drimane is typically abundant in both types of samples. In comparison, the Woodford Shale has abundant homodrimane and only trace drimane.

The absence of proxies for salinity and water column stratification is also characteristic of all the Goddard oils and source rocks in this study. The *m/z* 133 and *m/z* 134 chromatograms are dominated by methyl- and alkylbenzenes rather than the aryl isoprenoids. The lack of aryl isoprenoids in the Goddard is a stark contrast to formations such as the Woodford Shale which are rich in aryl isoprenoids (Connock, 2015).

5.5.2. Non-Goddard Oils and Source Rocks

While the majority of oil and core samples conformed to the biomarker fingerprint described above, three samples deviated from the biomarker assemblage associated with the Goddard: OC-1, AS-1, and SR-15. The distribution of n-alkanes for OC-1 was similar to that seen in the Goddard; the short-chain C_{12}-C_{18} n-alkanes are most abundant and the sample displayed a low wax content. Sample SR-15 had a bimodal n-alkane distribution unlike any other rock extract. The absence of n-alkanes in AS-1 was attributed to biodegradation.

The three rock extracts also lacked the abundant tricyclic terpane seen in the Goddard. Instead, all three extracts had the more typical distribution of hopanes (Figure 27). The low abundance of tricyclic terpanes suggests that the depositional environment and the organic matter input for these three samples was different than the Goddard oils and source rocks. Sample AS-1 was the most highly degraded sample in this study; the absence of the tricyclic terpane signal in AS-1 strongly implies that the abundant tricyclic terpane signal in the Goddard is not caused by biodegradation. Sample SR-15 is also likely within the same range of thermal maturity as the Goddard core samples, which suggests that thermal maturity is not the primary cause for the abundant tricyclic terpane signal.

The sterane fingerprint for the three extracts are also distinct from the Goddard samples. The dominant regular sterane in OC-1, AS-1, and SR-15 was stigmastane (C_{29}) and not cholestane (C_{27}). The 24-n-propylcholestane is also only abundant in the AS-1 extract. In SR-15 and OC-1, 24-n-propylcholestane is present in relatively low abundance

compared to the Goddard oils and source rocks. Sample OC-1 also had abundant MAS, although this abundance is likely due to the lower maturity of the sample.

Aryl isoprenoids were observed in OC-1 and SR-15 and possibly in AS-1 sample. Biodegradation may have affected the aryl isoprenoid abundance in AS-1.

The biomarker signatures for the three extracts are still consistent with a Type B, siliciclastic marine organofacies. However, the depositional environment for these samples may have been more saline than the depositional environment inferred for the Goddard oils and source rocks. A more saline depositional environment may partially explain the dominance of pentacyclic terpanes relative to the tricyclic terpanes.

Both OC-1 and SR-15 were originally identified as Springer (Ham et al., 1990; Jones and Philp, 1990). It is possible that both samples are from one of the unnamed shales of the Springer Group rather than the Goddard Formation. As mentioned by both Westheimer (1956) and Peace (1965), the physical appearance of the Goddard Formation and overlying shales in the Springer group is almost identical. Sample OC-1 was also collected from the Ardmore Basin. The distinct depositional and biologic conditions present in the Anadarko Basin during the Late Mississippian may have been absent from the Ardmore Basin. Sample AS-1 was collected from an oil seep anecdotally attributed to the Goddard Formation (Ardmore Geological Society, 2015). Based on the data collected in this study, the source of the oil at this seep does not exhibit any of the biomarker characteristics associated with the Goddard Formation. The biomarker assemblage for AS-1, specifically the abundant aryl isoprenoids, is more characteristic of the Woodford Shale (Connock, 2015).

6. Conclusions

Geochemical analyses of source rock extracts and oils characterize the Goddard as a Type B organofacies. The Type B organofacies describes a marine depositional environment dominated by siliciclastic sedimentation. Biomarkers associated with hypersalinity, water column stratification, and euxinia were not observed in any Goddard samples; this distinctive absence distinguishes the Goddard from the Woodford Shale, which is rich in monoaromatic steranes, carotenoids, and aryl isoprenoids and is highly associated with euxinic, saline, and stratified waters.

The abundance of tricyclic terpanes in oils and source rocks from the Goddard is likely related to unique climatic and biologic conditions present in the Anadarko Basin during the Late Mississippian. The Late Mississippian Serpukhovian mass extinction would have favored low-diversity communities with the potential to leave undiluted geochemical signatures in the rock record. The similarity between the biomarker assemblages of oils and source rocks supports such a homogeneous organic matter source. The onset of glaciation in the Late Mississippian and subsequent increase in loess production would also have facilitated nutrient seeding and algal blooms in marine environments. An algal bloom model is consistent with the laterally homogeneous biomarker fingerprint for the oils and source rocks of the Goddard and the inferred algal precursor for the tricyclic terpanes.

A specific precursor for the tricyclic terpanes is still undetermined. While tricyclic terpanes have long been associated with *Tasmanites*, petrographic and SEM analysis identified very few of these algal-like fossils. It is more likely that the tricyclic terpanes in

the Goddard are sourced from a yet-unknown algal precursor. Whether tricyclic terpanes are sourced from *Tasmanites* or another green alga, the paleoclimate interpretation for the Late Mississippian supports a low-diversity, high-abundance community consistent with the laterally and vertically homogeneous biomarker signal of the Late Mississippian Goddard across the Anadarko Basin.

The abundance of tricyclic terpanes in the Goddard may have been enhanced by thermal stress.; the majority and of the oil and source rock samples in this study were within the late oil window. Thermal alteration may have caused preferential decomposition of hopanes relative to the tricyclic terpanes. However, thermal stress alone does not explain the relative abundance of tricyclic terpanes relative to hopanes; if that was the case, then one would expect to see abundant tricyclic terpanes in all highly mature source rocks and fluids. Evidence for biodegradation in the Goddard was also minimal. Biodegradation likely played only a small role in enhancing the abundant tricyclic terpane signature.

The above interpretation has several implications for unconventional exploration and production in the Goddard. A fairly homogeneous source rock could reduce risk regarding product quality as the characteristics of produced fluids would be consistent. The exception to this observation is the apparent mixing in the oils. Identification of the Goddard as a Type B organofacies will also improve the basin models for the Goddard. The possibility of a single, algal organic matter source would influence the kinetic behavior of the Goddard; source rocks dominated by a homogeneous source of algal sources are well correlated with narrow generation and expulsion windows. The potential for early expulsion from the Goddard should be considered when placing wells

and calculating estimated ultimate recovery (EUR). Additionally, oil expelled from the Goddard may have migrated and mixed with Woodford or Mississippian sourced oils. While the Goddard has a chemical fingerprint distinct from the other major source rocks in the Anadarko Basin, it is undetermined how much mixing is needed to obscure the abundant tricyclic terpanes and introduce sufficient abundances of biomarkers typically absent from the Goddard. The uncertainty regarding mixing has implications for mass-balance accounting for source rock generation in the Anadarko Basin of Oklahoma.

7. Future Work

The intent of this study was to evaluate the geochemistry of the Goddard Formation and assess depositional organofacies, thermal maturity, and possible reasons for an unusually high abundance of tricyclic terpanes. However, there were additional areas of work not explored in this study which would add value to exploration in the Goddard Formation. Suggested areas of future work are listed below.

- Stable isotope analysis using carbon isotopes could be used to detect signatures indicative of algal blooms or for particular local climate conditions. Such work could use the core and outcrop samples from this study as no isotope analysis has been done on the samples.

- As the source rocks in this study are rare examples of a tricyclic terpane-rich, *Tasmanite* fossil-poor source rock, additional SEM and petrographic analysis may help identify non-*Tasmanite* precursors.

- High-resolution outcrop studies of the Goddard could reveal vertical trends in biomarker fingerprints. No suitably extensive Goddard outcrops were able to be located for this study. The samples used in this study were only able to reveal lateral trends within the Anadarko Basin

- Additional outcrop and core samples from the Ardmore Basin could be evaluated. Sample OC-1 was collected in the Ardmore Basin from a location mapped as Springer but did not display the typical biomarker assemblage associated with the Goddard source rock and oil samples in this study. As the Goddard is physically

indistinguishable from the shales of the Springer Group in the field, OC-1 may have come from one of the unnamed Springer shales. Another possibility is that conditions responsible for the Goddard Formation's distinct biomarker assemblage may only have existed in the Anadarko Basin and not in the Ardmore Basin.

- The biomarker fingerprint developed for the Goddard Formation could assist with surficial mapping of the Goddard Formation and the overlying Springer Shales, specifically the Rod Club Shale. While the physical appearance of the Goddard Formation and the Rod Club shale may be similar, the biomarker assemblage may be sufficient to distinguish the two shales.

References

Alberdi, M., Moldowan, J. M., Peters, K. E., Dahl, J. E., 2001. Stereoselective biodegradation of tricyclic terpanes in heavy oils from the Bolivar Coastal Fields, Venezuela. Organic Geochemistry 32, 181-191.

Alexander, R., Kagi R., Woodhouse, G. W., 1981. Geochemical correlation of Windalia oil and extracts of Winning Group (Cretaceous) potential source rocks, Barrow Subbasin, Western Australia. American Association of Petroleum Geologists Bulletin 65, 235-250.

Alexander, R., Kagi, R., Noble, R., 1983. Identification of the bycyclic sesquiterpenes, drimane, and eudesmane in petroleum. Journal of the Chemical Society Chemical Communications 5, 226-228.

Anders, D. E., Robinson, W. E., 1971. Cycloalkane constituents of the bitumen from Green River Shale. Geochimica et Cosmochimica Acta 35, 661-678.

Andrews, R. D., 2008. Morrow and Springer strata in the Southern Midcontinent. In: Andrews, R. D. (Ed.), Morrow and Springer in the Southern Midcontinent. Oklahoma Geological Survey Circular 111, 1-11.

Aquino Neto, F. R., Restle, A., Connan, J., Albrecht, P., Ourisson, G., 1982. Novel tricyclic terpanes (C_{19}, C_{20}) in sediments and petroleums. Tetrahedron Letters 23, 2027-2030.

Aquino Neto, F. R., Cardoso, J .N., Rodrigues, R., Trindade, L. A. F., 1986. Evolution of tricyclic alkanes in the Espirito Santo Basin, Brazil. Geochimica et Cosmochimica Acta 50, 2069-2072.

Aquino Neto, F. R., Trigüis, J., Azevedo, D. A., Rodrigues, R., Simoneit, B. R. T., 1992. Organic geochemistry of geographically unrelated *Tasmanites*. Organic Geochemistry 18, 791-803.

Ardmore Geological Society, 2015. Reservoir Characteristics of the Springer Shale in the SCOOP Play of the Eastern Anadarko Basin, Meeting.

Arinobu, T., Ishiwatari, R., Kaiho K., Lamolda, M. A., 1999. Spike of pyrosynthetic polycyclic aromatic hydrocarbons associated with an abrupt decrease in δ^{13}C of a terrestrial biomarker at the Cretaceous-Tertiary boundary at Caravaca, Spain. Geology 27, 723-726.

ASTM, 2011. Standard test method for microscopical determination of the reflectance of vitrinite dispersed in sedimentary rocks. American Society for Testing Materials, D7708-11.

Azevedo, D. A., Aquino Neto, F. R., Simoneit, B. R. T., Pinto, A. C., 1992. Novel series of tricyclic aromatic terpanes characterized in Tasmanian *Tasmanite*. Organic Geochemistry 18, 9-16.

Azevedo, D. A., Andre Zinu, C. J., Aquino Neto, F. R., Simoneit, B. R. T., 2001. Possible origin of acyclic (linear and isoprenoid) and tricyclic terpane methyl ketones in a Tasmanian *Tasmanite* bitumen. Organic Geochemistry 32, 443-448.

Bates, M., 2015. Springer: New Shale in Town Oil and Gas Investor 35 (3) 21.

Beckman, W. A., and Sloss, L. L., 1965. Possible pre-Springeran unconformity in southern Oklahoma. American Association of Petroleum Geologists Bulletin 50, 1342-1384.

Bendoraitis, J. G., Brown, B. L., Hepner, L. S., 1962. Isolation of 2,6,10,14-Tetramethylpentadecane by high temperature gas-liquid chromatography. Analytical Chemistry 34, 49-53.

Bennett, B., Aitken, C. M., Jones, D. M., Farrimond, P., Larter, S. R., 2007. The occurrence and significance of 25-norhopanic acids in petroleum reservoirs. Organic Geochemistry 38, 1977-1985.

Bennison, A. P., 1956. Springer and related rocks of Oklahoma. Tulsa Geological Society Digest 24, 111-115.

Blumer, M., Thomas, D. W., 1965. Phytadienes in zooplankton. Science 147, 1148-1149.

Bonelli, J. R., Patzkowsky, M. E., 2008. How are global patterns of faunal turnover expressed at regional scales? Evidence from the Upper Mississippian (Chesterian Series), Illinois Basin, USA. Palaios 23, 760-772.

Boalch, G. T., Guy-Ohlson, D. 1992. *Tasmanites*, the correct name for Pachysphaera (Prasinophyceae, Pterospermateceae). Taxon 41, 529-531.

Boyd, D. T., 2002. Oklahoma oil: Past, present, and future. Oklahoma Geology Notes 62, 97-106.

Boyd, D. T., 2008. Fighting the tide: Morrow-Springer gas in Oklahoma. In: Andrews, R. D. (Ed.), Morrow and Springer in the Southern Midcontinent. Oklahoma Geological Survey Circular 111, 27-38.

Branson, C. C., 1957. Some regional features of Mississippian and early Pennsylvanian rocks in the mid-continent. Abilene & Fort Worth Geological Societies. Joint Field Trip Guidebook 79-83.

Brocks, J. J., Summons, R. E., 2003. Sedimentary hydrocarbons, biomarkers for early life In: Schlesinger W.H. (Ed.), Treatise on Geochemistry 8, 63-115.

Brooks, J. D., Gould, K., Smith, J. W., 1969. Isoprenoid hydrocarbons in coal and petroleum. Nature 222, 257-259.

Brown, T. O., Northcutt, R. A., 2008. Springer gas-play development–Anadarko Basin In: Andrews, R. D. (Ed.), Morrow and Springer in the Southern Midcontinent. Oklahoma Geological Survey Circular 111, 137-138.

Bylinkin, G. P., 1987. The informativeness of the pristane/phytane ratio as a genetic index. International Geology Review 29, 1117-1120.

Cardott, B. J., 2012a. Introduction to vitrinite reflectance as a thermal maturity indicator. American Association of Petroleum Geologists Search and Discovery, 40928.

Cardott, B. J., 2012b. Thermal maturity of Woodford Shale gas and oil plays, Oklahoma, USA. International Journal of Coal Geology 103, 109-119.

Cardott, B. J., 2013. Woodford Shale: From hydrocarbon source rock to reservoir. American Association of Petroleum Geologists Search and Discovery, 50817.

Cardott, B., Oklahoma Geological Survey, Personal Communication, March 16th, 2016.

Carter, L. S., Kelley, S. A., Blackwell, D. D., and Naeser, N. D., 1998, Heat flow and thermal history of the Anadarko Basin, Oklahoma. American Association of Petroleum Geologists 82, 291-316.

Chicarelli, M. I., Aquino Neto, F. R., Albrecht, P., 1988. Occurrence of four stereoisomeric tricyclic terpane series in immature Brazilian Shales. Geochimica et Cosmochimica Acta 52, 1955-1959.

Coale, K. H., Johnson, K. S., Fitzwater, S. E., Gordon, R. M., Tanner, S., Chavez, F. P., Ferioli, L., Sakamoto, C., Rogers P., Millero, F., Steinberg, P., Nightingale, P., Cooper, D., Cochlan, W. P., Landry, M. R., Constantinou, J., Rollwagan, G., Trasvina, A., Kudela, R., 1996. A massive phytoplankton bloom induced by an ecosystem-scale iron fertilization experiment in the equatorial Pacific Ocean. Nature 383, 495-501.

Connock, G. T., 2015. Paleoenvironmental interpretations of the Woodford Shale, Wyche Farm Shale Pit, Pontotoc County, Oklahoma with a primary focus on water column chemistry and structure. M.S. Thesis, The University of Oklahoma, 1-253.

Continental Resources, 2014. Mapping out future: Investor & analyst day. Presentation.

Crowell, J. C., 1978. Gondwanan glaciation, cyclothems, continental positioning, and climate change. American Journal of Science 278, 1345-1372.

Davis, C., Manger, W., Lemke, S., 2015. Reservoir characteristics of the Springer Shale in the SCOOP Play of the Eastern Anadarko Basin, Oklahoma. American Association of Petroleum Geologists Search and Discovery 90221.

Dembicki, H. Jr., 2009. Three common source rock evaluation errors made by geologists during prospects or play appraisal. American Association of Petroleum Geology Bulletin 93, 341-356.

Didyk, B. M., Simoneit, B. R. T., Brassell, S. C., Eglinton, G., 1978. Organic geochemical indicators of paleoenvironmental conditions of sedimentation. Nature 272, 216-222.

Dutta, S., Greenwood, P. F., Brocke, R., Schaefer, R. G., Mann, U., 2006. New insights into the relationship between *Tasmanites* and tricyclic terpenoids. Organic Geochemistry 37, 117-127.

Eagle Rock Energy Partners, L.P., 2015. National Association of Publicly Traded Partnerships. Master Limited Partnership. Conference presentation materials.

Ekweozor, C. M., 1984. Tricyclic terpenoid derivatives from chemical degradation reactions of asphaltenes. Organic Geochemistry 6, 51-61.

Farrimond, P., Bevan, J. C., Bishop, A. N., 1999. Tricyclic terpane maturity parameters: Response to heating by an igneous intrusion. Organic Geochemistry 30, 1011-1019.

Gallegos E. J., 1971. Identification of new steranes, terpanes and branched paraffins in Green River by combined capillary gas chromatography and mass spectrometry. Analytical Chemistry 43, 1151-1160.

Girty, G. H., Roundy, P. V., 1923. Notes on the Glenn Formation of Oklahoma with consideration of new paleontologic evidence. American Association of Petroleum Geologists Bulletin 6, 331-349.

Graham, J. B., Dudley, R., Aguilar, N. M., Gans, C., 1995. Implications for the late Paleozoic oxygen pulse for physiology and evolution. Nature 375, 117-120.

de Grande, S. M. B., Aquino Neto, F. R., Mello, M. R., 1993. Extended tricyclic terpanes in sediments and petroleum. Organic Geochemistry 20, 1039-1047.

Greenwood, P. F., Arouri, K. R., George, S. C., 2000. Tricyclic terpenoids composition of *Tasmanites* kerogen as determined by pyrolysis GC-MS. Geochimica et Cosmochimica Acta 64, 1249-1263.

Grice, K., Nabbefeld, B., Maslen, E., 2007. Source and significance of selected polycyclic aromatic hydrocarbons in sediments (Hovea-3 well, Perth Basin, Western Australia) spanning the Permian–Triassic boundary. Organic Geochemistry 38, 1795-1803.

Grice, K., Lu, H., Atahan, P., Asif, M., Hallmann, C., Greenwood, P., Maslen, E., Tulipani, S., Williford, K., Dodson, J., 2009. New insights into the origin of perylene in geological samples. Geochimica et Cosmochimica Acta 73, 6531-6453.

Guy-Ohlson, D., Boalch, G. T., 1992. Comparative morphology of the genus *Tasmanites* (Pterospermales, Chlorophyta). Phycologia 31, 523-528.

Ham, W. H., McKinley, M. E., Johnson, K., 1990. Geologic map and sections of the Arbuckle Mountains, Oklahoma. In: Fairchild, R. W., Hanson, R. L., Davis, R. E. (Eds.), Hydrology of the Arbuckle Mountains Area, South-Central Oklahoma. Oklahoma Geological Survey Circular 91. Plate 2.

Hasegawa, T., 2001. Predominance of terrigenous organic matter in Cretaceous marine fore-arc sediments, Japan and Far East Russia. International Journal of Coal Geology 47, 207-221.

Heissler, D., Ocampo, R., Albrecht, P., Riehl, J., Ourisson, G., 1984. Identification of long-chain tricyclic terpene hydrocarbons (C_{21}—C_{30}) in geological samples. Journal of the Chemical Society, Chemical Communications 496-498.

Hemish, L. A., Andrews, R. D., 2001. Stratigraphy and depositional environments of the sandstones of the Springer Formation and the Primrose Member of the Golf Course Formation in the Ardmore Basin, Oklahoma. Oklahoma Geological Survey. Guidebook 32.

Henry, A. A., Lewan, M. D., 1999. Comparison of kinetic-model predictions of deep gas generation. U.S. Department of the Interior, U.S Geological Survey. Open-File Report 99-326.

Huang, W-Y., Meinschein, W. G., 1979. Sterols as ecological indicators. Geochimica et Cosmochimica Acta 43, 739-745.

Huang, H., Zhang, S., Su, J., 2015. Geochemistry of tri- and tetracyclic terpanes in the Paleozoic oils form the Tarim Basin, Northwest China. Energy Fuels, 29, 7014-7025.

Hunt, J. M., 1996. Petroleum geochemistry and geology, second edition. W. H. Freeman Publishers, New York.

Jacobs, T., Rassenfoss, S., Betz, J., 2014. Springer Shale rising: Continentals new niche play. Journal of Petroleum Technology Exploration and Production Notes 66 (12).

Jarvie, D. M., Hill, R. J., Pollastro, R. M., 2005. Assessment of the gas potential and yields from shales: The Barnett Shale model. In Cardott, B. J. (Ed.), Unconventional energy resources in the southern Mid-continent, 2004 symposium: Oklahoma Geological Survey Circular 110, 37-50.

Jarvie, D. M., 2012. Shale resource systems for oil and gas: Part 2–Shale-oil resource systems. In Breyer, J. A. (Ed.), Shale reservoirs–Giant resources for the 21st century. American Association of Petroleum Geologists Memoir 97, 89-119.

Johnson, K. S., Amsden, T. W., Denison, R. E., Dutton, S. P., Goldstein, A. G., Rascoe, B., Sutherland, P. K., Thompson, D. M., 1989. Geology of the Southern Midcontinent. Oklahoma Geological Survey. Special Publication 89-2.

Johnson, K. S., 2008. Geologic history of Oklahoma. Oklahoma Geological Survey. Educational Publication 9.

Jones, D. M., Douglas, A. G., Connan, J., 1988. Hydrous pyrolysis of asphaltenes and polar fractions of biodegraded oils. In: Mattavelli, L., Novelli, L. (Ed.), Advances in Organic Geochemistry 1987. Pergamon Press, Great Britain. Organic Geochemistry 13, 981-993.

Jones, P. J., Philp, R. P., 1990. Oils and source rocks from Pauls Valley, Anadarko Basin, Oklahoma, U.S.A. Applied Geochemistry 5, 429-448.

Kaiho, K., Yatsu, S., Oba, M., Gorjan, P., Casier, J-G., Ikeda, M., 2013. A forest fire and soil erosion event during the Late Devonian mass extinction. Paleogeography, Paleoclimatology, Paleoecology 392, 272-280.

Kim, D., Philp, R. P., 2001. Extended tricyclic terpanes in Mississippian rocks from the Anadarko Basin, Oklahoma. In: Johnson, K. E. (Ed.), Silurian, Devonian, and Mississippian Geology and Petroleum in the Southern Midcontinent. Oklahoma Geological Survey Circular 105, 109-127.

Van Krevelen, D. W., 1950. Graphical-statistical method for the study of structure and reaction processes of coal. Fuel 29, 269-283.

Kruge, M. A., Hubert, J. F., Akes, R. J., Meriney, P. E., 1990a. Biological markers in Lower Jurassic synrift lacustrine black shales, Hartford basin, Connecticut, U.S.A. Organic Geochemistry 15, 281-289.

Kruge, M. A., Hubert, J. F., Bensley, D. F., Crelling, L, C., Akes, R. J., Meriney, P. E., 1990b. Organic geochemistry of a Lower Jurassic synrift lacustrine sequence, Hartford basin, Connecticut, U.S.A. In: Durand, B., Behar, F. (Eds.), Advances in Organic Geochemistry 1985. Pergamon Press, Great Britain. Organic Geochemistry 16, 689-701.

López-Gamundí, O. R., and Buatois, L. A., 2010. Introduction: Late Paleozoic glacial events and postglacial transgressions in Gondwana. In: López-Gamundí, O. R., and Buatois, L. A. (Eds.), Late Paleozoic Glacial Events and Postglacial Transgressions in Gondwana. Geological Society of America Special Paper 468, v-viii.

Mackenzie, A. S., Hoffman, C. F., Maxwell, J. R., 1981. Molecular parameters of maturation in the Toarcian shales, Paris Basin, France—III. Changes in aromatic steroid hydrocarbons. Geochimica et Cosmochimica Acta 45, 1345-1355.

Mackenzie, A. S., Lamb, N. A., Maxwell, J. R., 1982. Steroid hydrocarbons and the thermal history of sediments. Nature 295, 223-226.

Magoon, L. B., Dow, W. D., 1994. The petroleum system—From source to trap. American Association of Petroleum Geologists Memoir 60.

Martin, J. H., Coale, K. H., Johnson, K. S., Fitwzwater, S. E., Gordon, R. M., Tanner, S. J., Hunter, C. N., Elrod, V. A., Nowicki, J. L., Coley, T. L., Barber, R. T., Lindley, S., Watson, A. J., van Scoy, K., Law, C. S., Liddicoat, M. I., Ling, R., Stanton, T., Stockel, J., Collins, C., Anderson, A., Bidigare, R., Ondrusek, M., Latasa, M., Millero, F. J., Lee, K., Yao, W., Zhang, J. Z., Friederich, G., Sakamoto, C., Chavez, F., Buck, K., Kolber, Z., Greene, R., Falkowski, P., Chisholm, S. W., Hoge, F., Swift, R., Yungel, J., Turner, S., Nightingale, P., Hatton, A., Liss P., Tindale, N. W., 1994. Testing the iron hypothesis in ecosystems of the equatorial Pacific Ocean. Nature, 371, 123-129.

Marynowski, L., Smolarek, J., Hautevelle, Y., 2015. Perylene degradation during gradual onset of organic matter maturation. International Journal of Coal Geology 139, 17-25.

Maxwell, J. R., Pillinger, C. T., Eglinton, G., 1971. Quarterly Review. Organic Geochemistry 25, 571-628.

McCaffrey, M. A., Legarre, H. A., Johnson, S. J., 1996. Using biomarkers to improve heavy oil reservoir management: An example from the Cymric Field, Kern County, California. American Association of Petroleum Geologists Bulletin 80, 898-912.

McGhee, G. R. Jr., Clapham, M. E., Sheehan, P. M., Bottjer, D. J., Droser, M. L., 2013. A new ecological-severity ranking of major Phanerozoic biodiversity crises. Paleogeography, Paleoclimatology, Paleoecology 370, 260-270.

Mello, M. R., Gaglianone, P. C., Brassel, S. C., Maxwell, J.R., 1988, geochemical and biological marker assessment of depositional environments using Brazilian offshore oils: Marine and Petroleum Geology 5, 205-223.

Moldowan, J. M., Seifert, W. K., Gallegos, E. G., 1983. Identification of an extended series of tricyclic terpanes in petroleum. Geochimica et Cosmochimica Acta 47, 1531-1534.

Moldowan, J. M., Seifert, W. K., Gallagos, E. J., 1985. Relationship between petroleum composition and depositional environment of petroleum source rocks. American Association of Petroleum Geologists Bulletin 69, 1255-1268.

Moldowan, J. M., Sundararaman, P., Schoell, M., 1986. Sensitivity of biomarker properties to depositional environments and/or source rock input in the Lower Toarcian of S.W. German. Organic Geochemistry 10, 912-915.

Moldowan, J. M., Fago, F. J., Lee, C. Y. Jacobson, S. R., Watt, D. S., Slougui, N-E, Jaganathan, A., Young, D. C., 1990. Sedimentary 24-n-Propylcholestanes, molecular fossils diagnostic of marine algae. Science 247, 309-312.

Nash, S. S., 2014. The Springer shale: A sleeping giant? American Association of Petroleum Geologists Search and Discovery 10664, 26.

Oil and Gas Investor This Week, 2015a. Continental announces results from four Springer Shale completions. Petroleum and Gas, Best of Activity Highlights 23, 12.

Oil and Gas Investor This Week, 2015b. Lower Springer shale well produces 1.303 Mbbl of Oil, 456 Mcf of gas per day. Petroleum and Gas, Drilling Highlights 23, 18.

Ourisson, G., Albrecht, P., Rohmer, M., 1982. Predictive microbial biochemistry–from molecular fossils to procaryotic membranes. Trends in Biochemical Sciences 7, 236-239.

Ourisson G., Albrecht, P., 1992. Hopanoids. 1. Geohopanoids: The most abundant natural products on Earth? Accounts of Chemical Research 25, 398-402.

Peace, M. W., 1965. The Springer Group of the Southeastern Anadarko Basin in Oklahoma. Oklahoma City Geologic Survey, The Shale Shaker 15, 280-297.

Pearson, A., Budin, M., Brocks, J. J., 2003. Phylogenetic and biochemical evidence for sterol synthesis in the Bacterium Gemmata Obscuriglobus. Proceedings of the Natural Academy of Science in the United States of America 100, 15353-15357.

Pepper, A. S., Corvi, P. J., 1995. Simple kinetic models of petroleum formation. Part I. Oil and gas generation from kerogen. Marine and Petroleum Geology 12, 291-319.

Perry, W. J. Jr., 1989, Tectonic evolution of the Anadarko basin region, Oklahoma. In: U.S. Geological Survey bulletin 1866-A, A multidisciplinary approach to research studies of sedimentary rocks and their constituents and the evolution of sedimentary basins, both ancient and modern.

Peters, K. E., 1986. Guidelines for evaluating Petroleum source rock using programmed pyrolysis. American Association of Petroleum Geologists Bulletin 70, 318-329.

Peters, K. E., Moldowan, J. M., Schoell, M., Hempkins, W. B., 1986. Petroleum isotopic and biomarker composition related to source rock organic matter and depositional environment. In: Leythaeuser, D., Rullkotter, J. (Eds.), Advances in Organic Geochemistry 1985. Pergamon Press, Great Britain. Organic Geochemistry 10, 17-27.

Peters, K. E., Moldowan, J. M., 1991. Effects of source, thermal maturity, and biodegradation on the distribution and isomerization of homohopanes in petroleum. Organic Geochemistry 17, 47-61.

Peters, K. E., Moldowan, J. M., 1993. The Biomarker Guide. Interpreting molecular fossils in petroleum and ancient sediments. Prentice-Hall, Englewood Cliffs, New Jersey.

Peters, K. E., Cassa, M. R., 1994. Applied source rock geochemistry In: Magoon. L. B., Dow W. G., The Petroleum System—from Source to trap. American Association of Petroleum Geologists Memoir 60.

Peters, K. E., Moldowan, J. M., McCaffrey, M. A., Fago, F. J., 1996. Selective biodegradation of extended hopanes to 25-norhopanes in petroleum reservoirs. Insights from molecular mechanics. Organic Geochemistry 24, 765-783.

Peters, K. E., 2000. Petroleum tricyclic terpanes: Predicted physicochemical behavior from molecular mechanics calculations. Organic Geochemistry 31, 497-507.

Peters, K. E., Walters, C. C., Moldowan, J. M., 2005. The Biomarker Guide: Biomarkers and isotopes in petroleum exploration and Earth history, second edition. Cambridge University Press, New York.

Philp, R. P., Gilbert, T. D., 1986. Biomarker distributions in Australian oils predominantly derived from terrigenous source material. In: Leythaeuser, D., Rullkotter, J. (Eds.), Advances in Organic Geochemistry 1985. Pergamon Press, Great Britain. Organic Geochemistry 10, 73-84.

Philp R. P., Zhao-An, F., 1987. Geochemical investigation of oils and source rocks from Qianjiang Depression of Jianghan Basin, a terrigenous saline basin, China. Organic Geochemistry 11, 549-562.

Philp, R. P., Jinggui, L., Lewis, C. A., 1989. An organic geochemical investigation of crude oils from Shanganning, Jianghan, Chaidamu, and Zhungeer Basins, Peoples Republic of China. Organic Geochemistry 14, 447-460.

Philp, R. P., Chen, J., Galvez-Sinibaldi, A., Wang, H., Allen, J. D., 1992. Effects of weathering and maturity on the geochemical characteristics of the Woodford Shale. In: Johnson, K. E., Cardott, B. J. (Ed.), Source Rocks in the Southern Midcontinent. Oklahoma Geological Survey Circular 93, 106-121.

Powell, M. G., 2008. Timing and selectivity of the Late Mississippian mass extinction of brachiopod genera from the Central Appalachian Basin. Palaios 23, 525-534.

di Primio, R., Horsfield, B., 2006. From petroleum-type organofacies to hydrocarbon phase prediction. American Association of Petroleum Geologists Bulletin 90, 1031-1058.

Qiao, L., Shen, S-Z., 2014. Global paleobiogeography of brachiopods during the Mississippian–Response to the global tectonic reconfiguration, ocean circulation, and climate changes. Gondwana Research 26, 1173-1185.

Ramon, J. C., Dzou, L., Giraldo, B., 1997. Geochemical evaluation of the Middle Magdalena Basin, Columbia. Ciencia, Technologia y Futuro, 1, 47-66.

Rascoe B. Jr., Adler, F. J., 1983. Permo-Carboniferous hydrocarbon accumulations, Mid-Continent, U.S.A. American Association of Petroleum Geologists Bulletin 67, 979-1001.

Reedy, H. J., Sykes, H. A., 1959 Carter-Knox oil field, Grady and Stephens counties. In: Mayes, J. W., Westheimer, J., Tomlinson, C. W., Putman, D. M. (Eds.), Petroleum Geology of Southern Oklahoma, Volume 2. American Association of Petroleum Geologists Special Publication, 198-219.

Revill, A. T., Volkman, J .K., O'Leary, T., Summons, R. E., Boreham, C. J., Banks, M. R., Denwer, K., 1994. Hydrocarbon biomarkers, thermal maturity, and depositional setting of *Tasmanite* oil shales from Tasmania: Australia. Geochimica et Cosmochimica Acta 58, 3803-3822.

Riolo, J., Hussler, G., Albrect, P., Connan, J., 1986. Distribution of aromatic steroids in geologic samples: Their evolution as geochemical parameters. In: Leythaeuser, D., Rullkotter, J. (Eds.), Advances in Organic Geochemistry 1985. Pergamon Press, Great Britain. Organic Geochemistry 10, 981-990.

Romero-Sarmiento, M-F., Letort, G., Pilot, D., Lamoureux-Var, V., Beaumont, V., Huc, A.Y., Garcia, B., 2015a. New rock-eval method for characterization of shale plays. Presentation.

Romero-Sarmiento, M-F., Letort, G., Pilot, D., Lamoureux-Var, V., Beaumont, V., Huc, A. Y., Garcia, B., 2015b. New rock-eval method for characterization of unconventional shale resource systems. Oil & Gas Science and Technology.

Rush, W., Personal Communication, February 2nd, 2016.

Rush, W., 2016. Reservoir characterization and chemostratigraphy of the Goddard Shale in the South Central Oklahoma Oil Province. M.S. Thesis (Unpublished), The University of Oklahoma. 1-84.

Scott, A. C., Jones, T. P., 1994. The nature and influence of fire in Carboniferous ecosystems. Paleogeography, Paleoclimatology, Paleoecology 106, 91-112.

Seifert, W. K., and Moldowan, J. M., 1978. Applications of steranes, terpanes, and monoaromatics to the maturation, migration, and source of crude oils. Geochimica et Cosmochimica Acta 42, 77-95.

Seifert, W. K. Moldowan, J. K., 1986. Use of biological markers in petroleum exploration In: Johns, R.B. (Ed.), Methods in geochemistry and geophysics 24, 261-290.

Shanmugam, G., 1985. Significance of coniferous rain forests and related organic matter in generating commercial quantities of oil, Gippsland Basin, Australia. American Association of Petroleum Geologists Bulletin 69, 1241-1254.

Shi, G. R., Waterhouse, J. B., 2010. Late Paleozoic global changes affecting high-latitude environments and biotas: An introduction. Paleogeography, Paleoclimatology, Paleoecology 298, 1-16.

Simoneit, B. R. T., Leif, R. N., Aquino Neto, F. R., Azevedo, D. A., Pinto, A. C., Albrecht, P., 1990. On the presence of hydrocarbons in Permian *Tasmanites* algae. Naturwissenschaft, 77, 380-383.

Simoneit, B. R. T., Schoell, M., Dias, R. F., Aquino Neto, F. R., 1993. Unusual carbon isotope compositions of biomarker hydrocarbons in a Permian *Tasmanite*. Geochimica et Cosmochimica Acta 57, 4205-4211.

Simoneit, B. R. T., McCaffrey, M. A., Schoell, M., 2005. Tasmanian *Tasmanite*: II–compound specific isotope analyses of kerogen oxidation and Raney Ni reduction products. Organic Geochemistry 36, 399-404.

Sinninghe Damasté, J. S., Kock-van Dalen, A. C., de Leeuw, J. W., Schenck, P. S., Guoying, S., Brassell, S. C., 1987. The identification of mono-, di-, and trimethyl 2-methyl-2(4,8,12-trimethyltridecyl)chromans and their occurence in the geosphere. Geochimica et Cosmochimica Acta 51, 2393-2400.

Sinninghe Damasté, J.A., Keely, B. J., Betts, S. E., Baas M., Maxwell, J. R., De Leeuw, J. W., 1993. Variations in abundances and distributions of isoprenoid chromans and long-chain alkylbenzenes in sediments of the Mulhouse Basin: A molecular sedimentary record of paleosalinity. Organic Geochemistry 20, 1201-1215.

Sinninghe Damasté, J. P., Kenig, F., Koopmans, M., Koster, J., Schouten, S., Hayes, J. M., Leeuw, J. W., 1995. Evidence for gammacerane as an indicator of water column stratification. Geochimica et Cosmochimica acta 59, 1895-1900.

Smith, L. B. Jr., Read, J. F., 2000. Rapid onset of late Paleozoic glaciation on Gondwana: Evidence from Upper Mississippian strata of the Midcontinent, United States. Geology 28, 279-282.

Soreghan, G. S., Soreghan, M. J., Hamilton, M. A., 2008. Origin and significance of loess in late Paleozoic western Pangaea: A record of tropical cold? Paleogeography, Paleoclimate, Paleoecology 268, 234-259.

Stratas Advisors, 2014. Springer Shale's Economic Leap out from the pack: Insights from North American Shale Service.

Summons, R. E., Powell, T. G., 1987. Identification of aryl isoprenoids in source rocks and crude oils: Biological markers for the green sulphur bacteria. Geochimica et Cosmochimica Acta 51, 557-566.

Tao, S., Wang, C., Du, J., Liu, L., Chen, Z., 2015. Geochemical application of tricyclic and tetracyclic terpanes biomarkers in crude oils of NW China. Marine and Petroleum Geology 67, 460-467.

Thompson, K. F. M., 1987. Fractionated aromatic petroleums and the generation of gas-condensates. Organic Geochemistry 11, 573-590.

Tissot, B. P., Califet-Debyser, Y., Deroo, G., Oudin, J. L., 1971. Origin and evolution of hydrocarbons in early Toarcian shales, Paris Basin, France. American Association of Petroleum Geologists 55, 2177-2193.

Tissot, B. P., Welte, D. H., 1984. Petroleum Formation and occurrence. Springer. Berlin.

Treibs, A., 1936. Chlorophyll and hemin derivatives in organic mineral substances. Angewandte Chemie 49, 682-686.

U.S. Energy Information Administration, 2011. Review of emerging resources: U.S. shale gas and shale oil plays: Analysis & Projections. http://www.eia.gov/analysis/studies/usshalegas

Visher, G. S., 1989. Anadarko Basin history from stratigraphic response patterns. In: Johnson, K. E. (Ed.), Anadarko Basin Symposium. Oklahoma Geological Survey Circular 90, 221-224.

Volkman, J. K., 1986. A review of sterol markers for marine and terrigenous organic matter. Organic Geochemistry 9, 83-99.

Wang, H .D., Philp, R. P., 2001. Geochemical characterization of selected oils and source rocks from the Chester Formation, Springer Formation, and Morrow Group of the Anadarko Basin. In: Johnson, K. E. (Ed.), Pennsylvanian and Permian Geology in the Southern Midcontinent. Oklahoma Geological Survey Circular 104, 41-57.

Waples, D. W., Curiale, J. A., 1999. Treatise of petroleum geology, Handbook of petroleum geology: Exploring for oil and gas traps. Chapter 8: Oil-oil and oil-source rock correlations: American Association of Petroleum Geologists Special Volumes.

Weete, J. D., Abril, M., Blackwell, M., 2010. Phylogenetic distribution of fungal sterols. PLoS ONE 5 (5) e10899.

Wenger, L. M., Davis, C. L., Isakson, G. H., 2002. Multiple controls on petroleum biodegradation and impact on oil quality. Society of Petroleum Engineers. Reservoir Evaluation & Engineering 5, 375-383.

West, N., Alexander, R., Kagi, R. I., 1990. The use of silicalite for rapid isolation of branched and cyclic alkane fractions of petroleum. Organic Geochemistry 15, 499-501.

Westheimer, J. M., 1956. The Goddard Formation. Petroleum Geology of Southern Oklahoma 1, 392-396.

Williams, J. A., Bjorøy, M., Dolcater, D. L., Winters, J. C., 1986. Biodegradation in South Texas Eocene oils—Effects on aromatics and biomarkers. In: Leythaeuser, D., Rullkotter, J. (Eds.), Advances in Organic Geochemistry 1985. Pergamon Press, Great Britain. Organic Geochemistry 10, 451-461.

ZetaWare Inc., 2015. KinEx [computer software]. Available from http://www.zetaware.com/products/kinex.

Zhao-An, F., Philp, R. P., 1987. Laboratory biomarker fractionations and implications for migration studies. Organic Geochemistry 11, 169-175.

Zhusheng, J., Philp, R. P., Lewis, C. A., 1988. Fractionation of biological markers in crude oils during migration and the effects on correlation and maturation parameters. In: Mattavelli, L., Novelli, L. (Eds.), Advances in Organic Geochemistry 1987. Pergamon Press, Great Britain. Organic Geochemistry 13, 561-571.

Zumberge, J. E., Illich, H., Brown S., Cameron, N., 2000. Biomarker geochemistry of lacustrine-sourced crude oils: A world-wide survey. In: American Association of Petroleum Geologists International Conference and Exhibition, October, 2000, Indonesia, American Association of Petroleum Geologists Search and Discovery, 90913.

Appendix A. Whole Oil-Gas Chromatograms

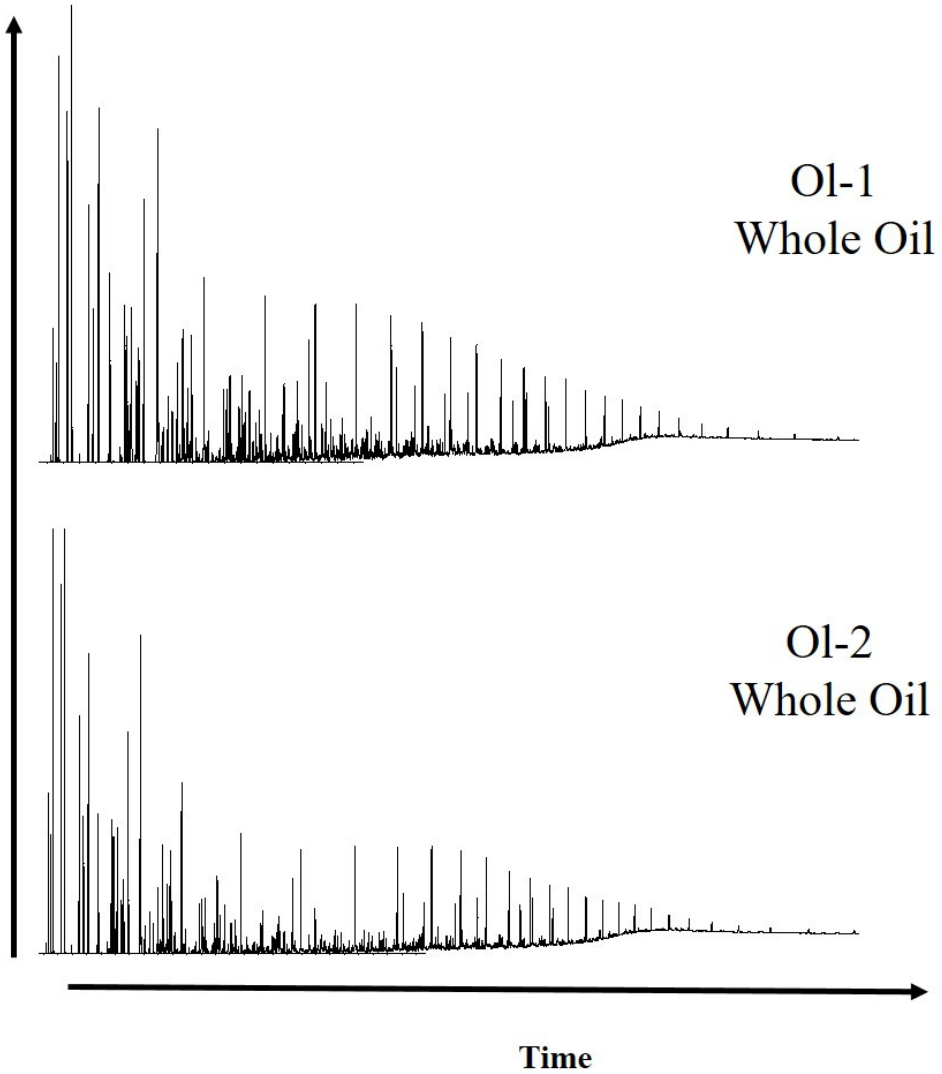

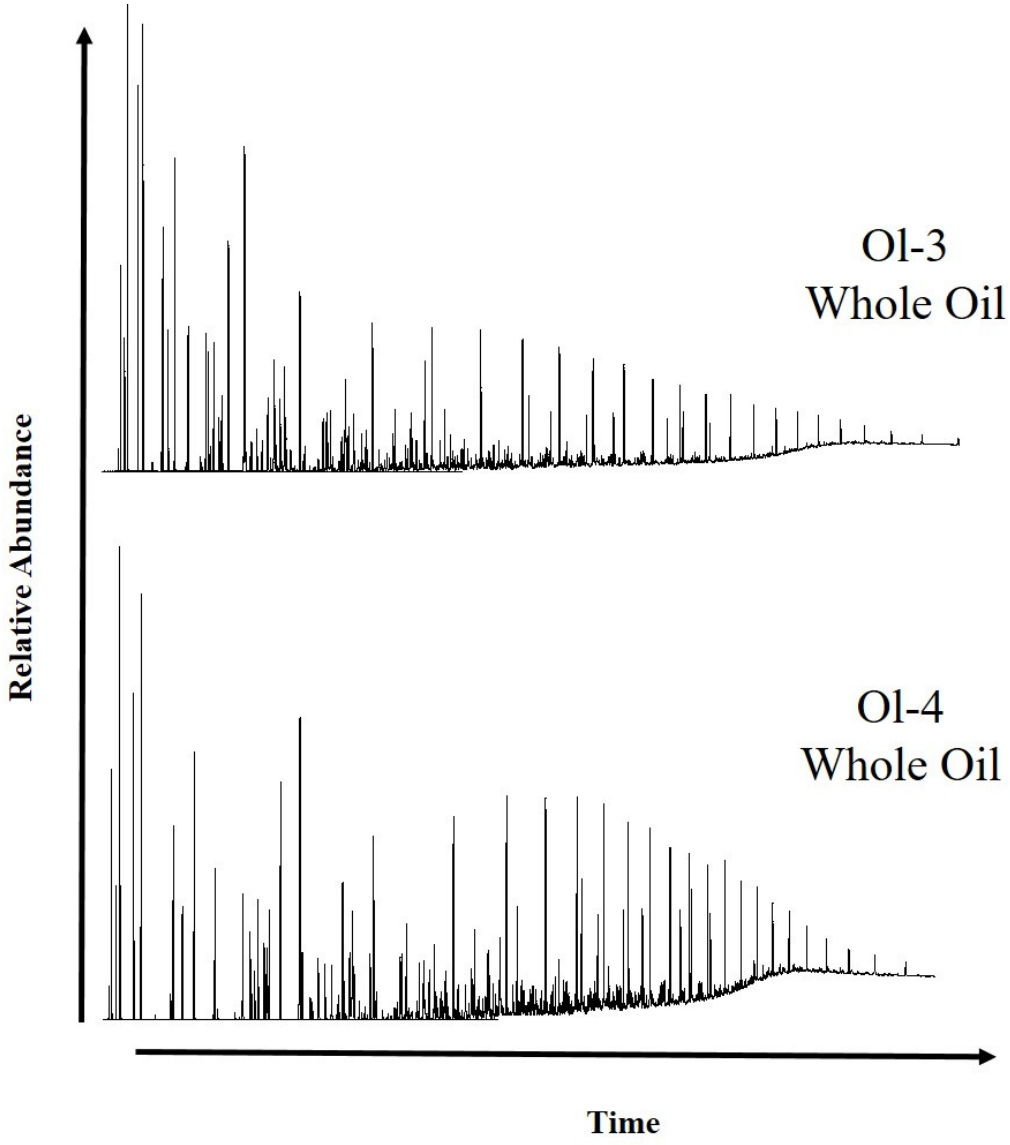
Ol-3
Whole Oil
Ol-4
Whole Oil
Relative Abundance
Time

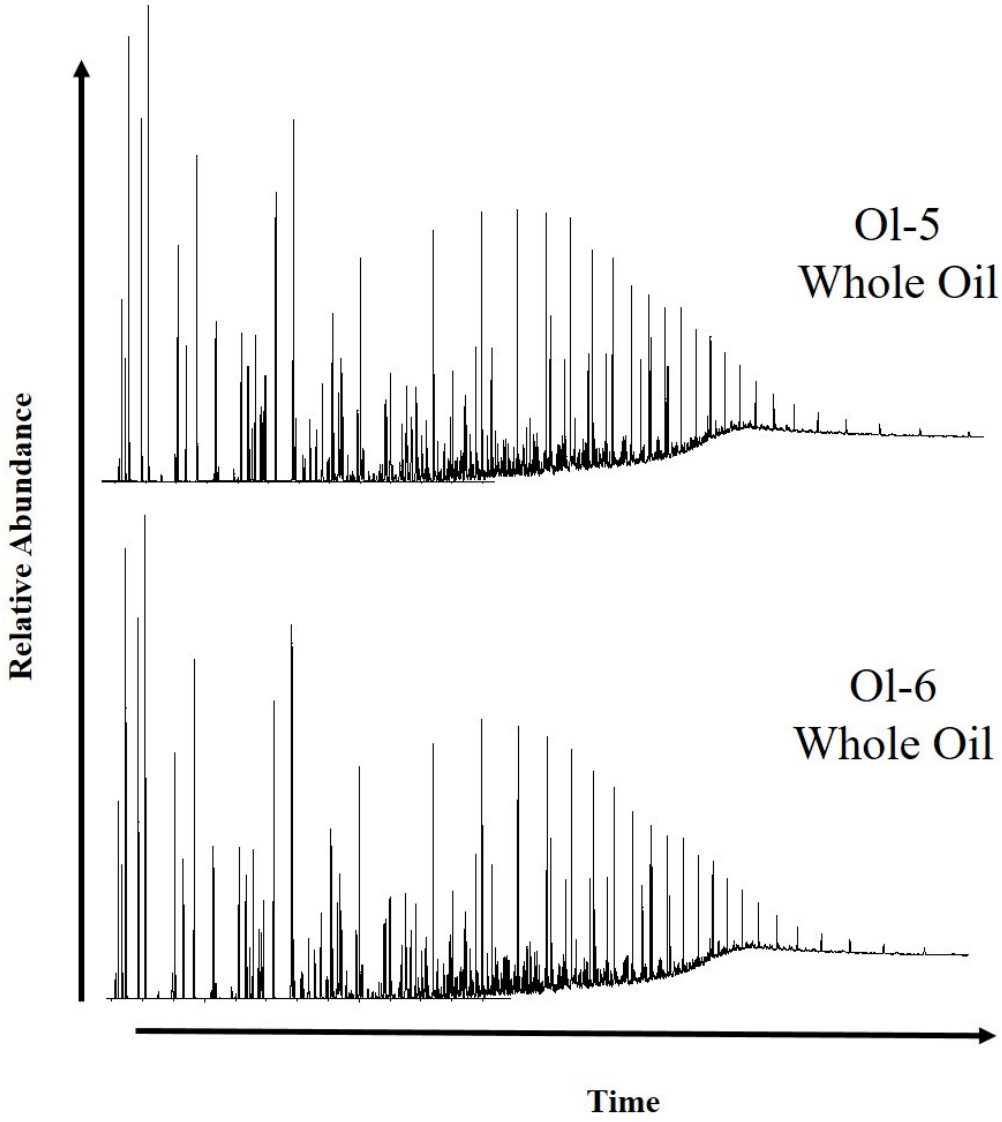
Ol-5
Whole Oil
Ol-6
Whole Oil
Relative Abundance
Time

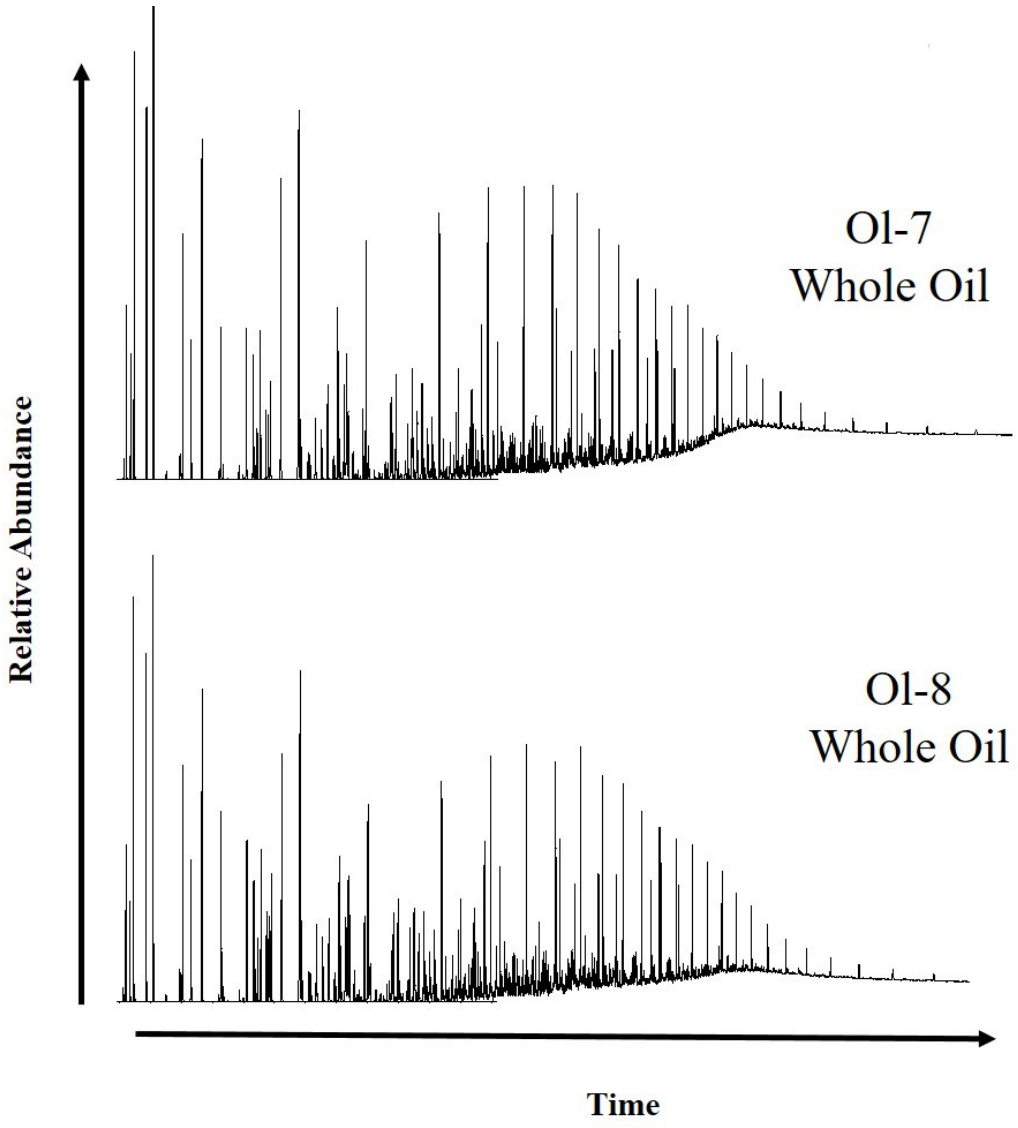
Ol-7
Whole Oil
Ol-8
Whole Oil
Relative Abundance
Time

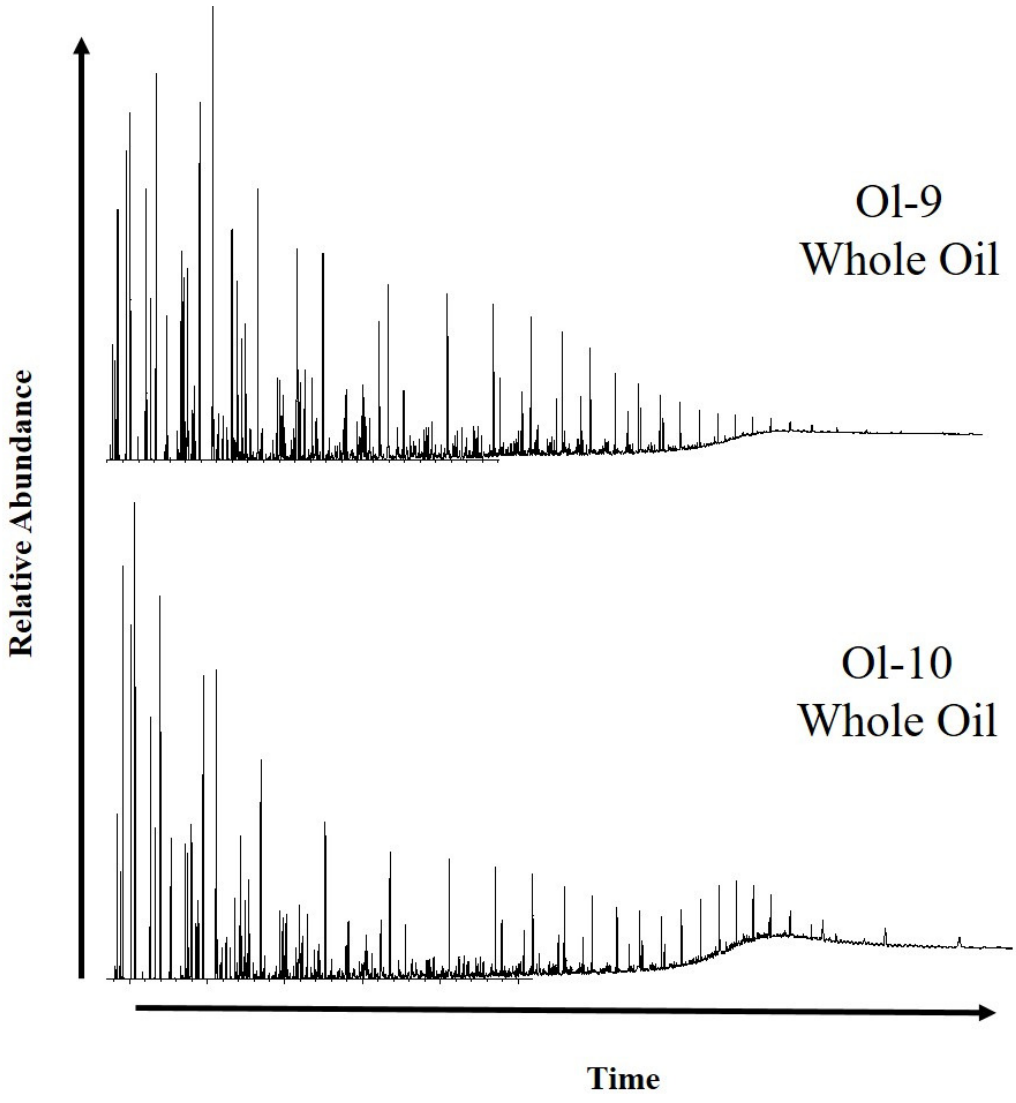
Ol-9
Whole Oil
Ol-10
Whole Oil
Relative Abundance
Time

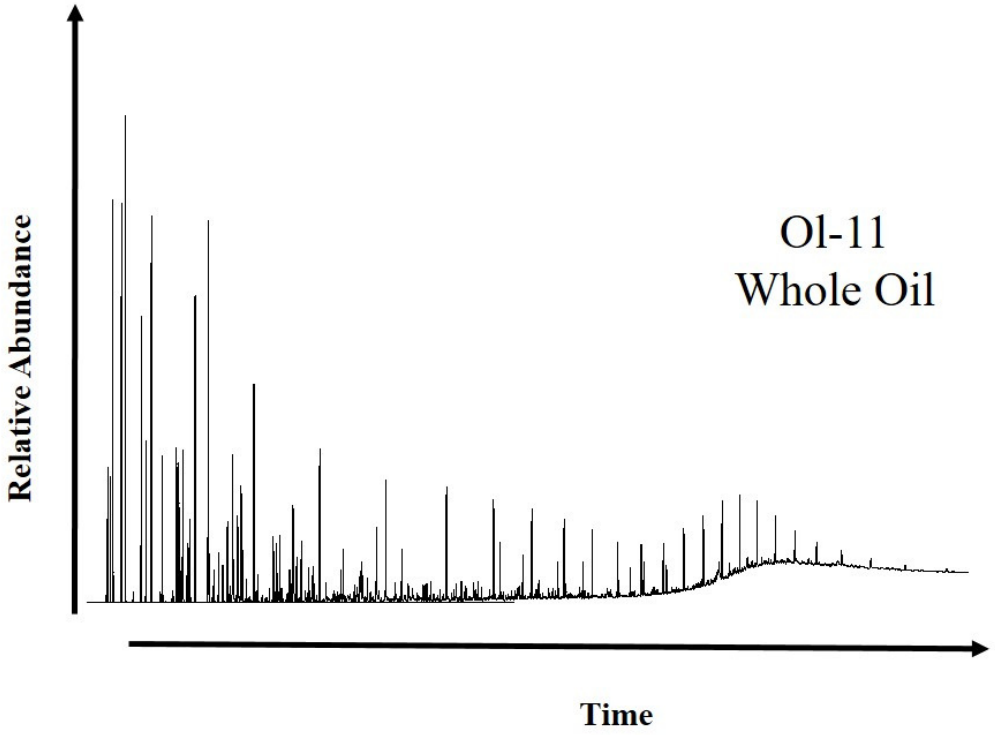
Relative Abundance
Ol-11
Whole Oil
Time

Appendix B. GC Aliphatic Chromatograms

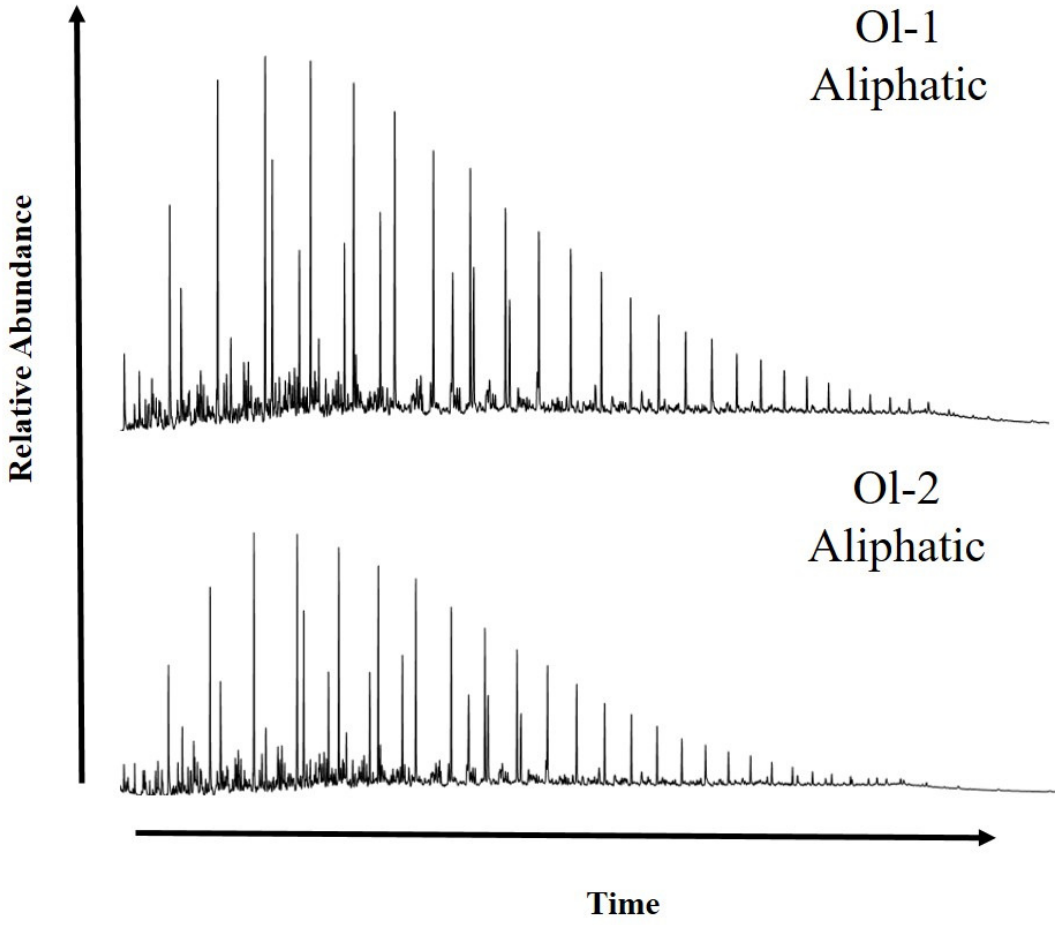

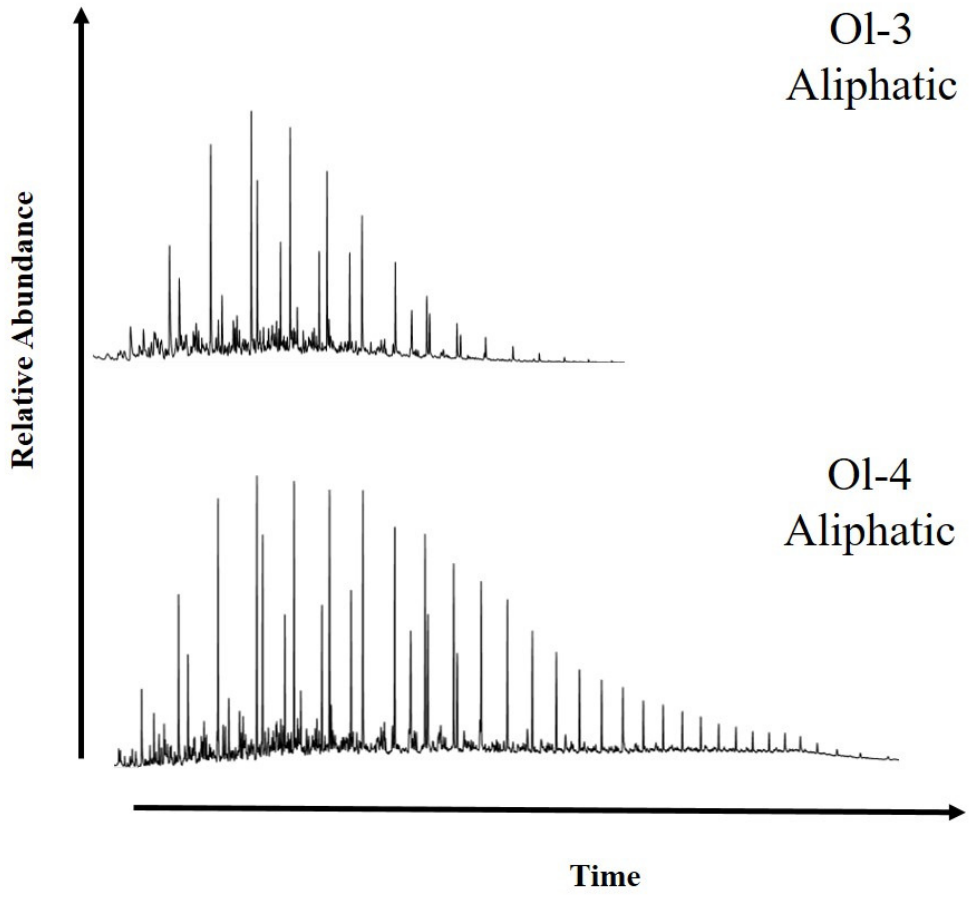
Ol-3
Aliphatic
Ol-4
Aliphatic
Relative Abundance
Time

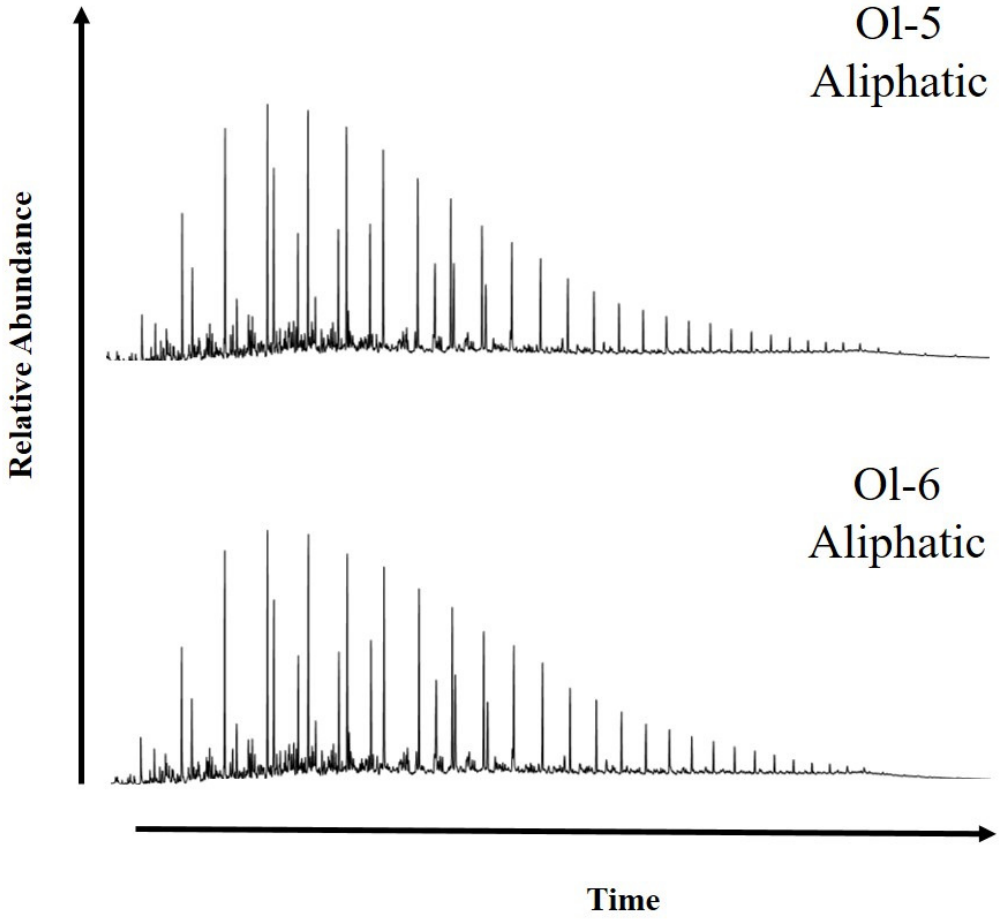
Ol-5
Aliphatic
Ol-6
Aliphatic
Relative Abundance
Time

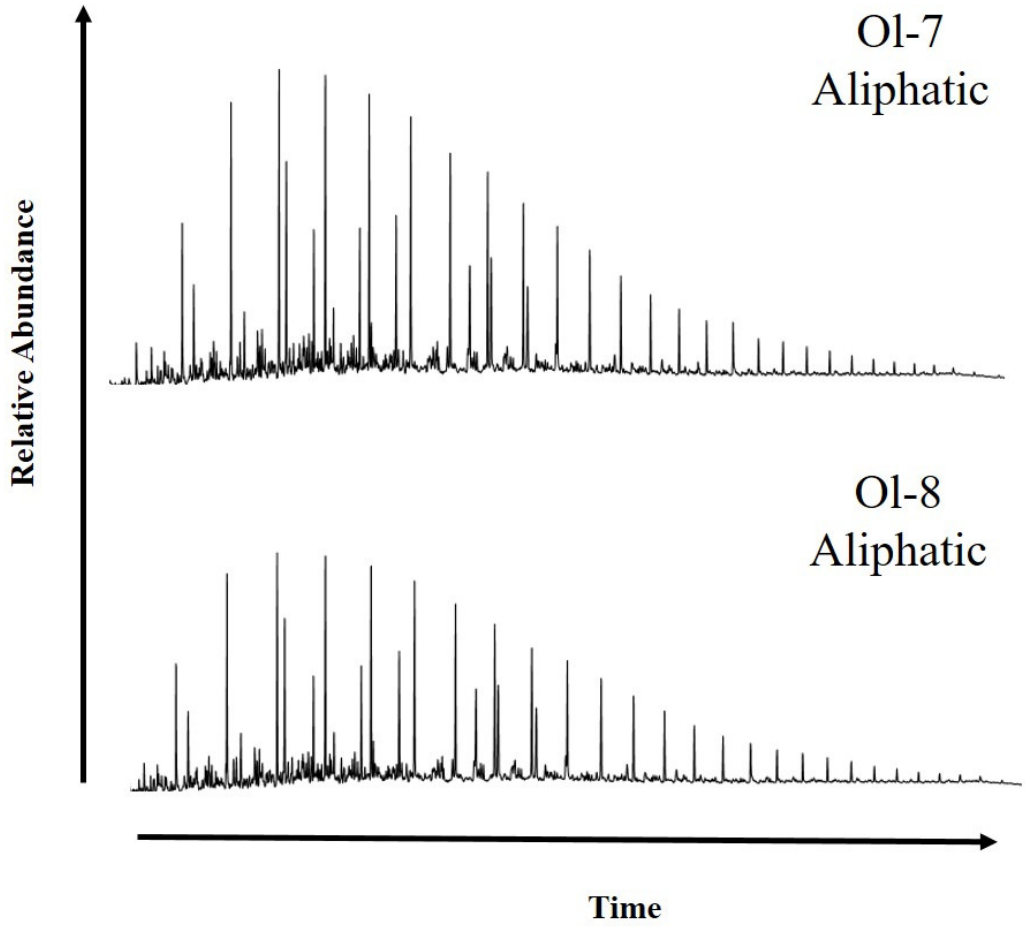
Ol-7
Aliphatic
Ol-8
Aliphatic
Relative Abundance
Time

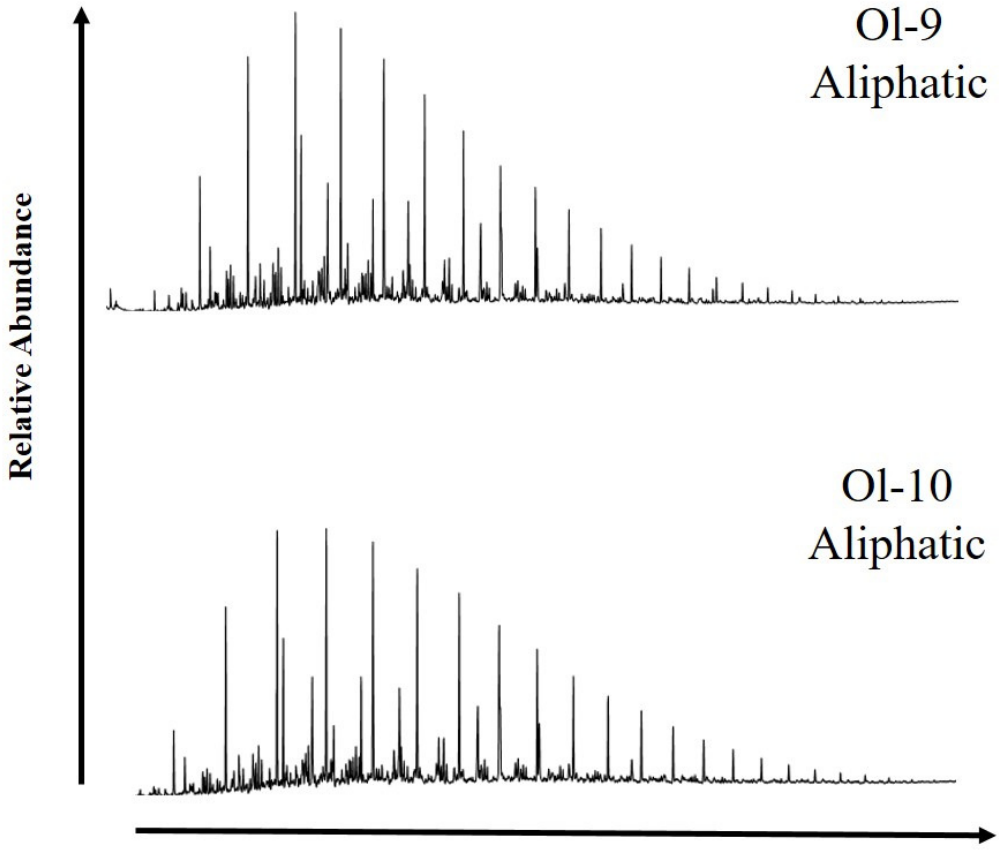
Ol-9
Aliphatic
Relative Abundance
Ol-10
Aliphatic

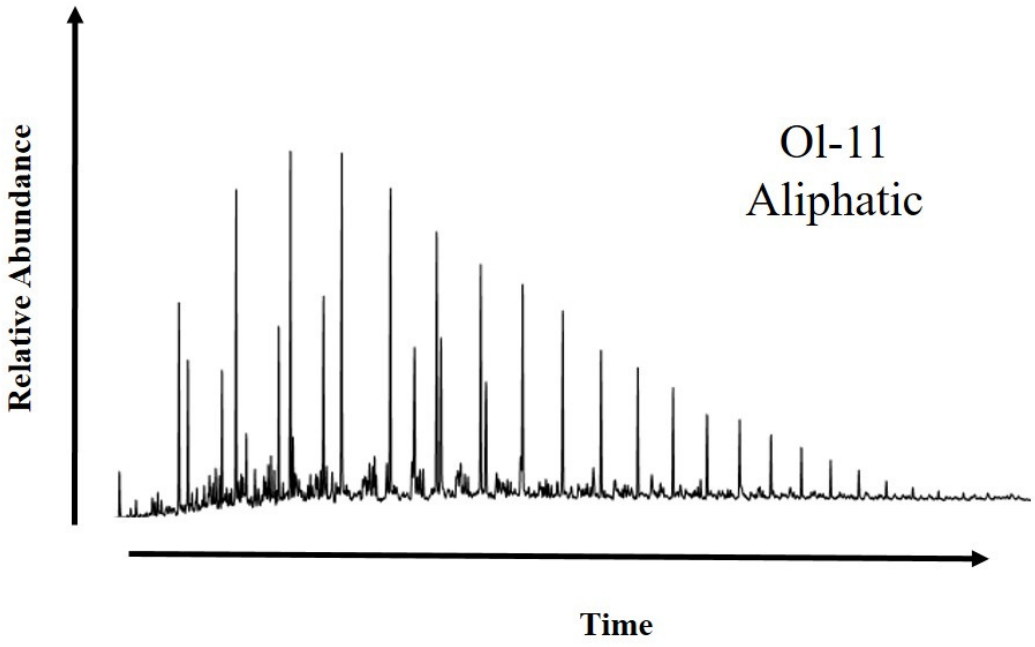
Relative Abundance
Ol-11
Aliphatic
Time

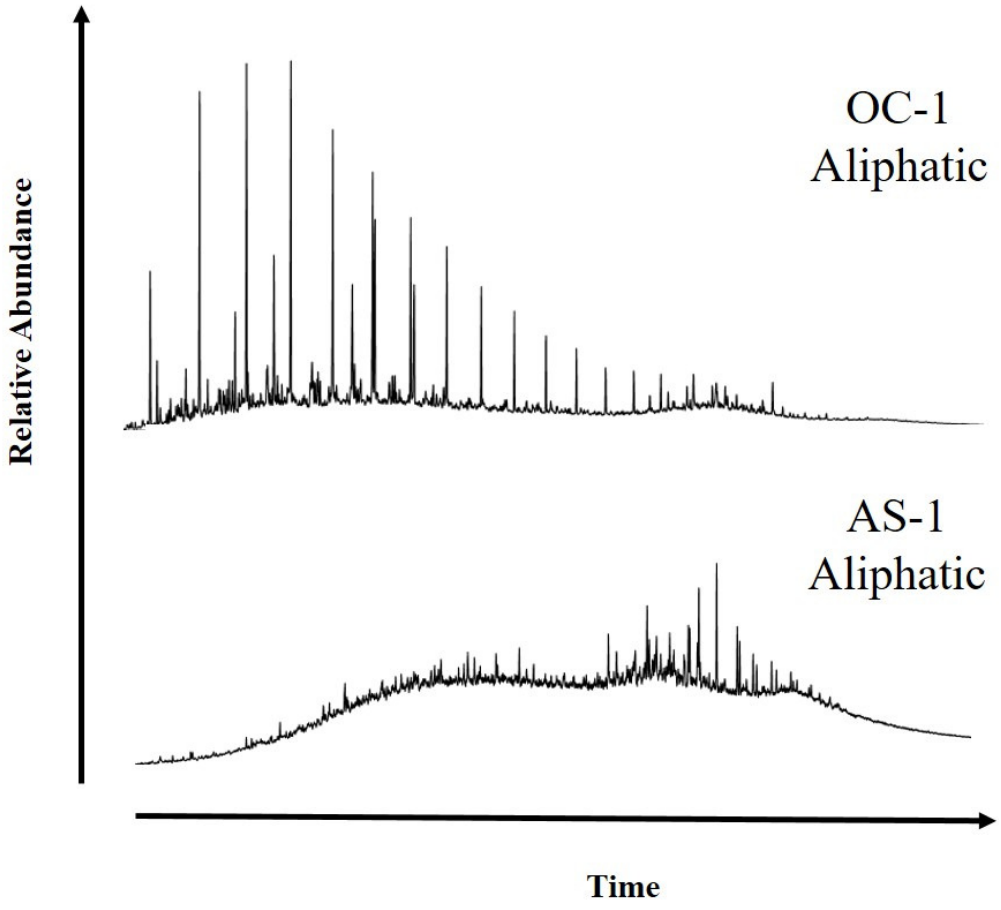
Relative Abundance
OC-1
Aliphatic
AS-1
Aliphatic
Time

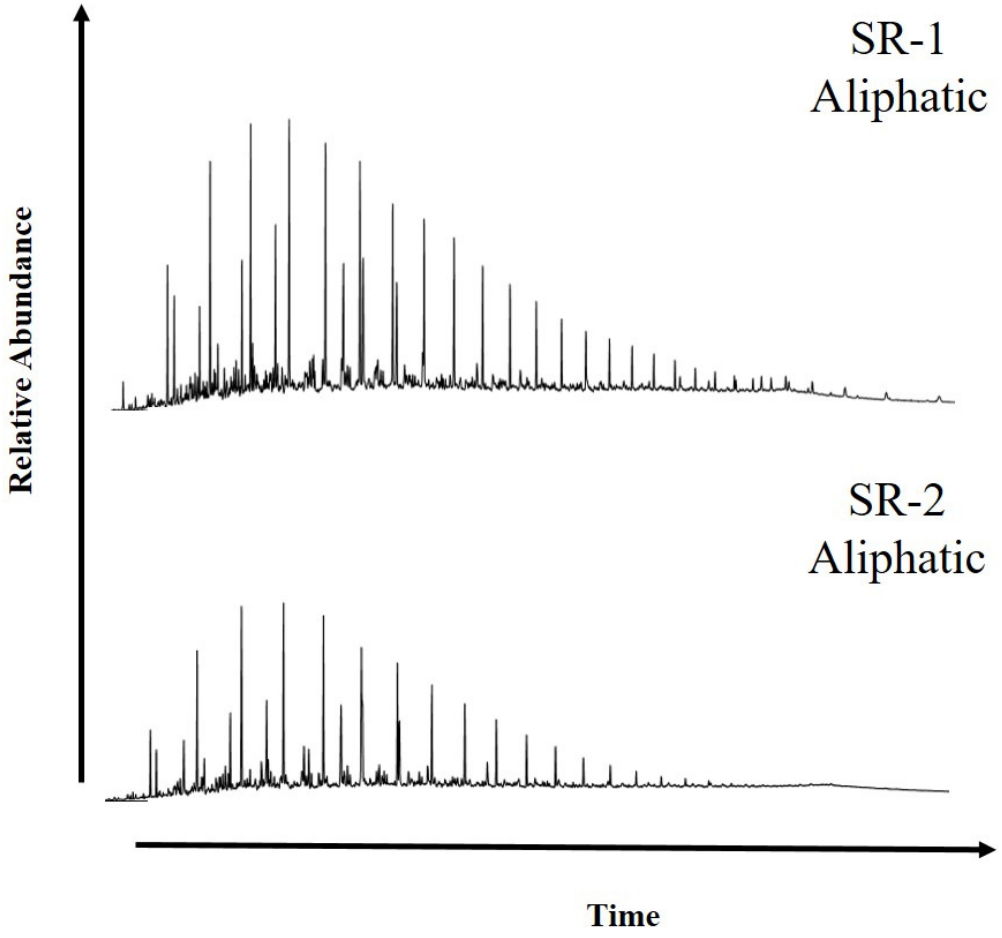
SR-1
Aliphatic
SR-2
Aliphatic
Relative Abundance
Time

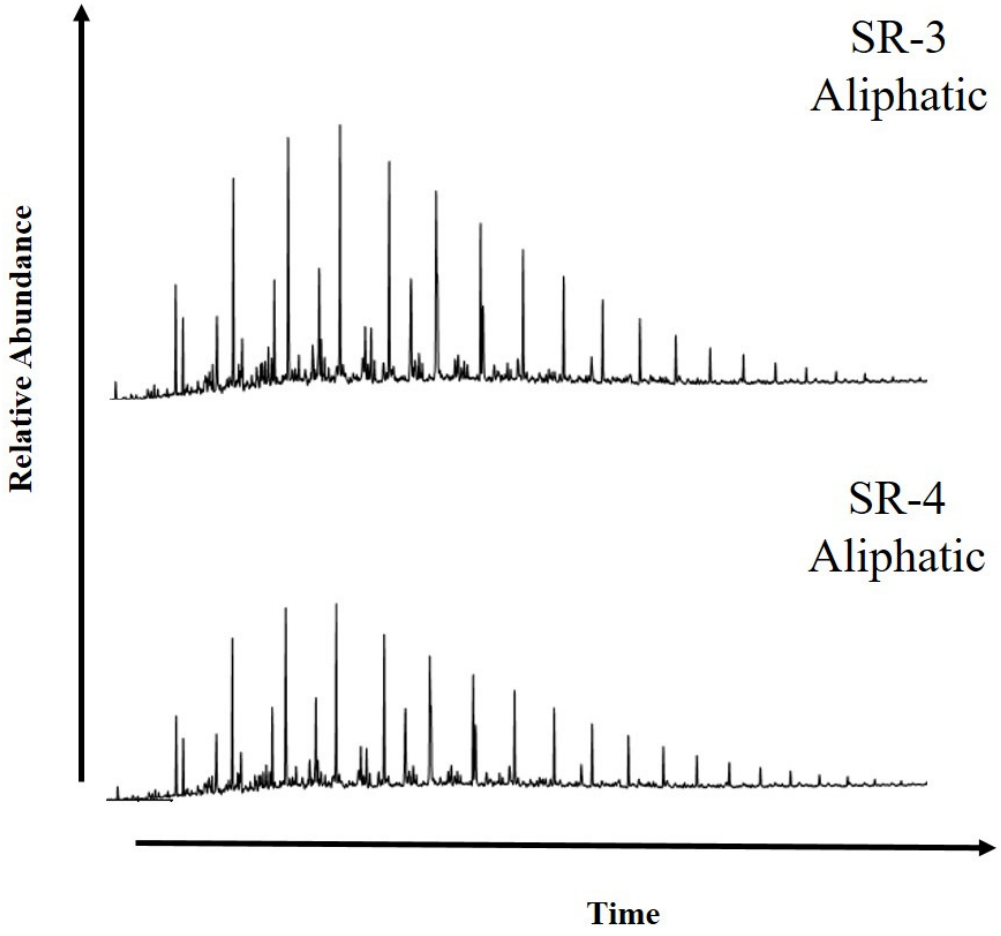
SR-3
Aliphatic
SR-4
Aliphatic
Relative Abundance
Time

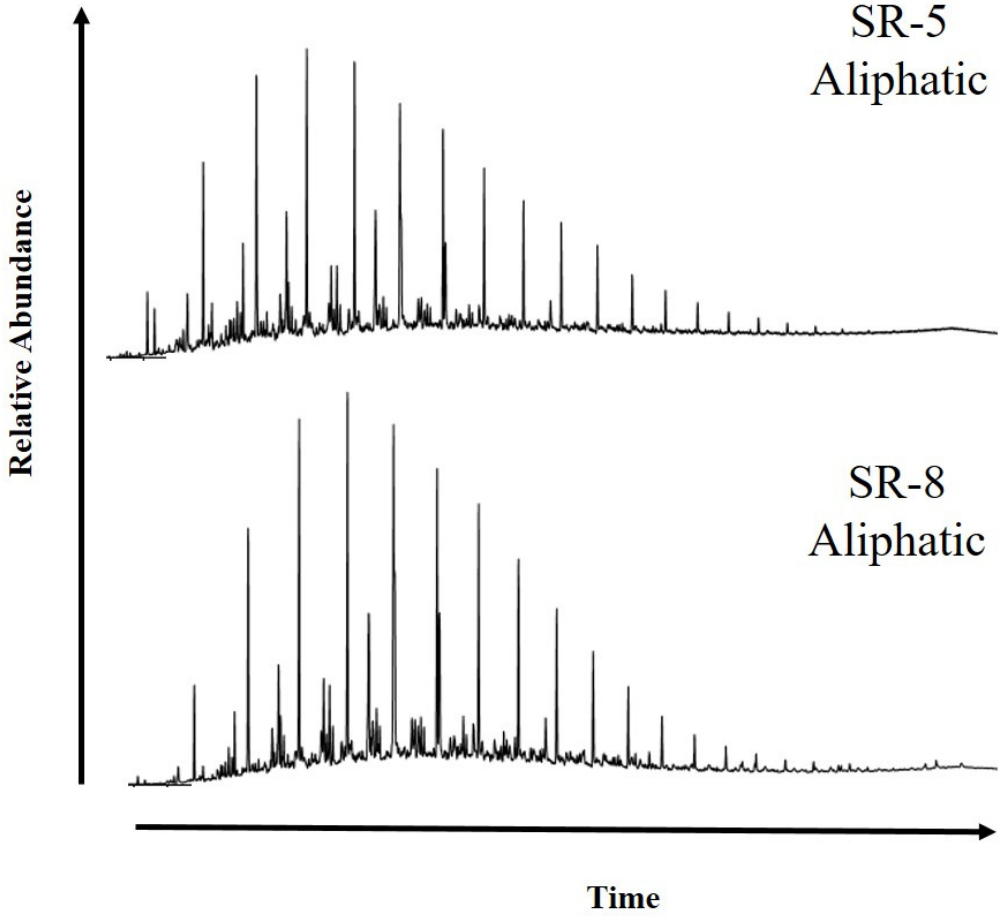
SR-5
Aliphatic
SR-8
Aliphatic
Relative Abundance
Time

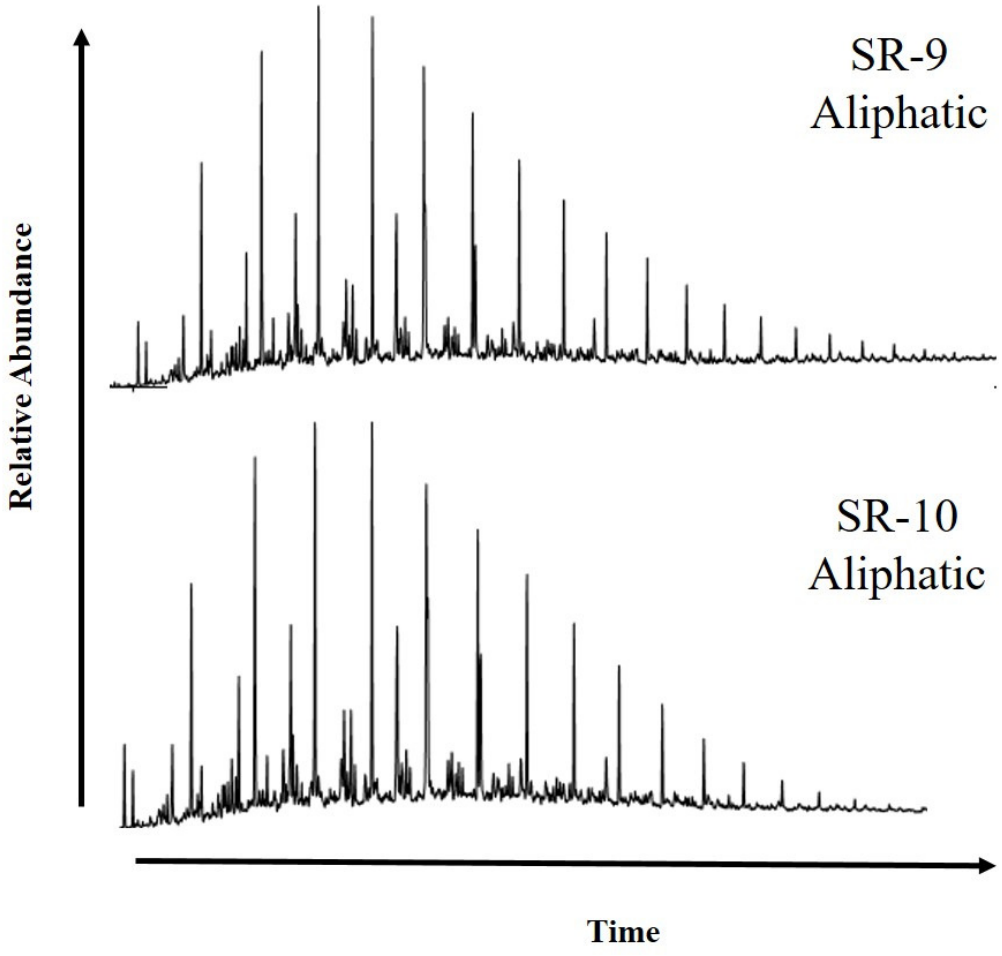
SR-9
Aliphatic
SR-10
Aliphatic
Relative Abundance
Time

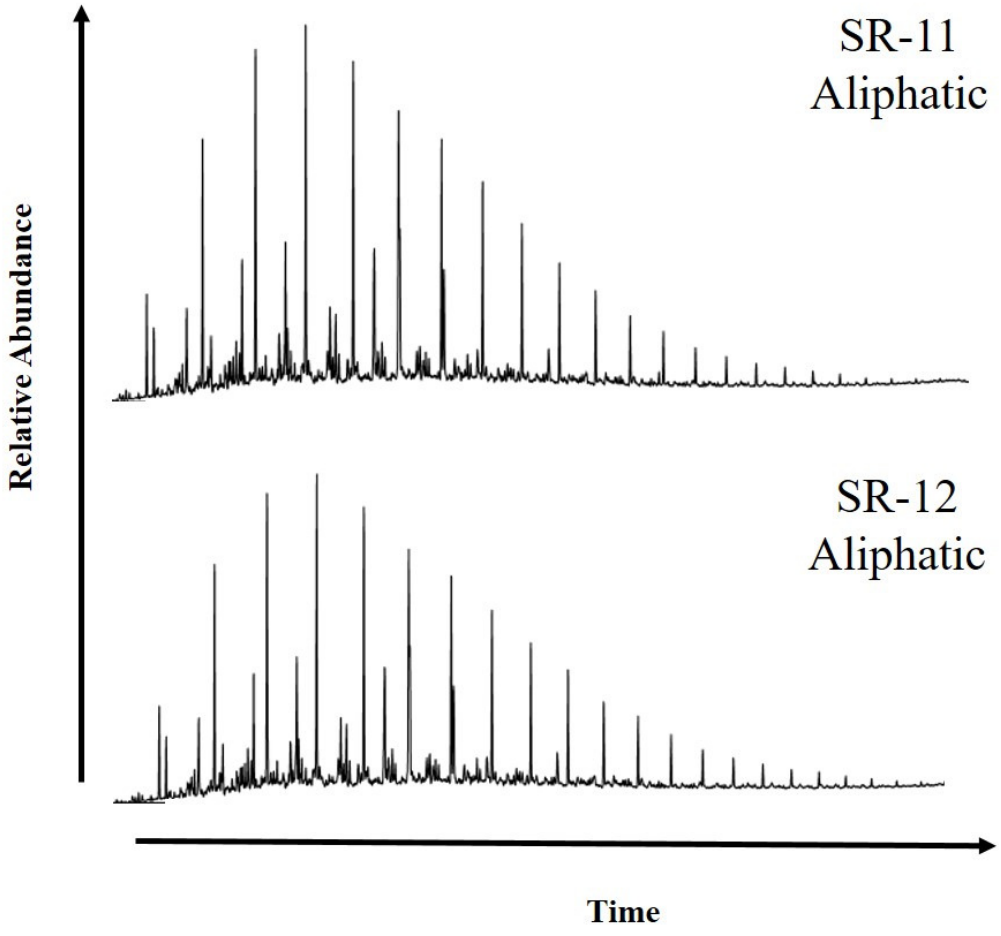
SR-11
Aliphatic
SR-12
Aliphatic
Relative Abundance
Time

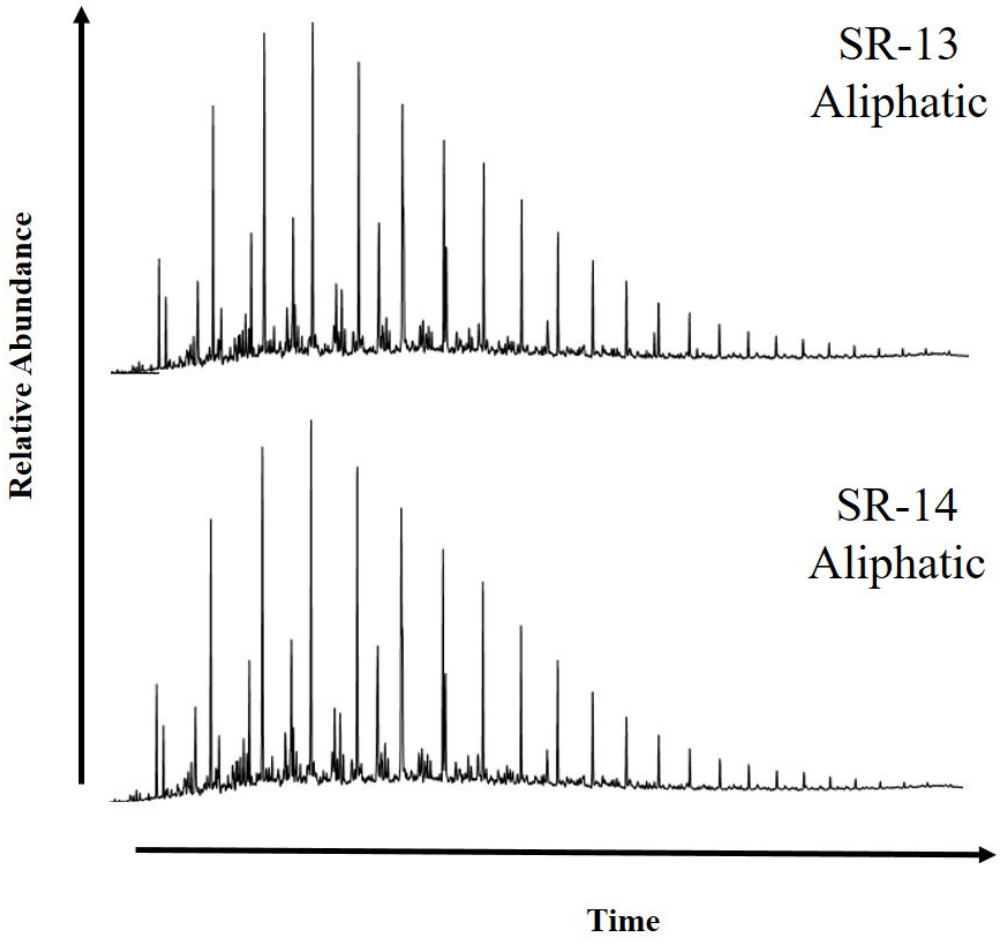
SR-13
Aliphatic
SR-14
Aliphatic
Relative Abundance
Time

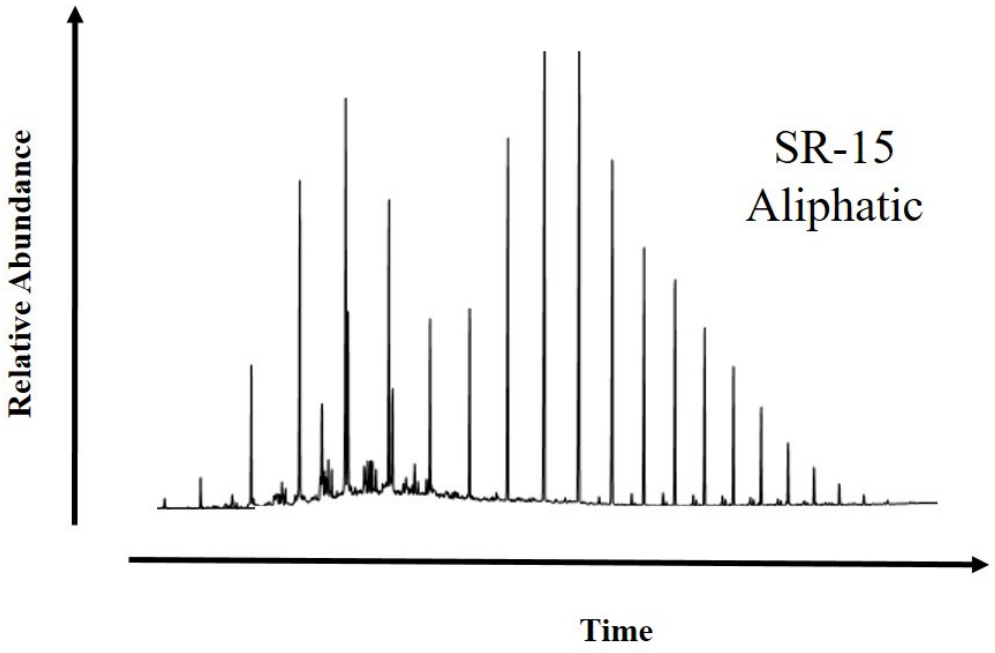
Relative Abundance
SR-15
Aliphatic
Time

Appendix C. GCMS *m/z* 191 Chromatograms

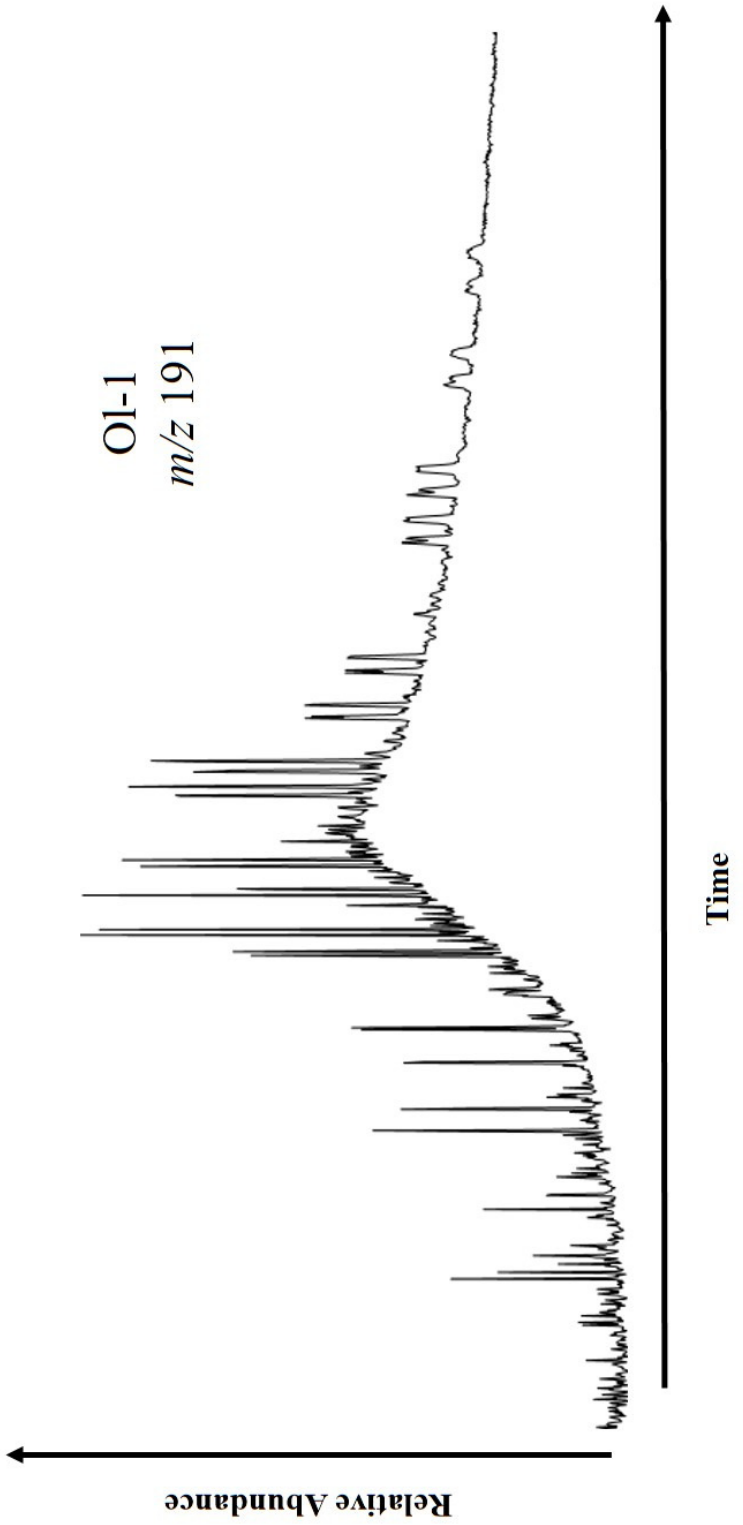

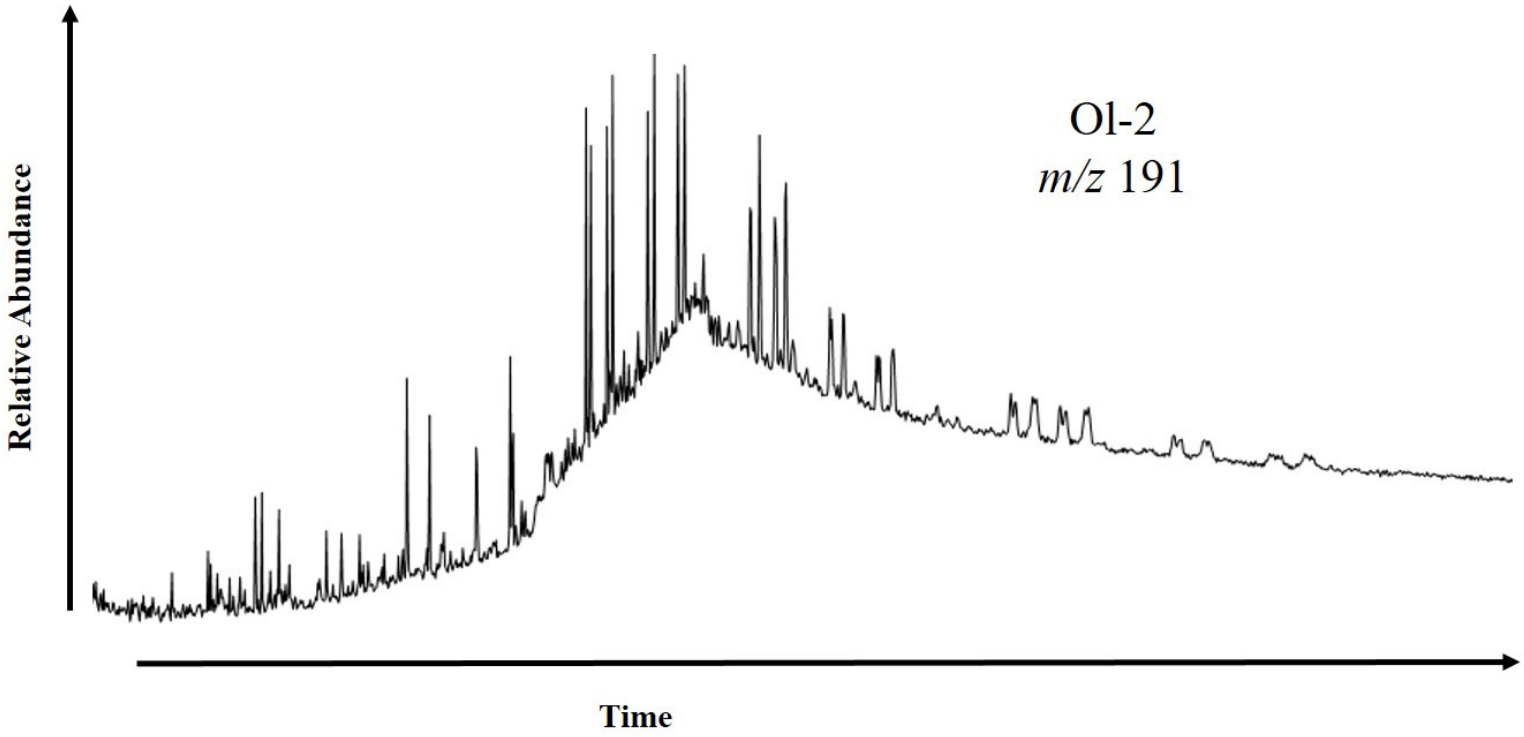
Ol-2
m/z 191
Relative Abundance
Time

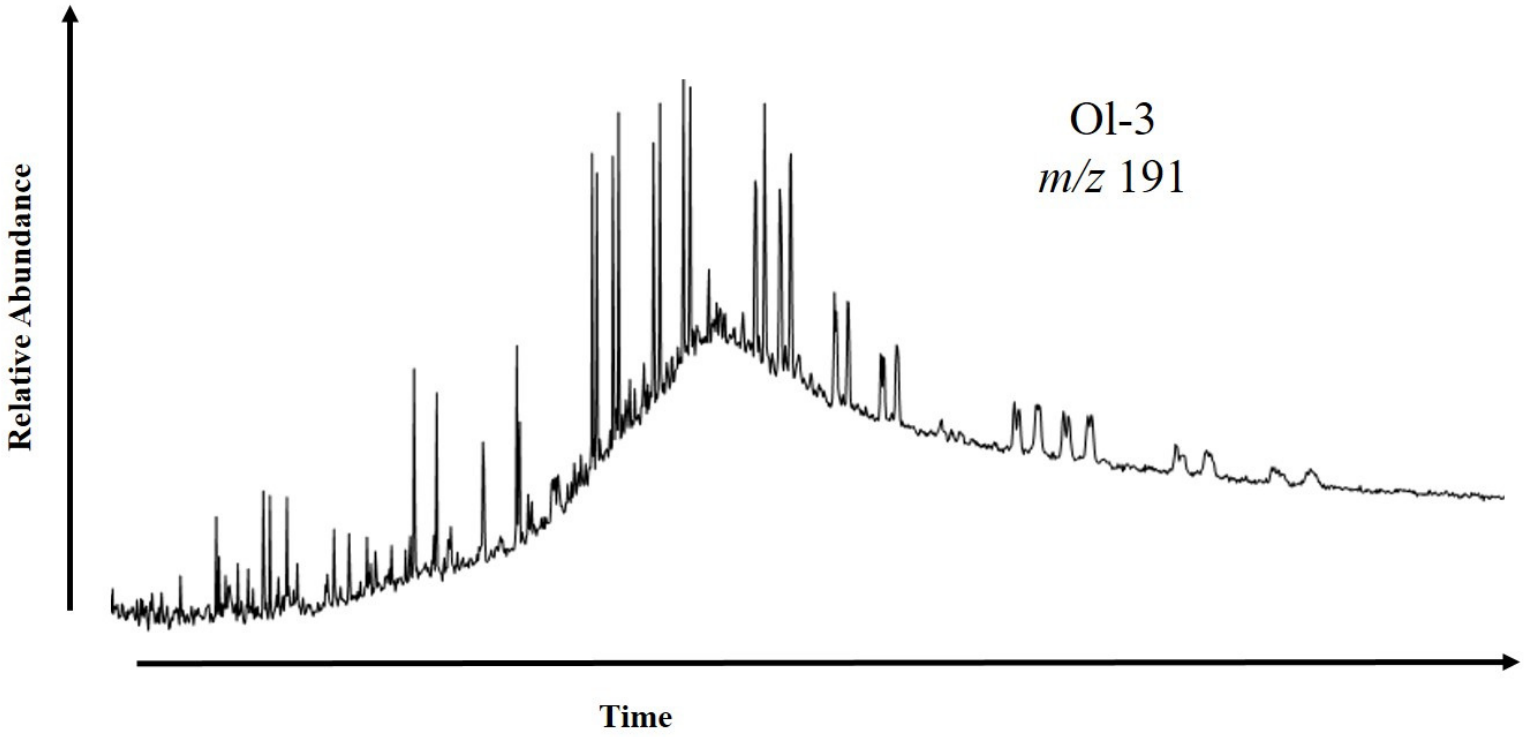
Ol-3
m/z 191
Relative Abundance
Time

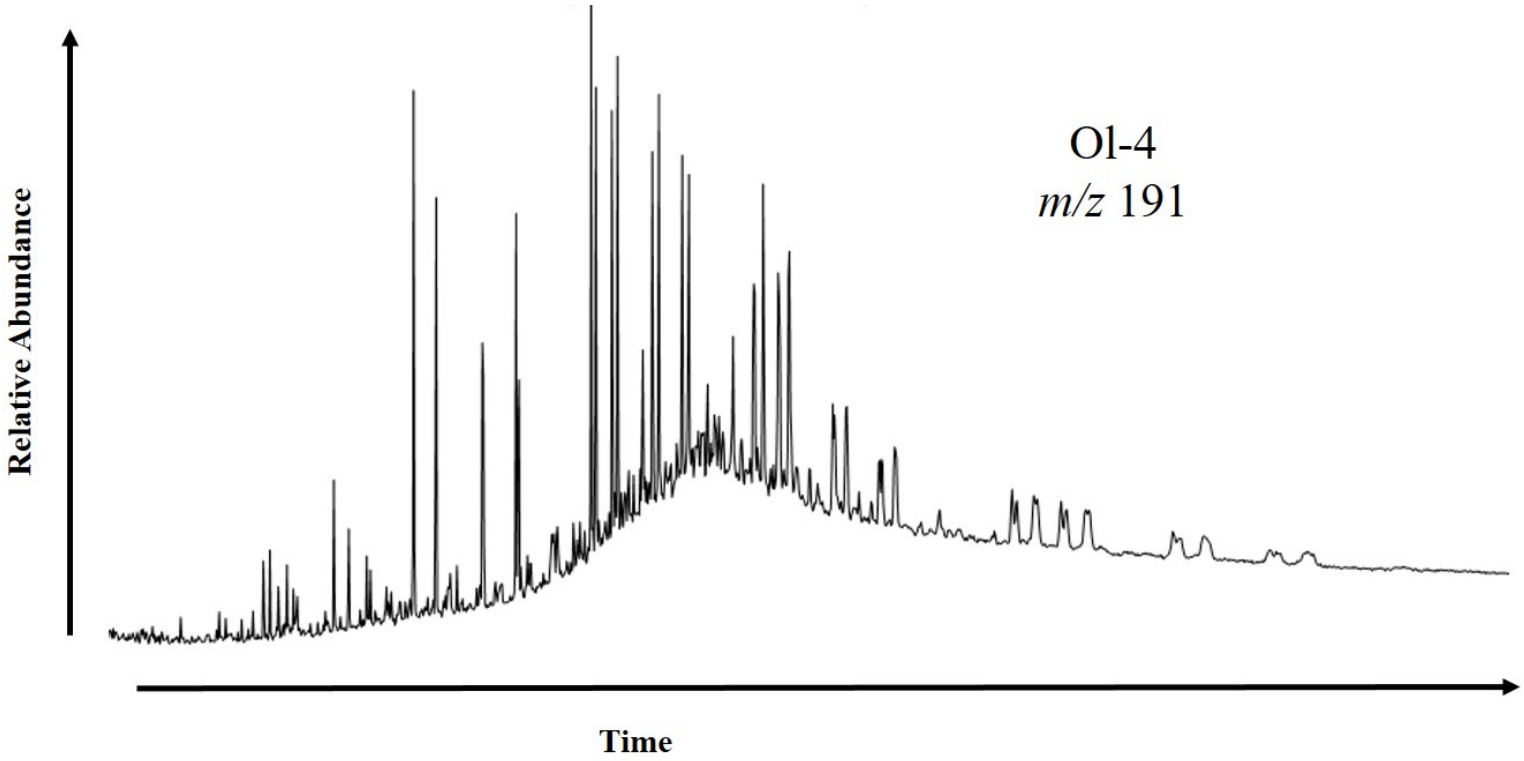
Ol-4
m/z 191
Relative Abundance
Time

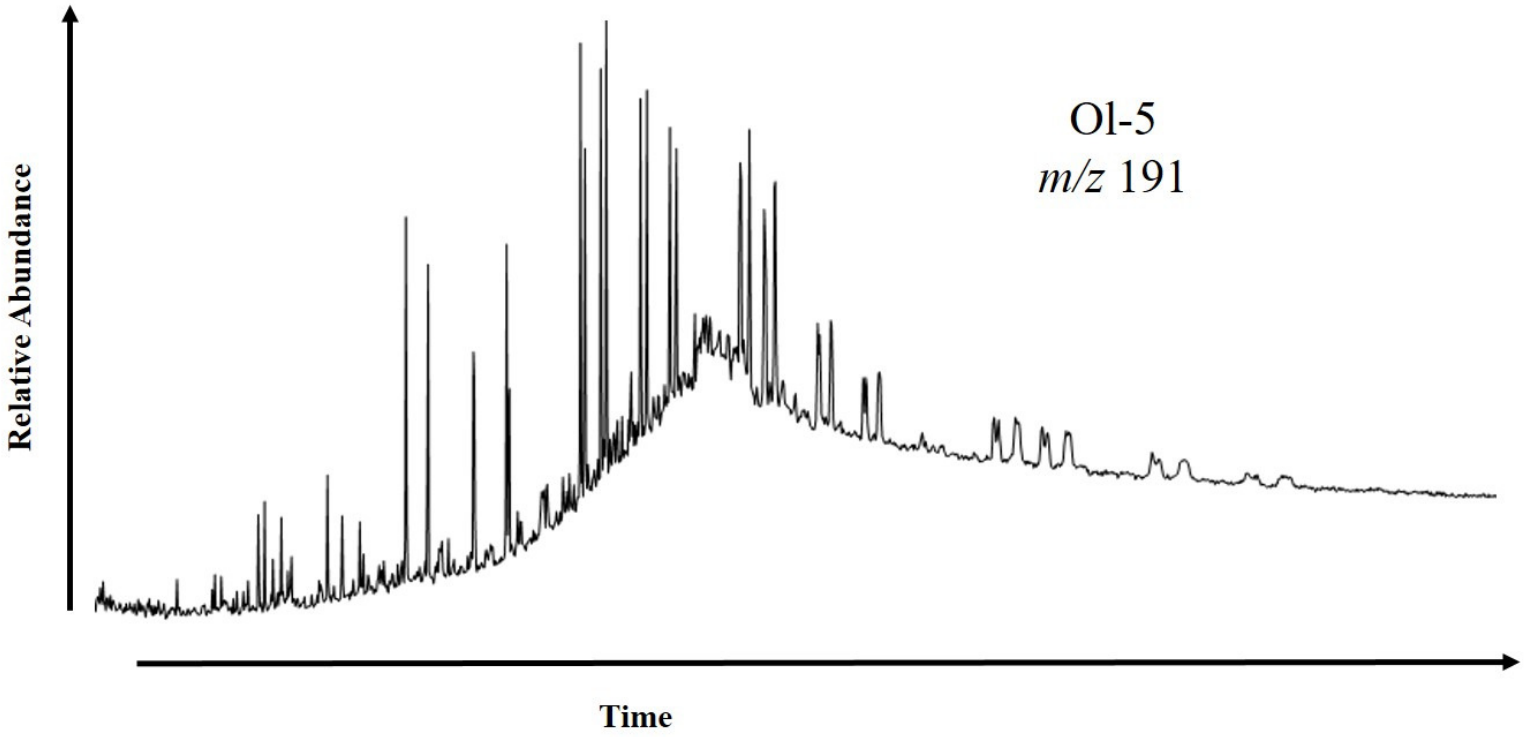
Ol-5
m/z 191
Relative Abundance
Time

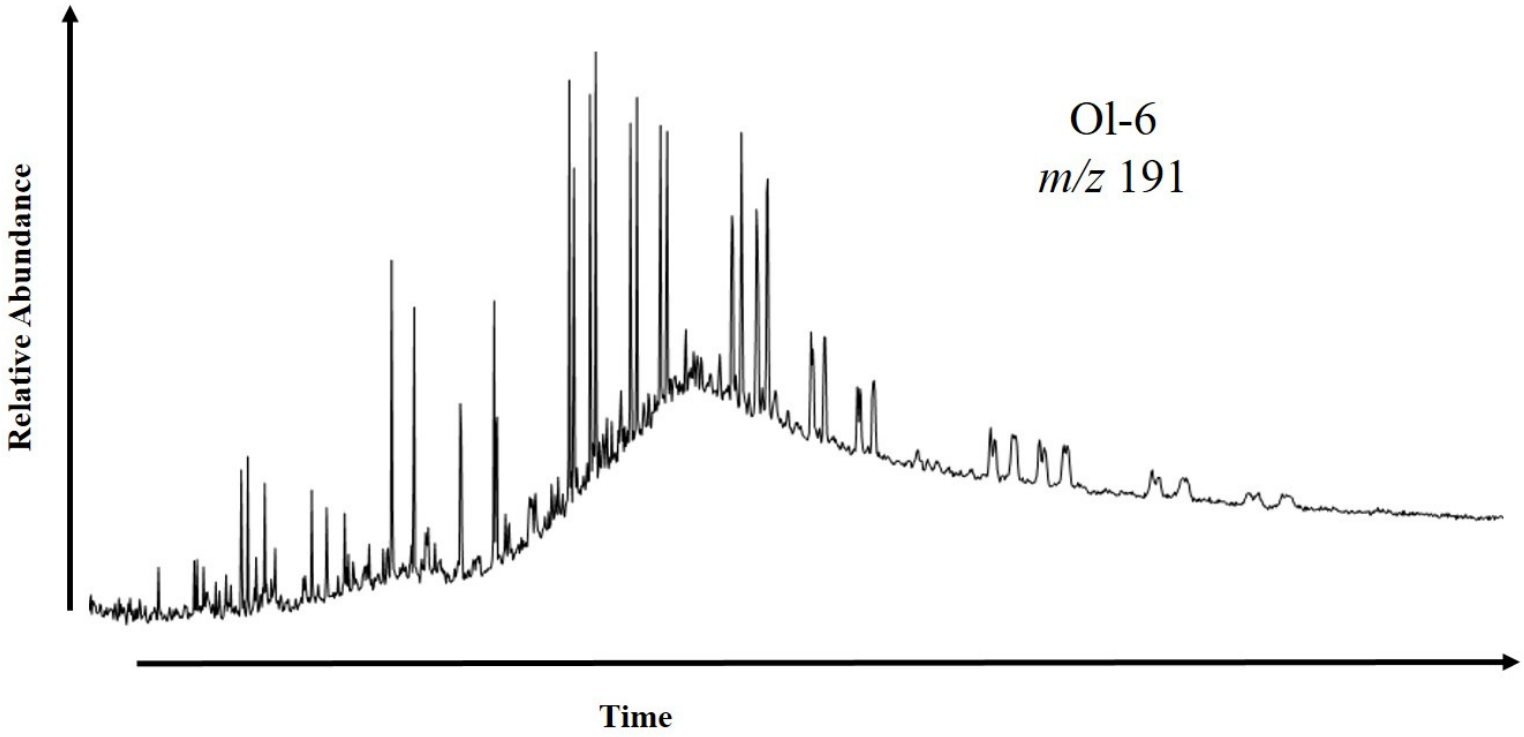
Ol-6
m/z 191
Relative Abundance
Time

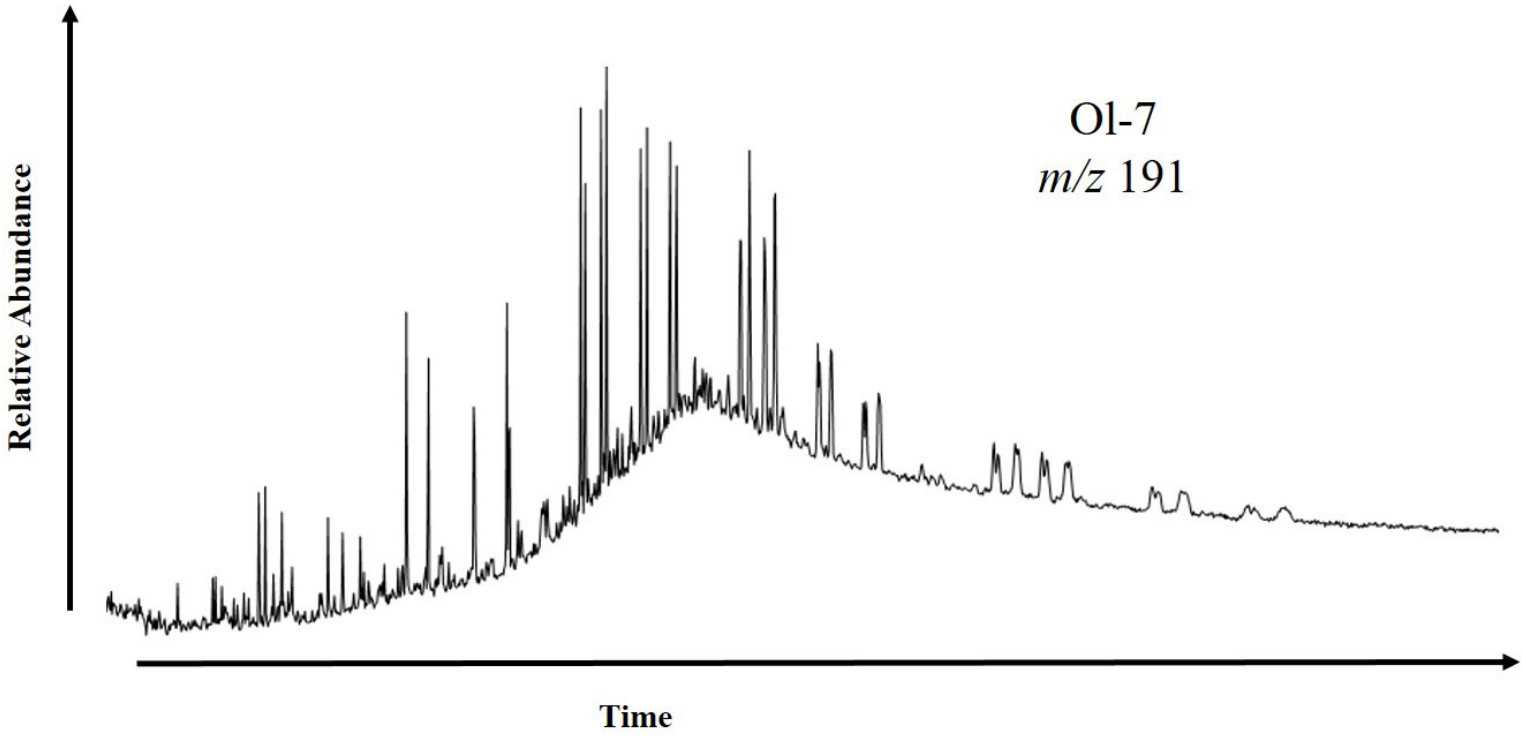
Ol-7
m/z 191
Relative Abundance
Time

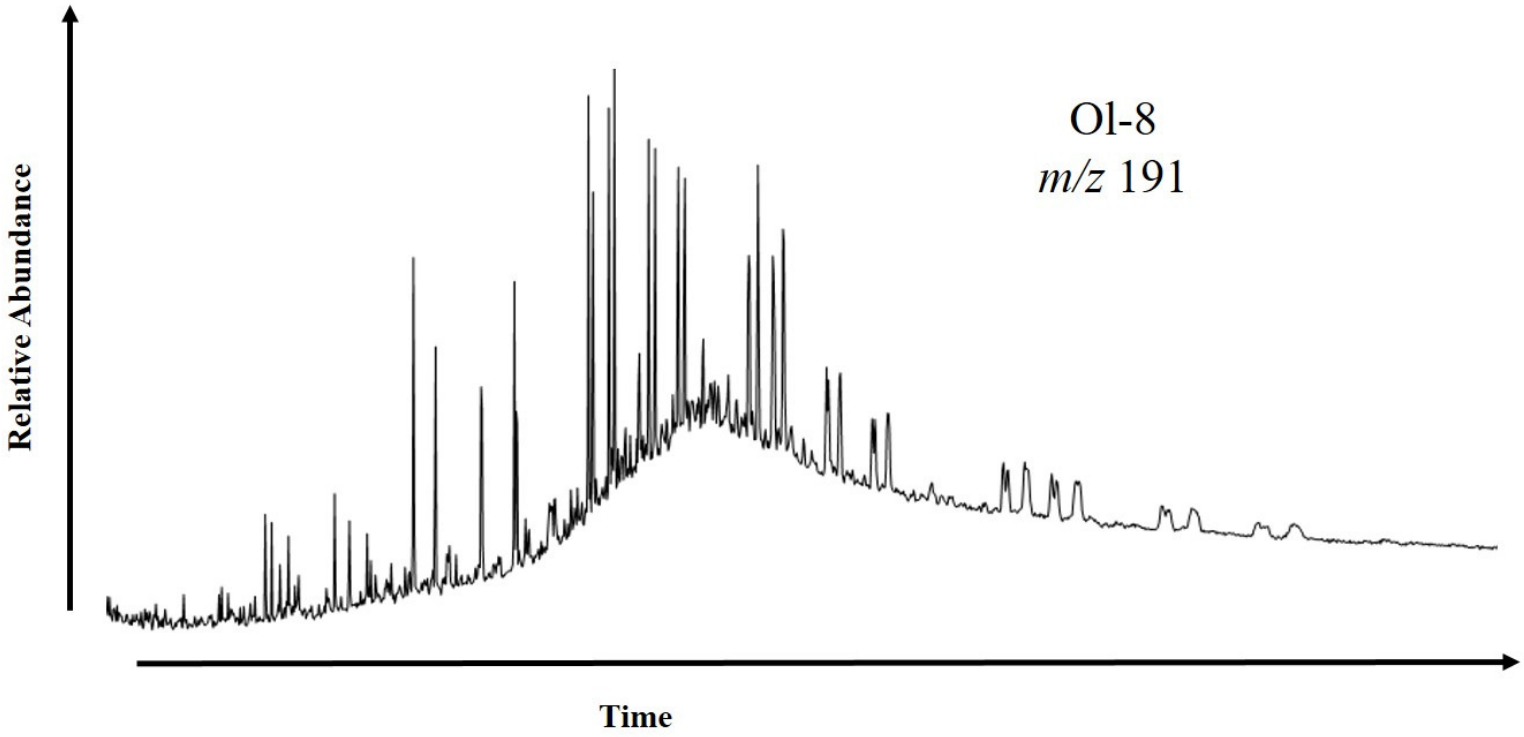
Ol-8
m/z 191
Relative Abundance
Time

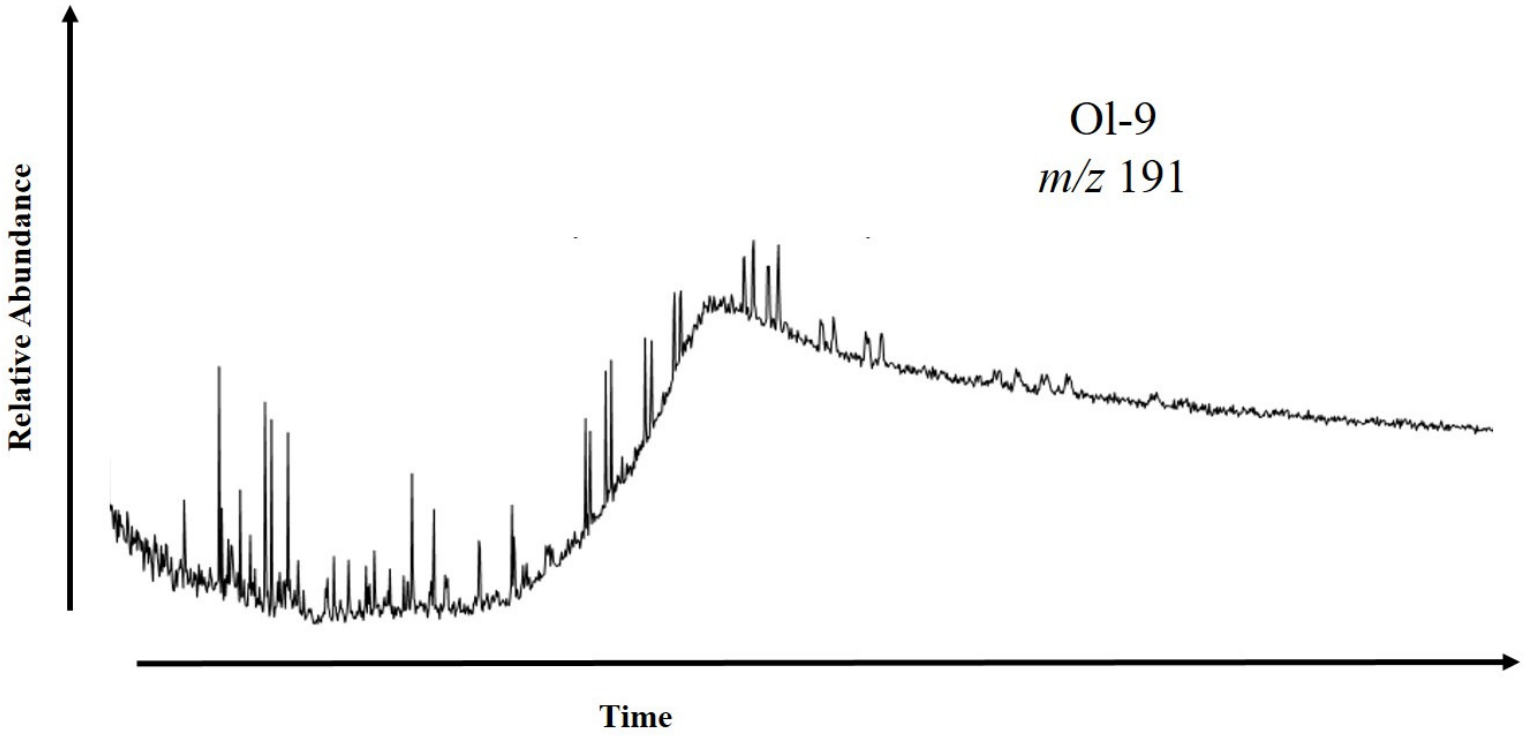
Ol-9
m/z 191
Relative Abundance
Time

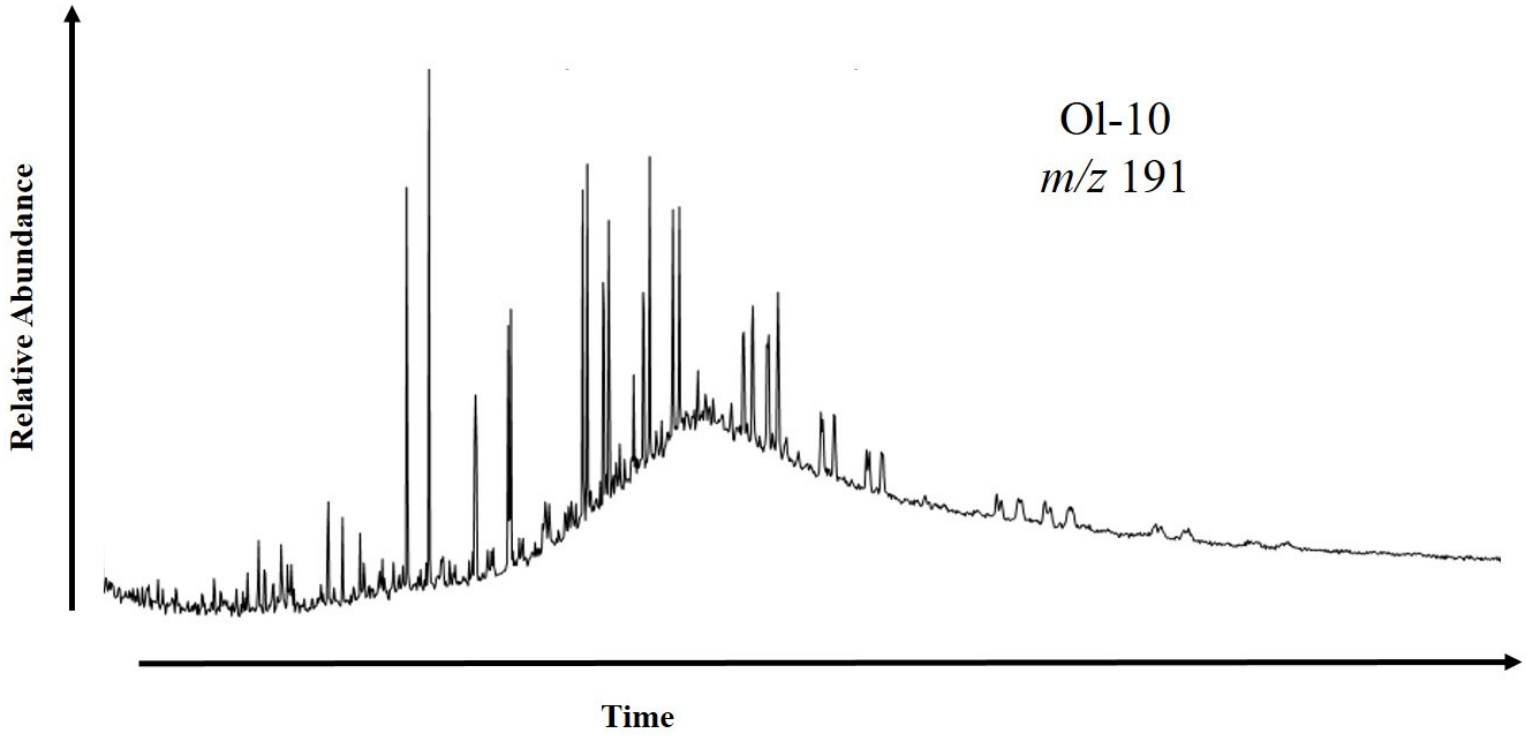
Ol-10
m/z 191
Relative Abundance
Time

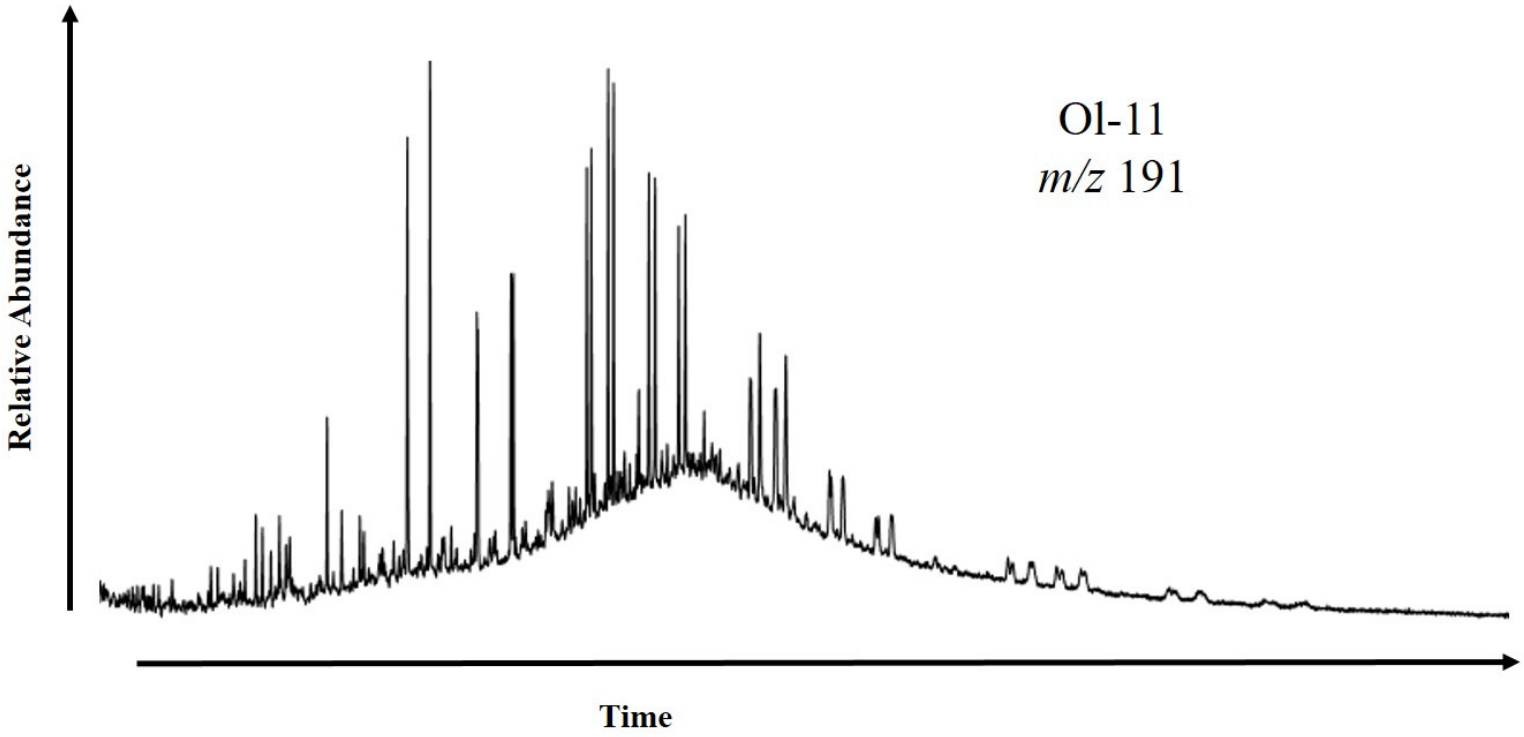
Ol-11
m/z 191
Relative Abundance
Time

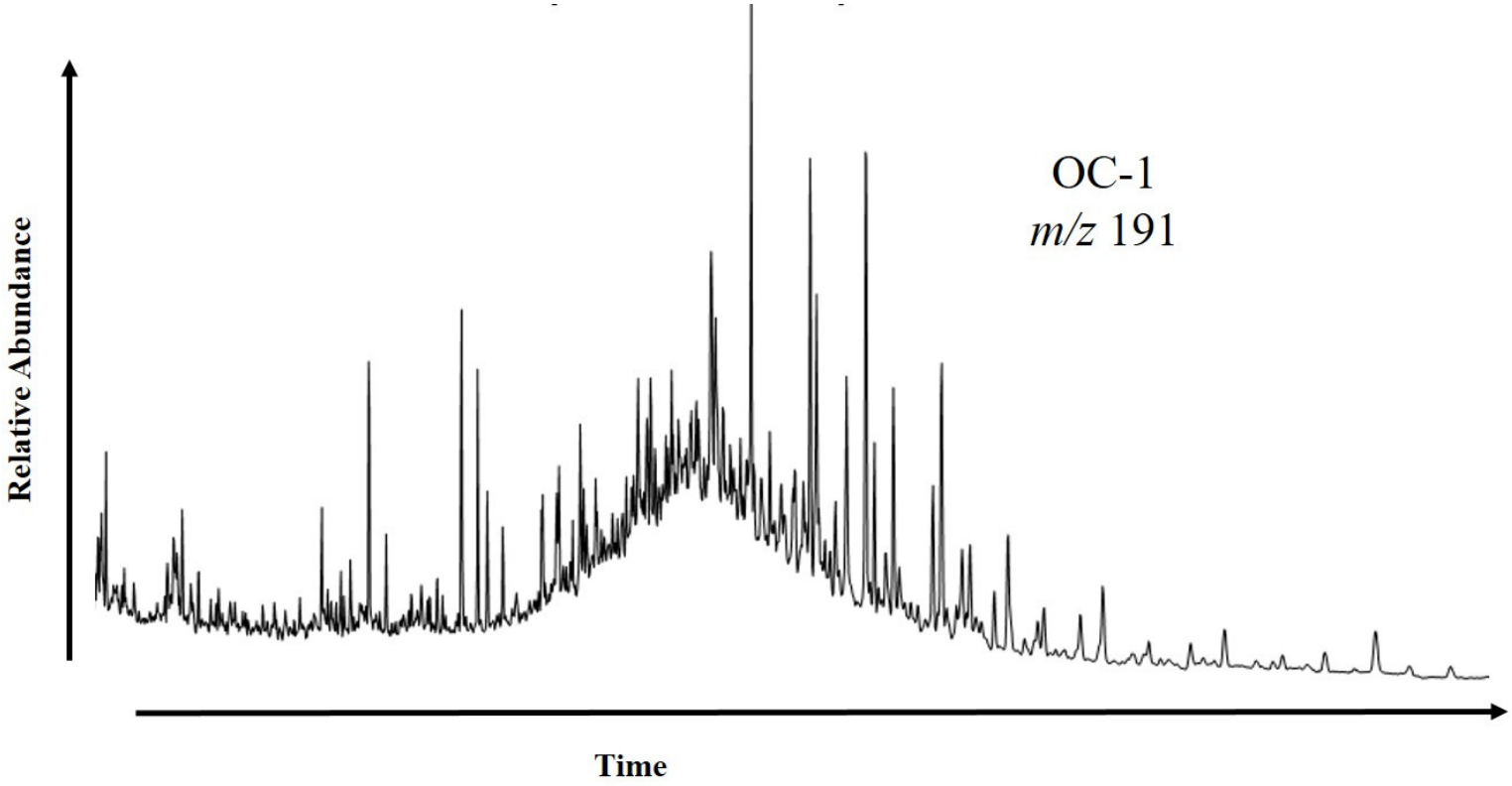
OC-1
m/z 191
Relative Abundance
Time

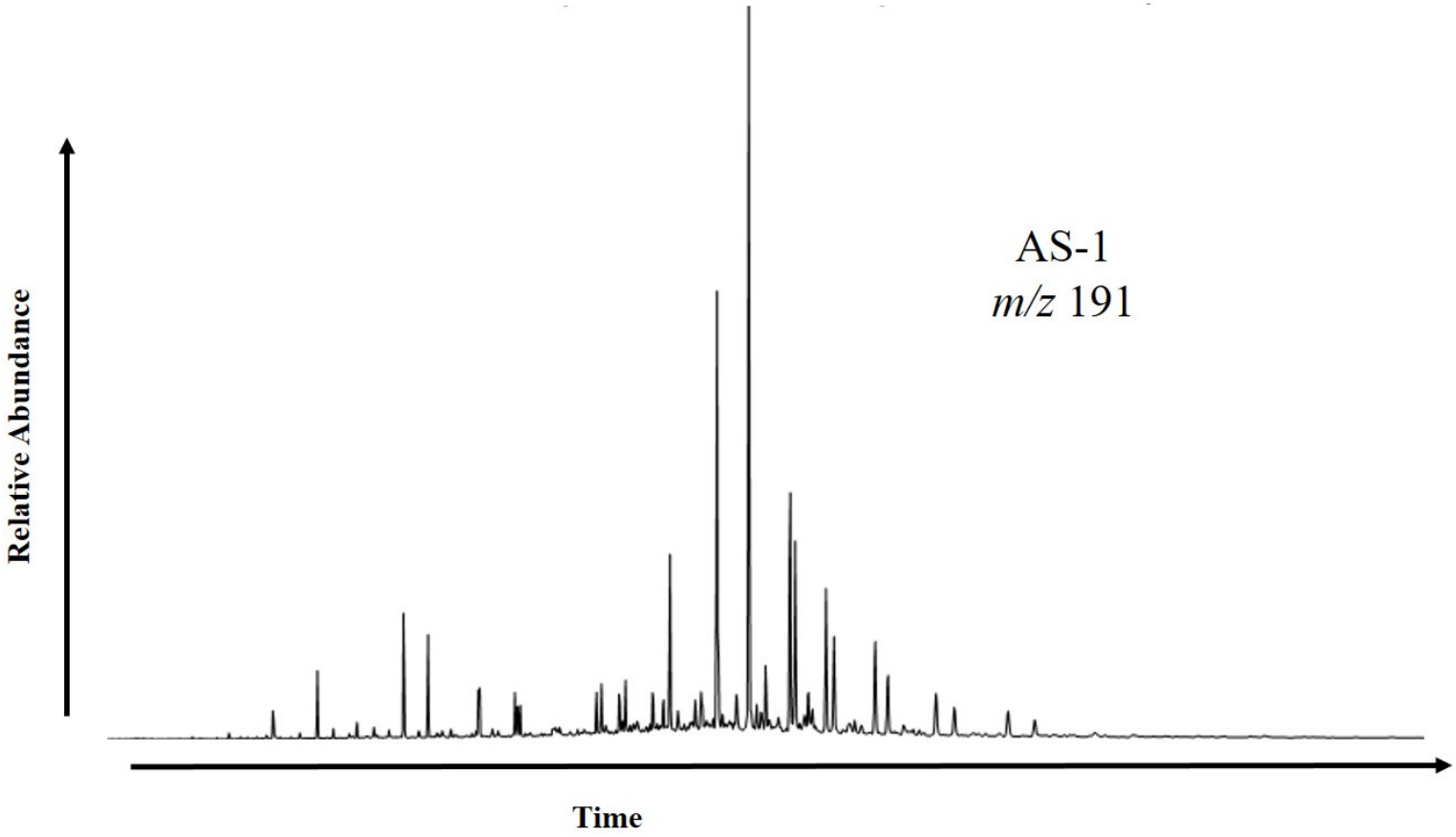
AS-1
m/z 191
Relative Abundance
Time

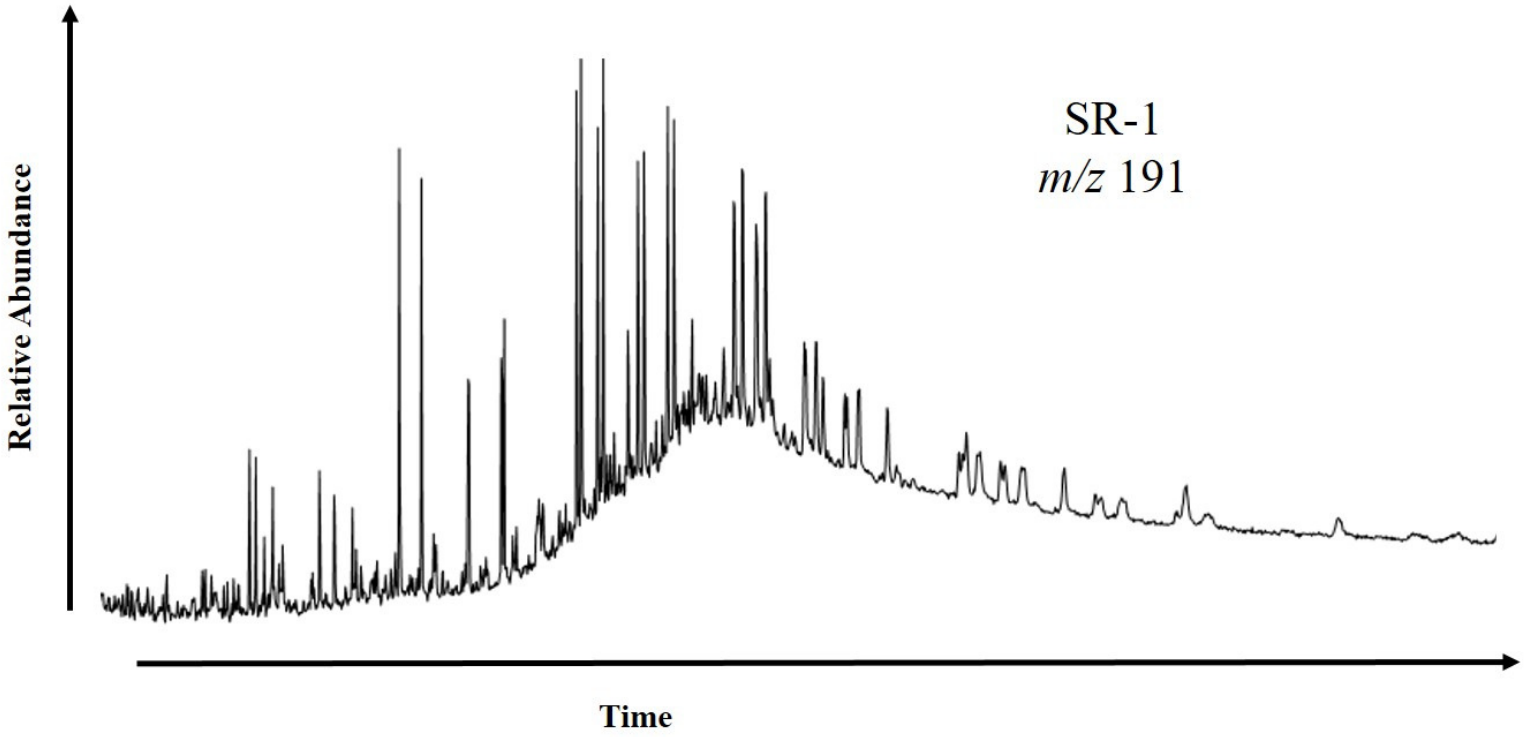
SR-1
m/z 191
Relative Abundance
Time

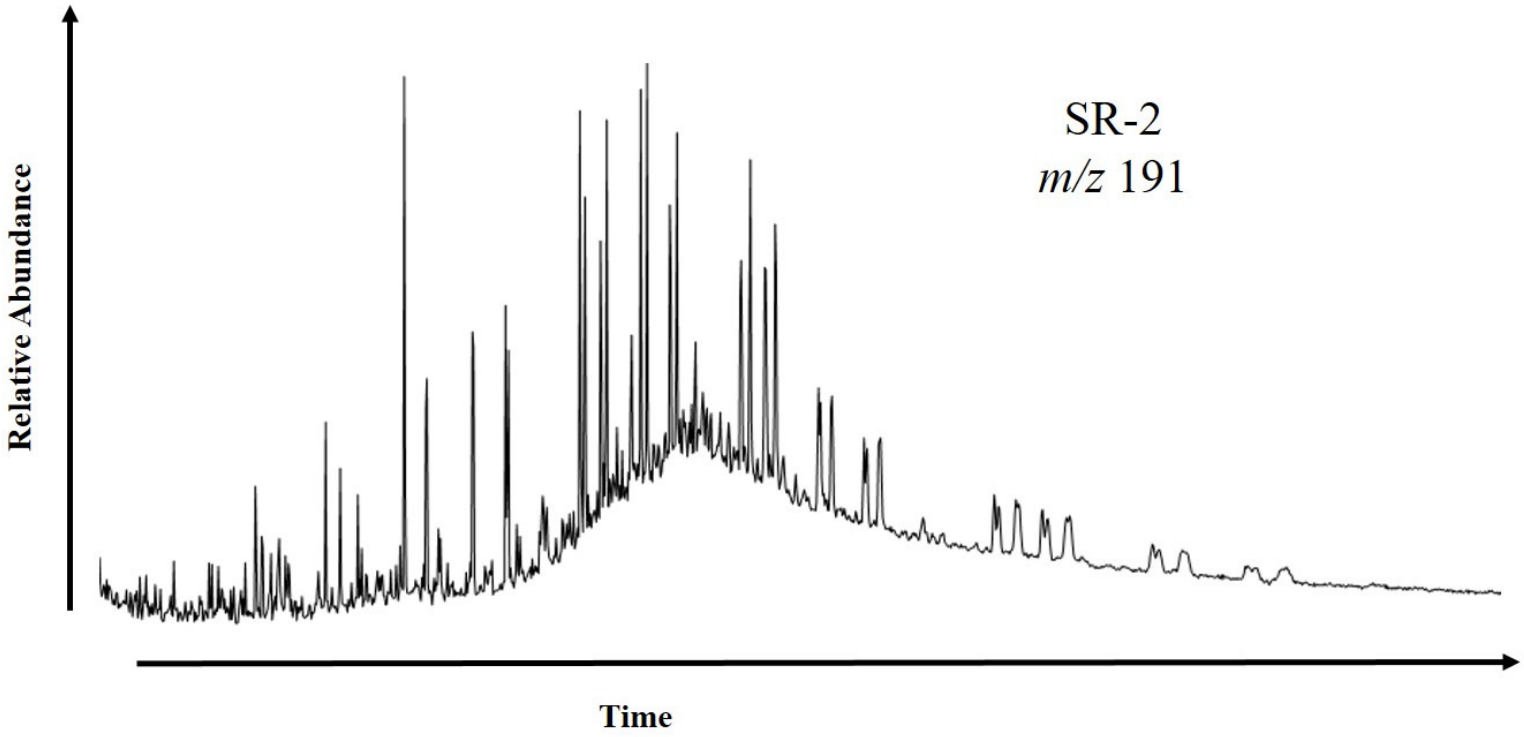
SR-2
m/z 191
Relative Abundance
Time

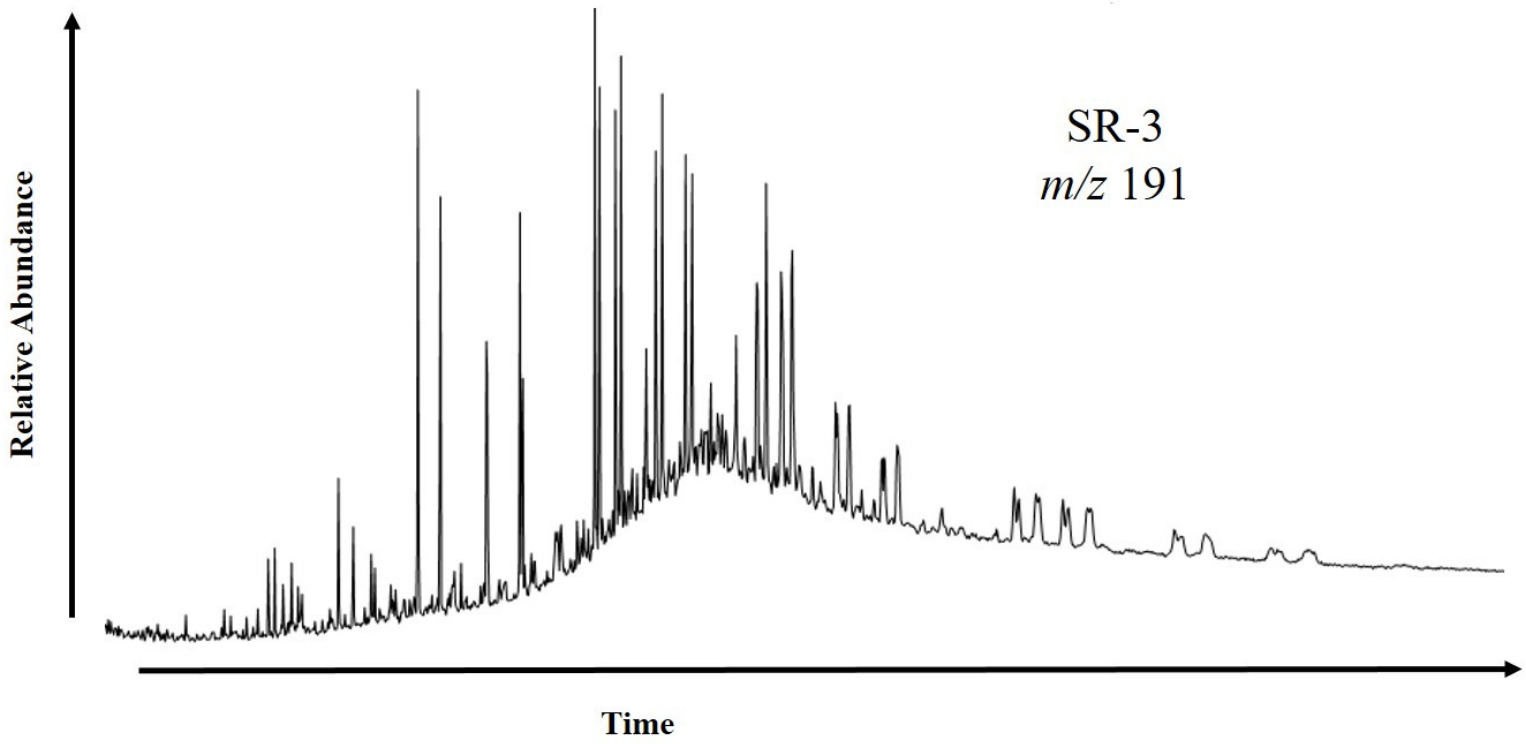
SR-3
m/z 191
Relative Abundance
Time

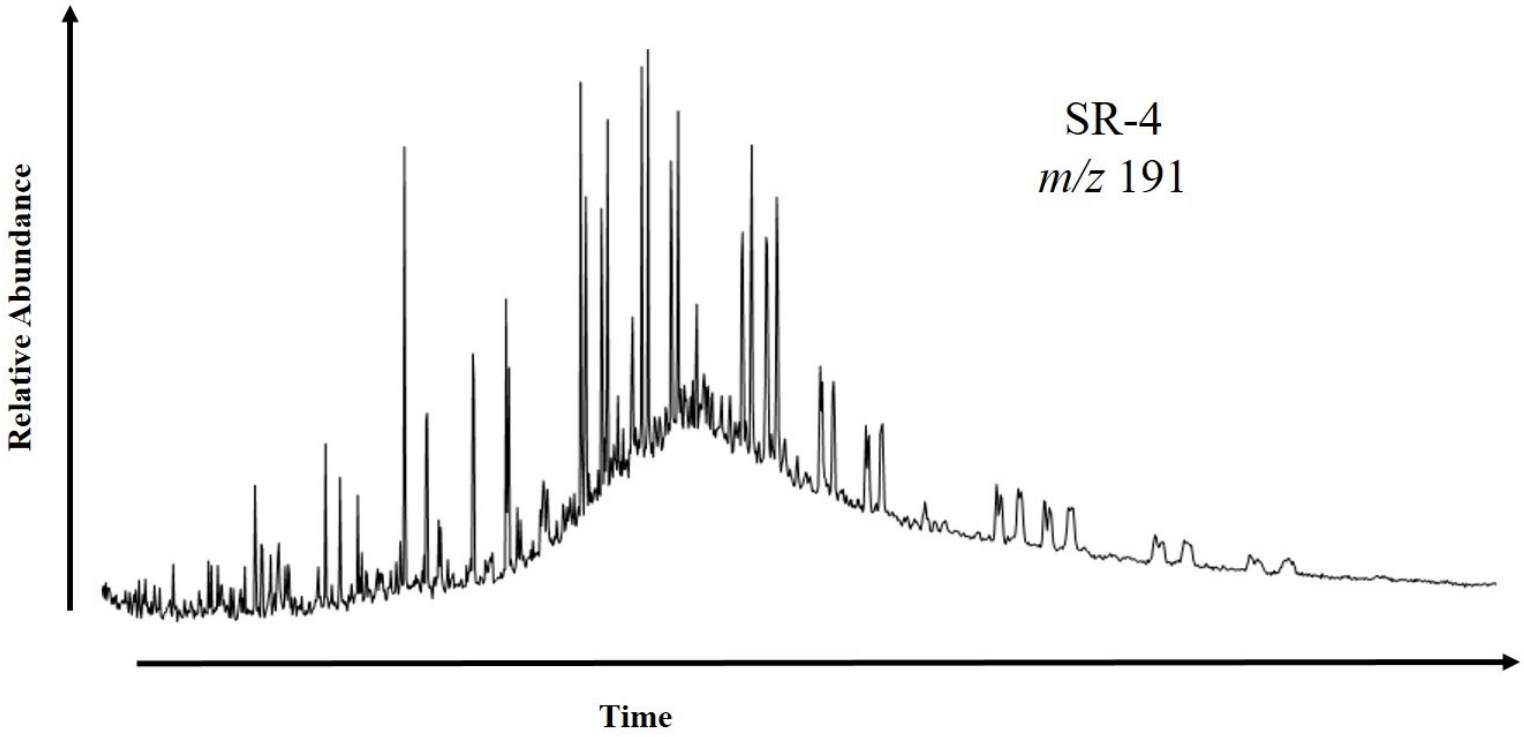
SR-4
m/z 191
Relative Abundance
Time

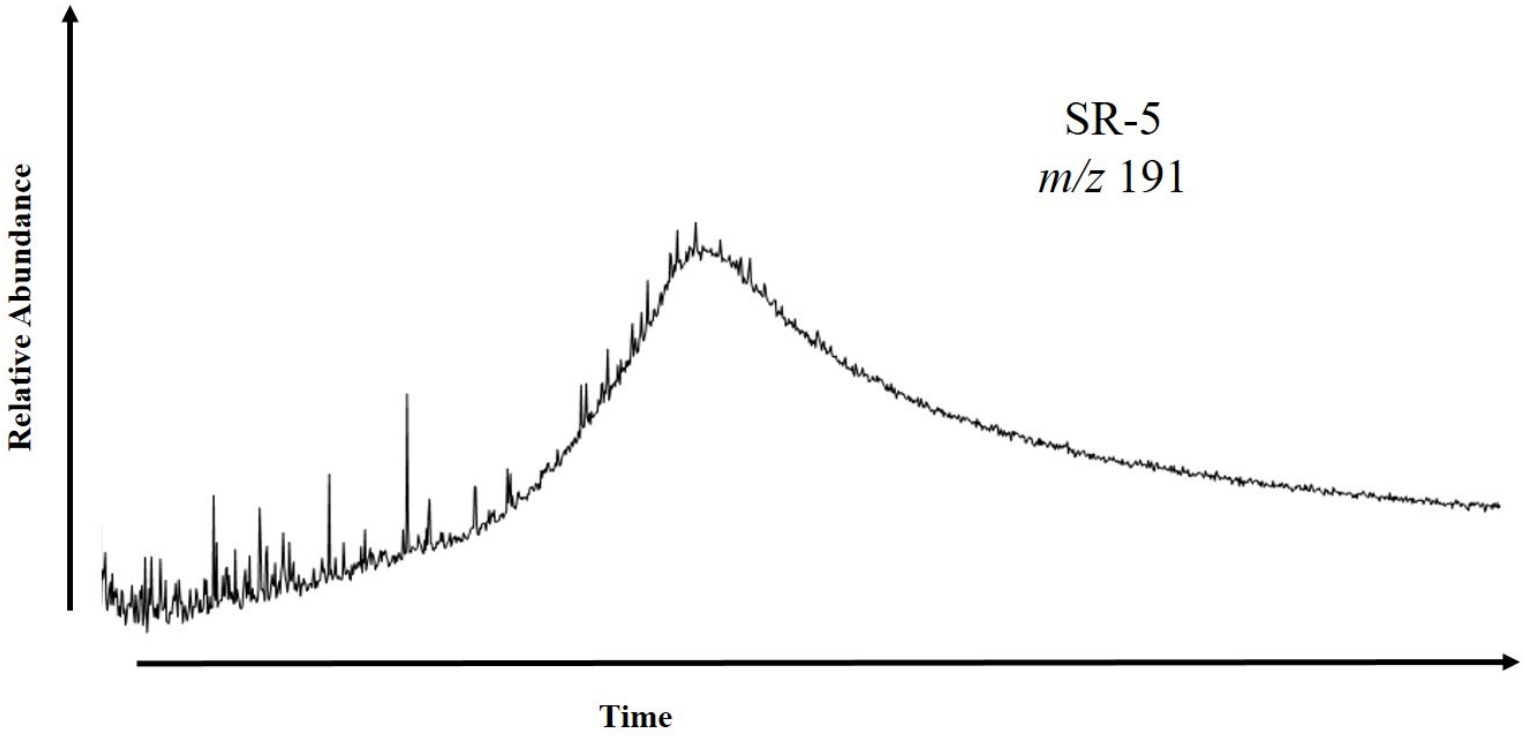
SR-5
m/z 191
Relative Abundance
Time

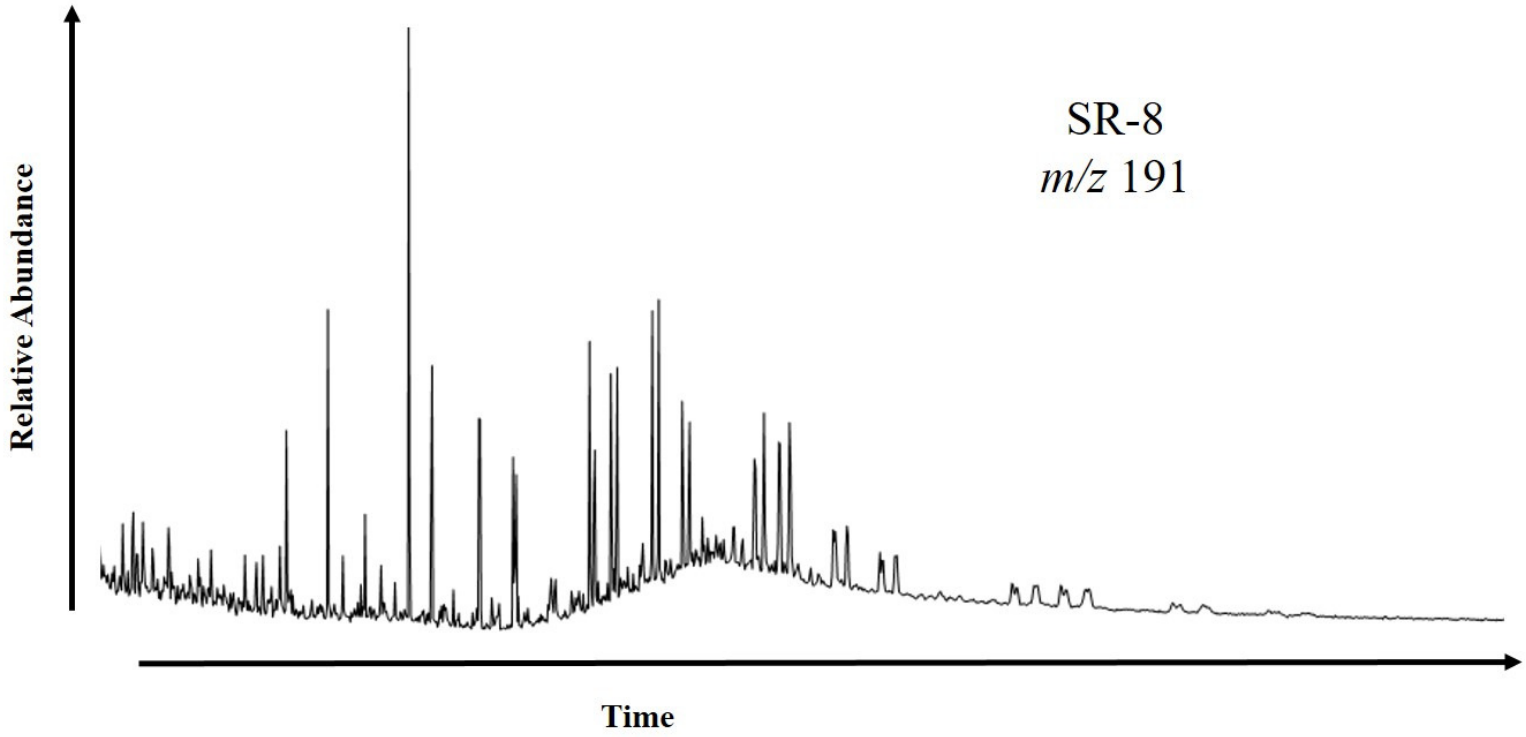
SR-8
m/z 191
Relative Abundance
Time

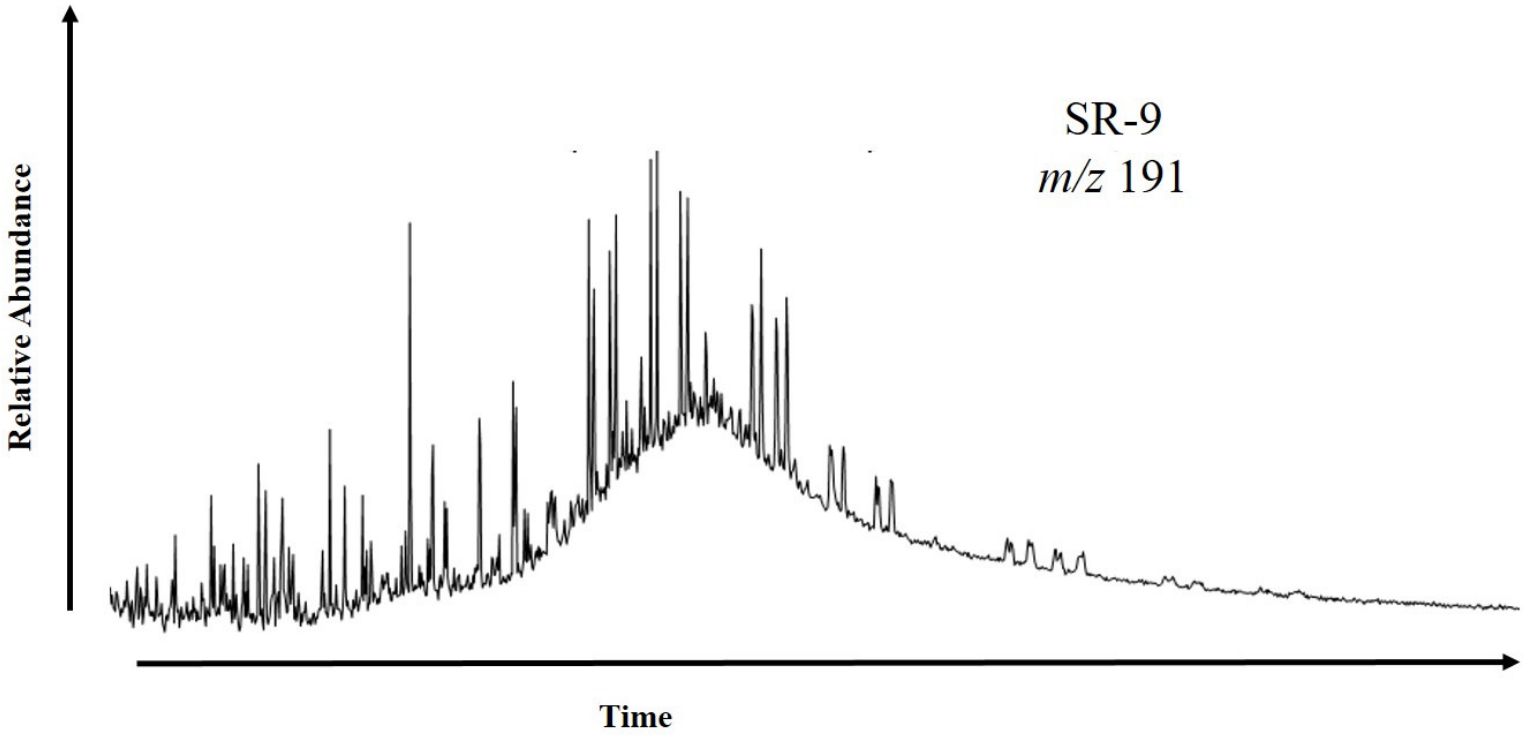
SR-9
m/z 191
Relative Abundance
Time

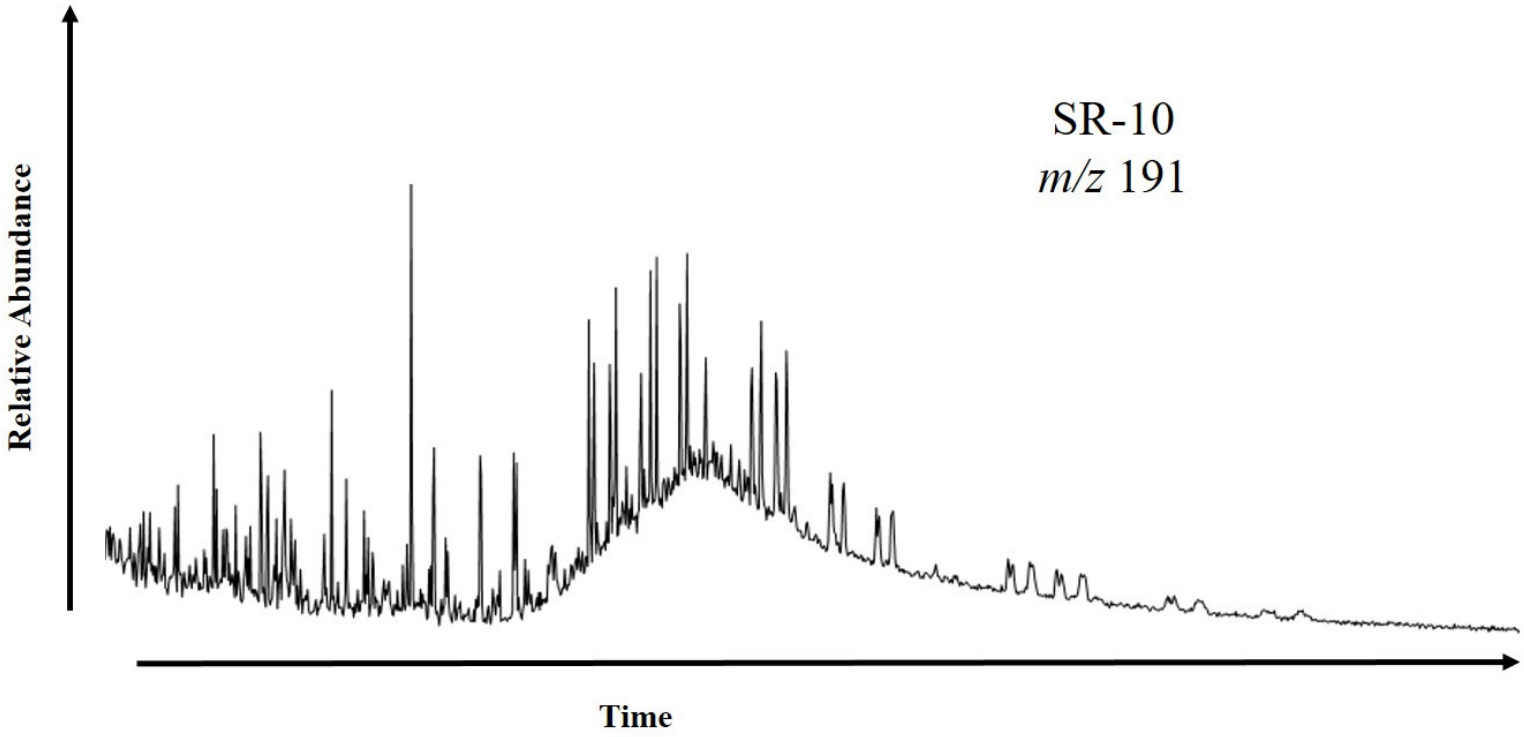
SR-10
m/z 191
Relative Abundance
Time

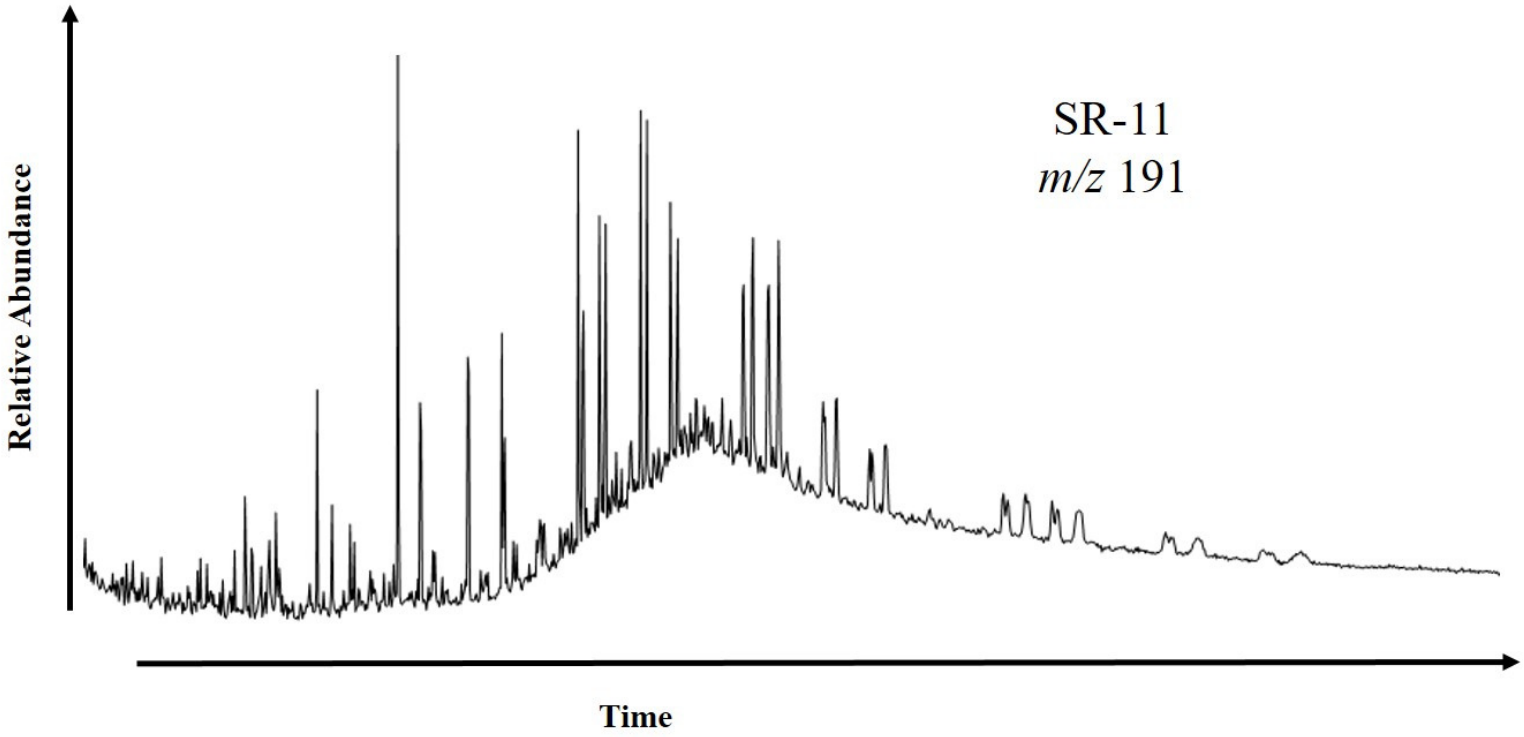
SR-11
m/z 191
Relative Abundance
Time

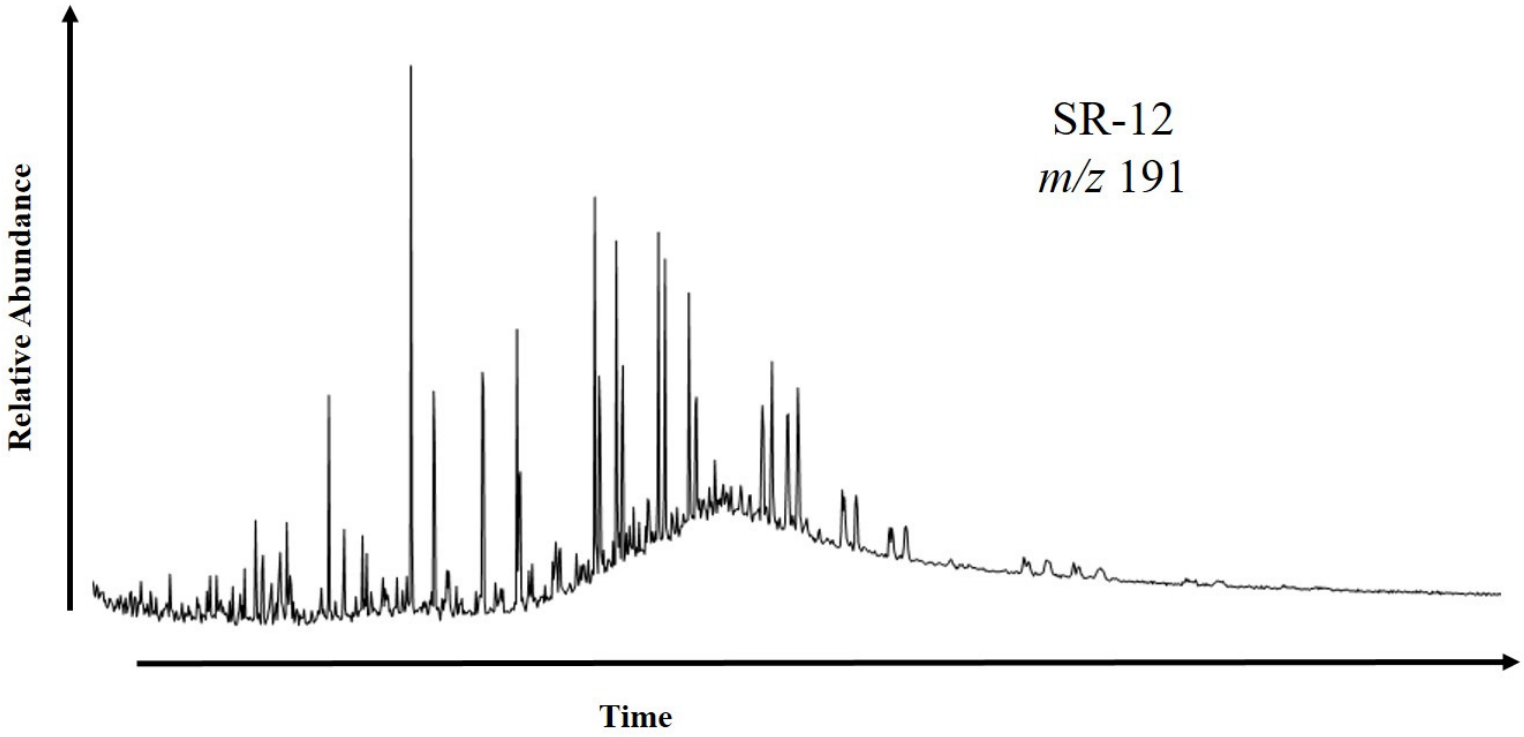
SR-12
m/z 191
Relative Abundance
Time

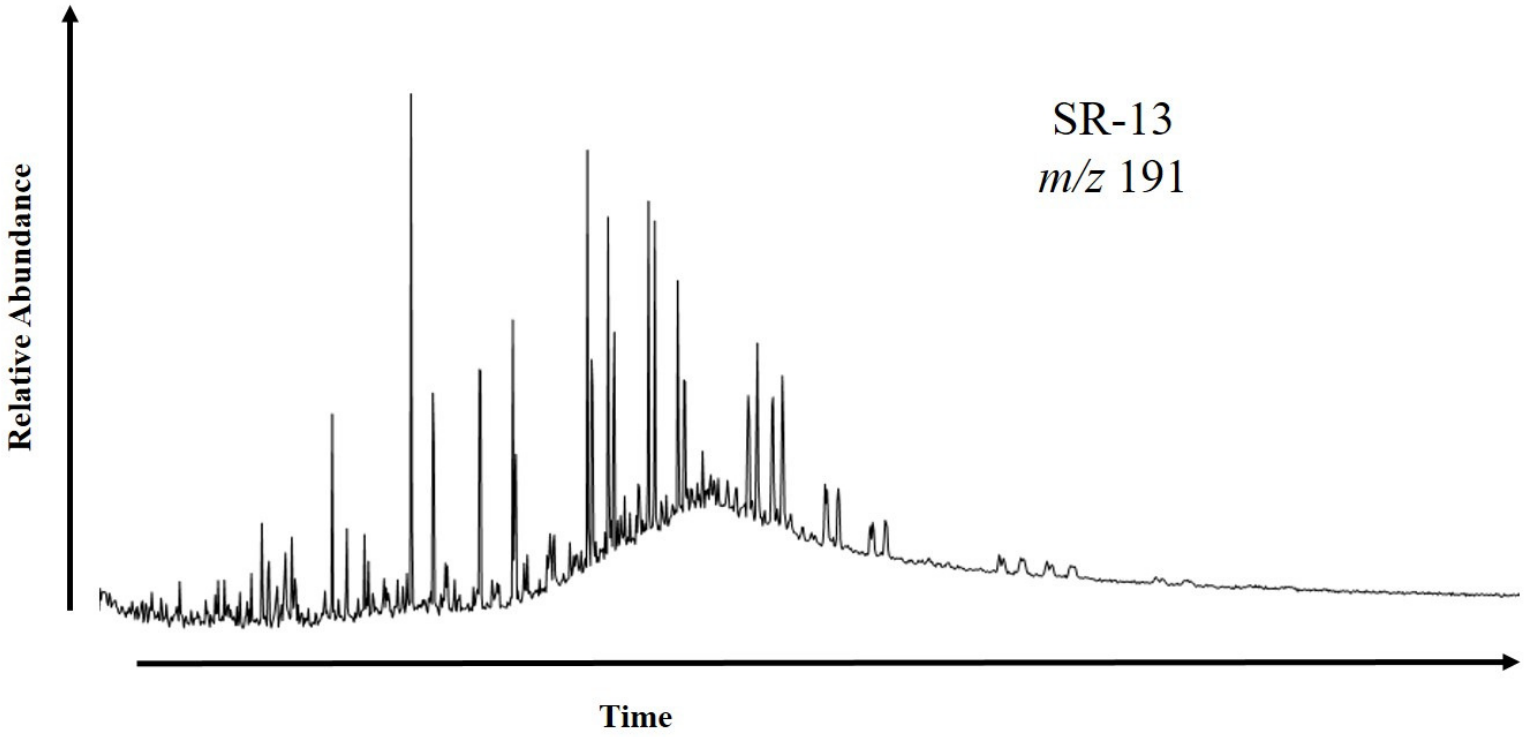
SR-13
m/z 191
Relative Abundance
Time

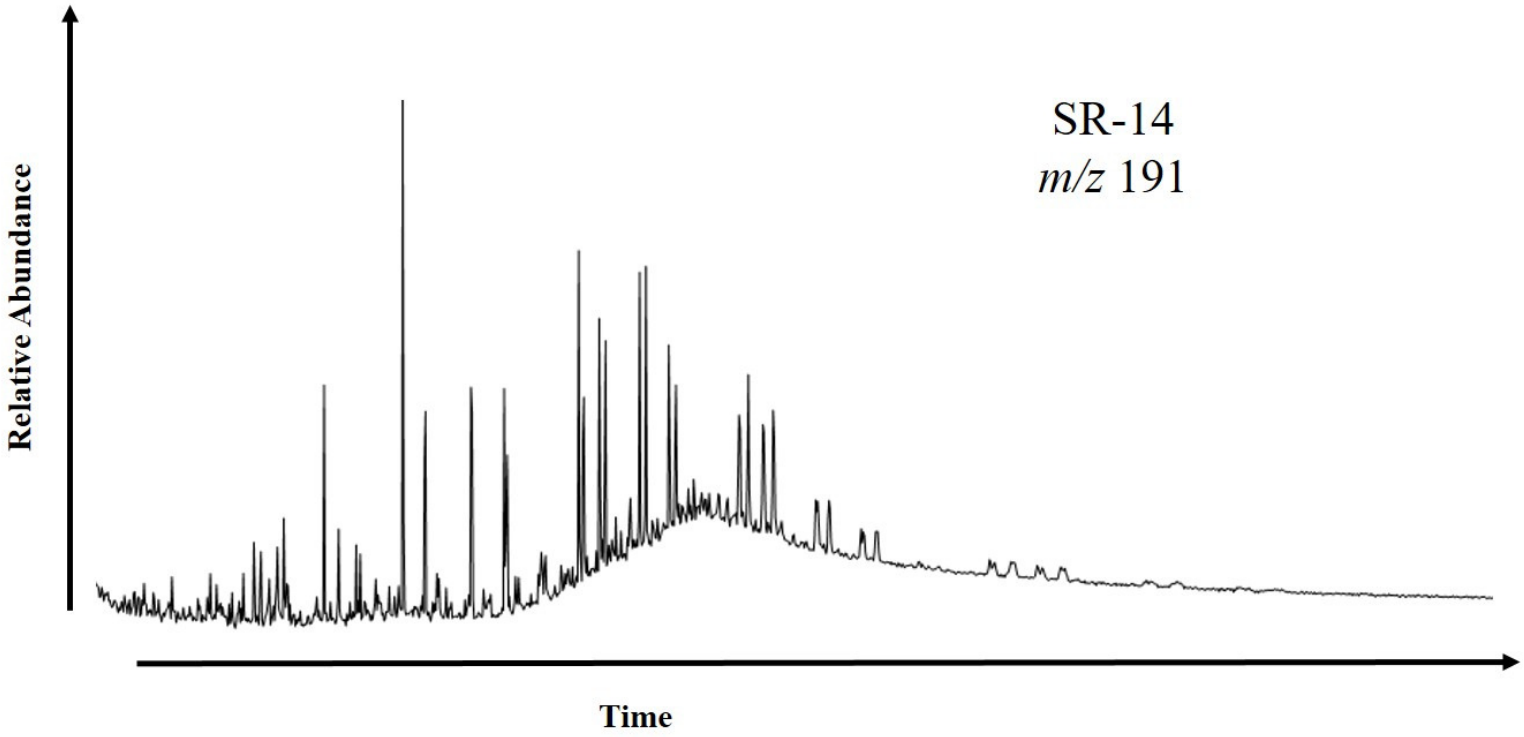
SR-14
m/z 191
Relative Abundance
Time

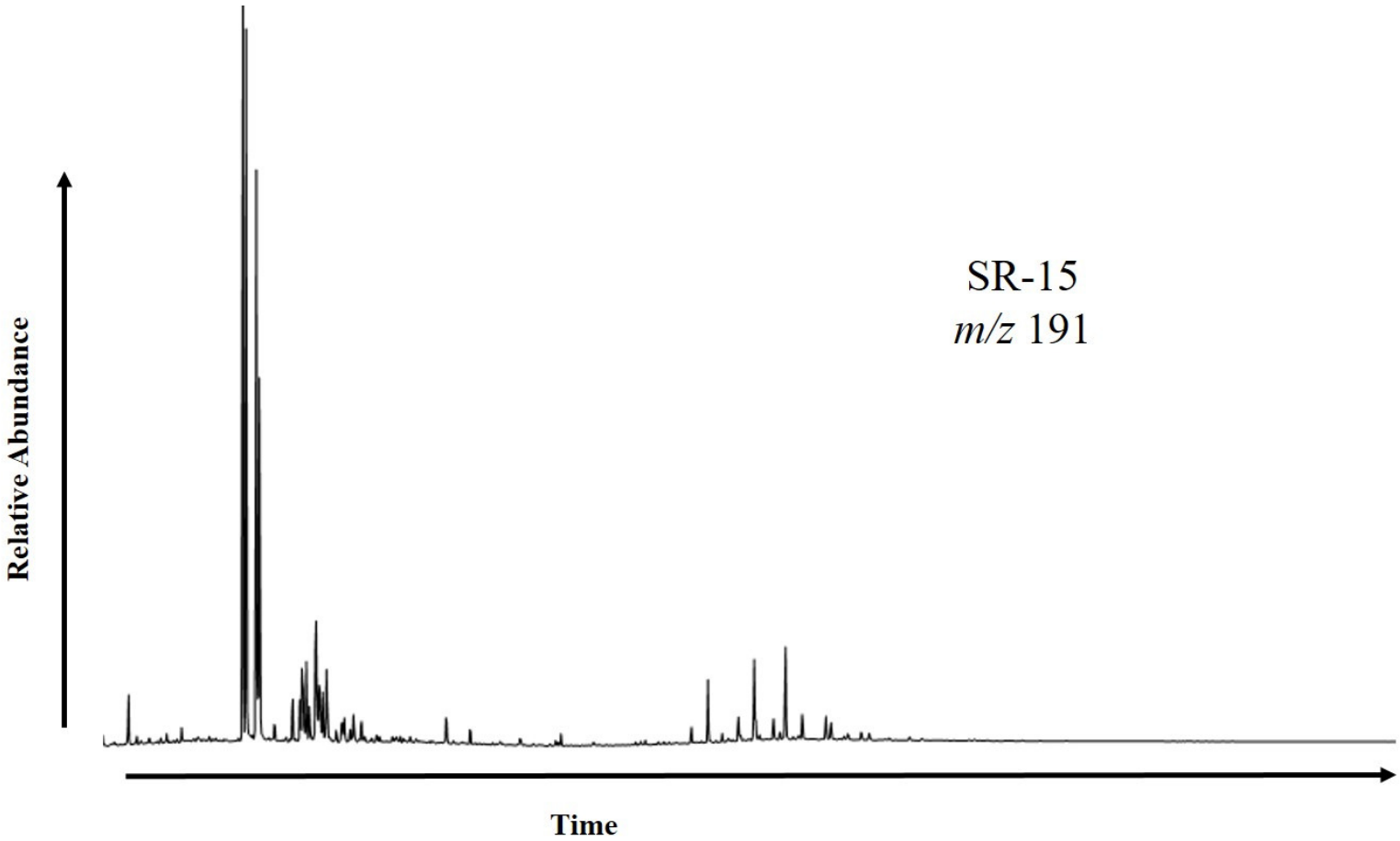
SR-15
m/z 191
Relative Abundance
Time